Discipline of Electrical and Computer Engineering

Real-time Power Management of Renewable Microgrid based on IEC 61850 Communication Protocol Using Adaptive Intelligent Petri Net

Navid Aghanoori

This thesis is presented for the Degree of

Doctor of Philosophy

of

Curtin University

May 2020

Declaration

To the best of my knowledge and belief this thesis contains no material previously published by any other person except where due acknowledgment has been made.

This thesis contains no material which has been accepted for the award of any other degree or diploma in any university.

Author: Navid Aghanoori

Date: 06/05/2020

Abstract:

The power consumption of all countries has undoubtedly increased in recent years. Utility scale microgrids (MGs) have been considered in the power system industry to provide cheaper power to remote communities. Renewable energy has made a major contribution to the energy supply of MGs. However, due to the intermittent nature of renewable energy, power system security has been the main concern of integrating these renewable energy-based microgrids into the utility grid. Therefore, sophisticated practical power management is needed to consider all aspects of connecting a renewable utility size microgrid.

This thesis utilises the author's practical experience in several renewable power plants, including Gullen Range Wind-Solar Farm (NSW, Australia), White Rock Wind-Solar Farm (NSW, Australia), Morton Lanes Wind Farm (NSW, Australia), Sydney Market Solar Farm (NSW, Australia), Stockyard Hill Wind Farm (Vic, Australia) and Moorabool Wind Farm (Vic, Australia) to propose a comprehensive Power Management Platform supported by a new data class model for the IEC 61850 substation protocol, which improves fundamental aspects of renewable MG operations on existing platforms.

The proposed method performs real-time power management of a microgrid to accommodate more renewable energy supported by a new proposed data class for the IEC 61850 substation protocol. This thesis not only supports the author's proposed contribution via simulation results conducted using the MATLAB software with a variety of case studies, but also supports the proposed solutions using field implementation.

The main components of the proposed and implemented platform, including the main contributions of the thesis, are:

1. An adaptive intelligent Petri Net as a high-level Power Management Platform. This Petri Net runs the top layer logic of Power Management and can be easily implemented in any SCADA platform for monitoring purposes. Due to its

adaptive elements, the Petri Net can simplify all the complex processes in high-level management.

2. A Co-evolutionary Particle Swarm Optimisation (CPSO) is run in one of the places of the Petri Net to provide the most optimal dispatch signals for Power Management.

   The CPSO continuously monitors the two main objectives, which satisfy network power demand and the stability of the microgrid. This comprehensive power management platform considers the stability of the microgrid and POCs in the renewable plants connected to the grid, while the power demand is the primary objective. This CPSO equips the power management platform with the consideration of the cascaded impact of the time delay on system stability and the impact of system stability on power management

3. New Voltage management platform for renewable microgrids.

   Most of the utility scale renewable plants are required to provide reactive power support to the gird at the POC. This thesis develops a voltage control strategy using the measurement of the virtual impedance of the line. The advantages of this method over the conventional voltage droop control is also shown and discussed.

4. The proposed power management platform requires a fast communication protocol. This thesis proposes, develops and tests a new data class model for the IEC 61850. The IEC 61850 protocol standard is proposed as the main backbone for fast communication; however, a new data class model is hereby proposed as the standard form for all renewable measurement and control components. This proposed communication platform reduces time delays in the feedforward and feedback loop control down to a few milliseconds versus conventional time delays at a few hundred milliseconds. This fast communication results in significant improvements in the stability of the microgrid, voltage control at the POC for renewable plants, as well as less harmonic distortion caused by time delays.

Statement of Contribution in publication by others

This thesis includes technical materials that have been published in international conferences and journals. These publications are listed below.

1- "Enhancement of Microgrid Operation by Cascaded Consideration of Communication Delay on System Stability and System Stability on Power Management"

This paper is the result of chapter four of the thesis and has been published in Elsevier – International Journal of Electrical Power and Energy Systems.

Main contribution of the candidate: generating the new idea of the publication, deriving the theory and computation, performing the lab tests, programming and configuration, troubleshooting the tests, collecting the data, running the main investigation, deriving the case studies, analysis and presentation of the results and preparing the manuscript.

Main contribution from the co-authors: encouraging and supporting the idea, assisting with the investigation of practicality of the idea, reviewing the results, reviewing and correcting the academic language and formatting. Further details are provided in the signed authorship statement in appendix C.

2- "Improving Voltage of Remote Connection Using Wind-Solar Farms Equipped with New Voltage Control Strategy Using Virtual Impedance Monitoring Enabled by IEC 61850 Communication".

This paper is the outcome of the results of the case study discussed in chapter five of the thesis and has been published in IET Generation Transmission and Distribution.

Main contribution of the candidate: generating the new idea of the publication, deriving the theoretical aspect of the simulation, performing the field tests, collecting the data, running the main investigation, deriving the case studies, analysis and presentation of the results and preparing the manuscript.

Main contribution from the co-authors: encouraging and supporting the idea, assisting with the investigation of practicality of the idea, performing the tests, reviewing the results, reviewing and correcting the academic language and formatting. Further details are provided in the signed authorship statement in appendix C.

3- “Investigation of microgrid instability caused by time delay”.

This paper is the outcome of the results of study of time delay in the power systems which was discussed in chapter three. This paper was published in IEEE conference ELECO.

Main contribution of the candidate: generating the new idea of the publication, deriving the theoretical aspect of the simulation, running the main investigation, deriving the case studies, analysis and presentation of the results and preparing the manuscript.

Main contribution from the co-authors: encouraging and supporting the idea, investigating the necessity of contribution, choosing the case studies and assisting with review and correction of language and formatting of the publication. Further details are provided in the signed authorship statement in appendix C.

4- “Voltage sag compensation in renewable plant using hydro-pump storage”.

This paper investigated the requirement of fast response for reactive power support from a hydro station in the event of grid fault for preventing a wind farm from tripping.

Main contribution of the candidate: generating the new idea of the publication, deriving the theoretical aspect of the simulation, running the main investigation, deriving the case studies, analysis and presentation of the results and preparing the manuscript.

Main contribution from the co-authors: Main contribution from the co-authors: encouraging and supporting the idea, investigating the necessity of contribution, choosing the case studies and assisting with review and correction of language and formatting of the publication. Further details are provided in the signed authorship statement in appendix C.

Candidate Signature:	Supervisor Signature:
Date: 06/05/2020	Date: 06/05/2020

ACKNOWLEDGMENTS

I am thankful to my supervisors, Ahmed Abu Saida, whose encouragement, supervision and support from the preliminary to the concluding stages enabled me to develop an understanding of the subject and complete my PhD thesis.

It is with pleasure that I would like to thank my chair and co-supervisor, associate professor Sumedha Rajakaruna and Dr. S. M. Muyeen for their advice, support and guidance towards the end of my research.

I would also like to thank all the authors who contributed to my publications and assisted me in presenting my results appropriately.

I am also thankful to Michael Haagensen from institute of professional editor for proofreading this thesis.

I offer my regards and blessings to my beloved parents who gave me their unwavering support, encouragement and prayers to the end of my education.

Finally, I heartily express my special appreciation to my wife for her endless dedication, love and patience throughout the completion of my PhD studies at Curtin University.

Table of Contents

1 CHAPTER ONE: Introduction 14
1.1 Research Incentives 14
1.2 Research Objectives 15
1.3 Thesis contributions 16
1.4 Thesis outline 18
1.3 References 20
2 CHAPTER TWO: Real-Time Power Management Using Petri PSO Equipped with Fast Communication 21
2.1 Problems 21
2.1.1 Power Management 23
2.2 Components of Proposed Power Management Platform 25
2.3 References 28
3 CHAPTER THREE: The Impact of Time Delays on System Performance 31
3.1 The Problem 31
3.1.1 Control Model for a Grid-connected Microgrid 32
3.1.2 Simulation and Results in Relation to the Effect of Time Delays 37
3.2 Proposed Communication Platform Solution 46
3.2.1 Introduction of IEC 61850 46
3.2.2 Proposed New Data Class Model 47
3.2.3 IEC 61850 Versus Industrial Communication Protocols 51
3.2.4 Conclusion 53
3.3 References 55
4 CHAPTER FOUR: Power Management Implementation 57
4.1 Three-Source Standalone Microgrid 57
4.2 State Space Modelling of the MG 58
4.2.1 Microgrid Control Layout 58
4.2.2 State Space Model of DG Inverters 61
4.2.3 MG State Space Model Considering Dispatch and Communication 67
4.2.4 Impact of Power Reference Upgrading 67
4.3 Proposed Real-Time Power Management and Stability Control Scheme 68

4.3.1 Adaptive Petri PSO 68
4.3.2 Petri PSO Cost Objective Function 70
4.3.3 Petri PSO Constraints 70
4.3.4 Adaptive Petri PSO 71
4.4 Implemented Fast Data Exchange Communication MG Based on IEC 61850 72
4.5 Results and Discussion 73
4.5.1 Real-time Power Management and Stability Analysis of an MG 73
4.5.2 IEC 61850 GOOSE and SV Test in the MG 80
4.6 Conclusion 83
4.6.1 Power Management and Stability Modelling 83
4.6.2 IEC 61850 GOOSE and SV Modelling 84
4.7 References 85
5 CHAPTER FIVE: Grid-Connected Voltage and Reactive Power Control Improvement Using Fast Communication and Virtual Impedance 86
5.1 Introduction 86
5.2 Problem 86
5.3 Voltage Control of a Wind-Solar farm in or outside a Microgrid 88
5.3.1 Droop Control Strategy 88
5.3.2 Wind-Solar White Rock Model 92
5.3.3 Adaptive Petri Net for Virtual Impedance Voltage Control Equipped with Fast Communication 93
5.4 Real-time Adaptive Petri Net Applied to Control the Voltage of the Wind-Solar Farm 95
5.4.1 Proposed Voltage Scheme 95
5.4.2 Proposed IEC 61850 Data Exchange Layout 97
5.5 Simulation and Results 97
5.5.1 Simulation Results 98
5.5.2 Field Test Results 105
5.6 Conclusion 110
5.7 References 112
6 CHAPTER SIX: Thesis Summary, Conclusions and achievement 115
6.1 Thesis Proposal and Implementation Summary 115
6.2 Conclusions and Achievements 116

6.2.1 Power System Related Conclusion 116
6.2.2 Communication Related Platform Conclusion 117
6.3 Future Works 118
APPENDIX A 118
APPENDIX B 123
APPENDIX C 124
APPENDIX D 130

List of Figures:

Figure 2.1 Power Management Overall Scheme Including Control and Communication Layout 27
Figure 3.1 Single-phase representation of microgrid system under study with specific voltage phasors indicated [5,9] 33
Figure 3.2 The RL feedforward current-limiting algorithm [5,9]; (a) control block diagram, (b) implementation. 34
Figure 3.3 Control Block representation of flux-charge model algorithm [5,9] 36
Figure 3.4 Modification of flux-charge-model control [5,9]. 36
Figure 3.5 Flux-charge model control with time delay [5,9] 37
Figure 3.6 (a) Critical load voltage (b). Critical load RMS voltage (c). Critical load current (d). Critical load RMS current for time delay = 1 μs [9] 40
Figure 3.7 Bode Plot of the Open Loop Control System of Microgrid Transfer Function with time delay 1 μs [9] 40
Figure 3.8 (a) Critical load voltage (b). Critical load RMS voltage (c). Critical load current (d). Critical load RMS current for time delay = 1 ms 42
Figure 3.9 Bode Plot of the Open Loop Control System of Microgrid Transfer Function with time delay = 1 ms [9] 43
Figure 3.10 (a) Critical load voltage (b). Critical load RMS voltage (c). Critical load current (d). Critical load RMS current for time delay = 5 ms [9] 45
Figure 3.11 Bode Plot of the Open Loop Control System of Microgrid Transfer Function with time delay = 5 ms [9] 45
Figure 3.12 Control and protection LNs combined in one physical device [9,10] 47
Figure 3.13 Peer-to-peer data value publishing model (conceptual) [10] 49
Figure 3.14 MG inverter and controller information proposed structure 49
Figure 3.15 GOOSE, SV, Proposed Data class and Client Server Communication on OSI layer 50
Figure 4.1The isolated MG under consideration with the addition of IEC 61850 GOOSE Messaging (similar to the MG of [1] with PV, micro-turbine and fuel cell generators) 58
Figure 4.2 Considered Microgrid Single Line Diagram 59
Figure 4.3 Inverter control, central controller and IEC 61850 bus block diagram 61
Figure 4.4 Proposed MG Petri Net simulated in HIPS software with the system status; (a) at place 1, (b) at place 2 69
Figure 4.5 Laboratory setup for communication test of the proposed new class of IEC 61850 GOOSE messaging 73
Figure 4.6 Low frequency MG eigenvalues plotted for τ=1 msec and τ=30 msec 75
Figure 4.7 Low frequency eigenvalues of MG for: (a) τ=5 msec, (b) τ=15 msec 76
Figure 4.8 (a) Power output from each inverter with τ=5 msec, (b) DC voltage of Solar and FC inverters with τ=5 msec, (c) Load Voltage (d) load Current. 78

Figure 4.9 (a) Power output from each inverter with τ=15 msec, (b) DC voltage of solar and FC inverters with τ=15 msec. 79
Figure 4.10 IEC 61850 Server and Client Running on Xelas Energy Management Graphic User Interface (GUI) 81
Figure 4.11 (a) Server SCL file in model designer software package of Xelas Energy, (b) Wireshark IEC 61850 captured SVs at Client End 82
Figure 5.1 Conventional Voltage Control Block Diagram [20] 91
Figure 5.2 Simplified Single Line Diagram of White Rock Solar Wind Farm used for Simulations and Field data Measurements 92
Figure 5.3 Voltage Management Platform Petri Net [28] 94
Figure 5.4 Simplified Network-Farm POC Model [28] 96
Figure 5.5 The Proposed Overall Communication Layout [28] 97
Figure 5.6 Plant Voltage Response using Droop and Virtual Impedance 99
Figure 5.7 Turbine Reactive Power Response using Droop and Virtual Impedance 100
Figure 5.8 Plant Active Power at POC Droop Virtual Impedance 100
Figure 5.9 Turbine Current at Terminal Droop Control Virtual Impedance 100
Figure 5.10 . a) Turbine Reactive Power. b) POC Voltage. c) Turbine Current. d) POC Active Power Droop Virtual Impedance 104
Figure 5.11 WRWSF Plant Response to 5% Voltage Setpoint Change using Droop Control (a) POC Voltage, (b) Individual Wind Turbine 106
Figure 5.12 WRWSF Plant Response to 5% Voltage Setpoint Change using Virtual Impedance Method (a) POC Voltage, (b) Individual Wind Turbine Reactive Power [28] 107
Figure 5.13 WRWSF Plant Response to Cap Switching in the Network Using (a) Droop Control (b) Virtual Impedance Control [28] 109
Figure 5.14 WRWF Substation Equipment; (a) VMP and SCADA Systems, (b) Substation Automation and IEDs Proposed to be used in the Presented New Communication Platform. 110

List of Tables:

Table 3.1 System Parameters 33
Table 3.2 shows a quick comparison between the most commonly used protocols. 51
Table 4.1 Inverter Detailed Parameters 59
Table 4.2 Initial Modelling Values 60
Table 4.3 Petri Net Configuration Elements [2] 69
Table 4.4 Summary of the simulation results 77
Table 5.1 Petri Net Configuration Elements [28] 94

List of Abbreviations:

AI	Artificial Intelligence
AEMO	Australian Energy Market Operator
ASCI	American Standard Code for Interchange
ASN1	Abstract Syntax Notation One
BD	Block Diagram
CPSO	Co-evolutionary Particle Swarm Optimisation
CT	Current Transformer
DC	Direct Current
DG	Distributed Generator
DF	Distribution Feeder
dr	Droop
FCMC	Flux-Charged Model Control
GOOSE	Generic Object-Oriented Substation Event
GPS	Generator Performance Standard
HVRT	High Voltage Ride Through
IEC	International Electrotechnical Commission
IED	Intelligent Electronic Device
IEEE	Institute of Electrical and Electronics Engineers
IP	Internet Protocol
LD	Logical Node

LVRT	Low Voltage Ride Through
MG	Microgrid
MMS	Multimedia Messaging Service
MW	Mega Watt
NER	National Electricity Rule
NSW	New South Wales
OSI	Open System Interconnection
PI	Proportional Integrator
PN	Petri Net
POC	Point of Connection
PLC	Programmable Logic Controller
PPC	Power Plant Controller
PSO	Particle Swarm Optimisation
PWM	Pulse Width Modulation
PU	Per Unit
SCADA	Supervisory Control and Data Acquisition
SCSM	System Centre Server Management
STATCOM	Static Compensator
SV	Sampled Value
TCP	Transmission Control Protocol
THD	Total Harmonic Distortion
VLAN	Virtual Local Area Network

VMP	Voltage Management Platform
VSI	Voltage Source Inverter
VT	Voltage Transformer

1 CHAPTER ONE: Introduction

1.1 Research Incentives

In the past few years, the renewable energy sector of the power industry has grown significantly. There have been many reasons for this movement including the need to reduce green-house gasses and air pollution caused by CO_2 and the dependency on fossil fuels. In addition, in some countries, such as Australia, recent government policies, such as the renewable energy target, have motivated the industry to replace fossil fuel generators with renewable fuel generators. For instance, according to the Renewable Energy Target, Australia needs to provide 20% of its power demand from renewable energy sources by 2020 [1]. Consequently, some state governments, such as Western Australia's pays a subsidy to the power suppliers for the power generated by microgrids. This also motivates investors to empower microgrids within the network to meet Large-Scale and Small-Scale Renewable Energy Targets. These targets financially incentivise large and small generators by offering LGCs (Large-Scale Generation Certificates) and STCs (Small-Scale Generation Certificates) to pay large and small investors for each megawatt of renewable energy [2].

Since the increase in the demand for renewable energy, especially in the form of grid connected microgrids, this has brought security concerns in the utility grid, especially in regard to frequency and voltage instability; much of the literature in the field has addressed the stability, power management and power quality provided by renewable sources including renewable microgrids. However, none of the research has provided a comprehensive platform for microgrids or a renewable plant control platform which has taken all the theoretical and practical aspects of renewable power management into account. Providing a comprehensive practical scheme to eliminate or reduce the network security concern is one of the two contributions of this thesis.

The literature used in this thesis, in addition to the several grid connection models and simulations, reveal the fact that time delays can affect all the above-mentioned power features such as stability, response time to grid faults, and harmonics. There is limited research investigating time delays within renewable plants and microgrids; however, a few have proposed solutions to improve the time delay but even these solutions do not seem practical and sufficiently effective. Among all these solutions, the integration of

faster communication with power system management has not been paid enough attention.

The author of this thesis has broad practical experience in control systems and communication packages, such as for wind farms and solar energy farms. The author's practical experience has revealed the fact that communication delays can only be minimised if the communication between the measurement and control system is interoperable. Therefore, a new data class model for the IEC 61850 is proposed in this thesis to bring reliable, fast and interoperable communication protocols between measurement and control components of different vendors in the power plant, while improving the stability of the microgrid, voltage control at POC and power quality. To prove the outstanding contribution of this thesis, the author has published chapter five to show how effective this platform can be even for a renewable energy plant connected to a utility size grid.

Finally, with a commitment to power quality for utility scale microgrids connected to the entire grid in relation to Harmonic distortion has motivated this research to investigate the effect of time delays in microgrids and indicate how THD can improve the use of a fast communication platform.

1.2 Research Objectives

This research proposes a comprehensive real-time power management platform which can enhance the reliability of renewable microgrids, and consequently enlarge the penetration of renewable power into the grid. Prior to this research, there has been no research that comprehensively explores and provides a solution for the cascaded impact of time delays on MG stability and MG stability on power management. This research aims to achieve this by developing a new power management scheme and a new communication platform to support the proposed power management, including active power management and reactive-voltage management. The active power, which in this case relates to dispatching, can be slower than the voltage control, so it can utilise an optimisation method; however, the voltage control shall be fast and bypass the optimisation step in the scheme. Therefore, this research introduces a new voltage control method which uses the proposed fast communication protocol. This voltage control platform, subject to network utility agreement, can make wind and solar

microgrids of utility size the master voltage controller of the local area that the renewable plant is connected to.

In summary the research objectives are as follows:

- To develop a real-time Power Management System (PMS) for MG to accommodate more renewables. This power management requires the following fundamental control schemes. These control schemes are contained in a state space model of the system further described in sections 4.2.2 to 4.2.4.
    - Active Power
    - Voltage Control
    - Stability consideration
    - Demand Response
- Customising the IEC 61850 GOOSE messaging based on the proposed PMS scheme and generating the PMS packets accordingly.
- Applying the IEC 61850 communication protocol on the source side of the renewable MG substations.
- Developing an Intelligent Adaptive Petri Net (IAPT) to generate and update the optimal PMS references.
- Integrating IAPT with IEC 61850.
- Improving the power quality of the plant using the new communication platform.

1.3 Thesis contributions

As mentioned in other sections, there is currently a lack of a comprehensive method for microgrid management which not only considers all aspects of dispatching and stability but also covers the transient responses to the grid. Therefore, this research proposes a comprehensive power management platform which, at high levels, is controlled and monitored by a Petri Net, while it runs a cost optimisation algorithm to consider the stability of the system. A detailed platform with the combination of these two critical aspects, does not currently exist in microgrid power management research.

This platform needs to be equipped with a communication platform supported by all the measurement and the control elements of the microgrid. This adds interoperability between the control system components and consequently reduces time delays while

dynamically providing the current time delay of the system to the CPSO used in the power management. The CPSO uses the time delay as one of the key elements in the optimisation and continuously needs this to be updated with a new time delay. Introducing the time delay into the control system in a real-time manner gives the control system a greater degree of freedom to optimally select power control parameters.

Moreover, based on the practical experience of the author, improving the time delay embedded in the system can also improve power quality. As extensive studies of this impact of the time delay on the power system have not been found, generators and loads have needed to use expensive solutions such as harmonic filters. This thesis also explores how the proposed communication platform improves the THD of a power plant.

Therefore, this thesis proposes:

2. The development of a comprehensive power management platform considering all the aspects of utility-sized renewable microgrids.
    a. Developing an intelligent Petri Net equipped with a CPSO for optimisation.
    b. Improving stability by adding eigenvalue stability analysis in the dispatch control to guarantee the stability of the plant while supplying the demanded power at optimal cost.
    c. Relying on the proposed fast communication, improving the voltage control strategy and reactive power support at the point of connection of the renewable microgrid.
        i. Performs some simulation sets and proposes an enhancement of the voltage control against the conventional droop method.
        ii. Implements the proposed method and the conventional droop method in a real wind-solar farm and provides valuable field data and relevant analysis.
3. A new data class model for the IEC 61850 to
        a. First, establish interoperable communication between the inverters, controllers (such as PLCs) and measurement equipment from different equipment suppliers, which reduces the time delay to a significant scale.

b. Second, improve the harmonic distortion of the plant by reducing the time delay using the fast communication system.
c. Third, minimise the engineering and installation cost and complexity.

1.4 Thesis outline

This thesis is presented in six chapters which are outlined in this section. Chapter two first discusses the problem which exists due to the absence of a comprehensive real-time power management scheme. It then proposes the solutions and the aspects that need to be considered in a comprehensive management scheme.

Chapter three presents the impact of the time delay in power systems and particularly renewable microgrids in terms of stability and power quality. Simulation and field results are used to explore the relationship between the time delay and stability as well as the Harmonics. Then the proposed communication platform is introduced to reduce the time delay within the control system.

Chapter three also introduces the IEC 61850 substation protocol and the new data class, which is proposed to be added to this standard for the pure purpose of improving microgrid plants. This chapter has its own brief conclusion to summarise the discussion of the chapter.

Chapter four investigates the proposed real-time power management platform that has been presented in chapter two. The microgrid's new data class model proposed in chapter three has been tested using an IEC 61850 software platform in order to prove the claimed time delay is achievable using the proposed data model. The results of this chapter are the combination of simulation in MATLAB Simulink and some field tests using the IEC 61850 software platform. This chapter also includes the main contribution of the thesis which is a cascaded analysis of power management impacted by stability and MG stability by the communication time delay. This chapter has its own brief conclusion to summarise the discussion of the chapter.

Chapter five focuses on the aspect of real-time voltage control of the real-time power management platform as this is one of the main concerns in grid-connected MGs. This case study is presented to provide another application of an adaptive PN equipped with fast communication in grid-connected scenarios. As there was no real MG available to perform the study on, this thesis considered a wind-solar farm in the state of NSW in

Australia to explore the proposed method, and the real-time data have been presented. This chapter has its own brief conclusion to summarise the discussion of the chapter.

Chapter six summarises the entire thesis by providing a comprehensive conclusion in relation to the power management platform on a PN considering the stability influenced by the time delay and the improvement of the voltage control using faster communication. Some future works are also proposed in Chapter six.

1.3 References

[1] https://www.aph.gov.au/About_Parliament/Parliamentary_Departments/Parliamentary_Library/Browse_by_Topic/ClimateChangeold/governance/domestic/national/mandatory

[2] https://www.environment.gov.au/climate-change/government/renewable-energy-target-scheme

2 CHAPTER TWO: Real-Time Power Management Using Petri PSO Equipped with Fast Communication

2.1 Problems

Many new methodologies in relation to power generation, transmission, distribution and management have been considered and investigated as electricity demand has increased. Microgrids, which use renewable sources such as wind or solar power, represent one of the recent tools with significant advantages to other methods for the purpose of reducing dependency on the main utility grid. Microgrids have also been effective in reducing centrally dispatched power by using local renewable sources of energy. This supplies power to the customer with less energy loss.

Another feature of microgrids is their ability to be operated in island microgrid and grid-connected modes. The operation mode is dictated by how the system is designed [1-3] based on the microgrid requirement and its connection point to the loads or the grid. Microgrids assist with the overall cost of the power supply, reducing CO2 emission, and energy waste throughout the grid [4-6]. However, there is significant potential for maximising MG usage in a network, and a significant gap in terms of a comprehensive power management scheme equipped with a sophisticated control and communication platform. A more sophisticated management platform can assist with achieving optimal outcomes in various operating conditions. For instance, one black out in the state of South Australia was reported due to a sudden and significant loss of power supply that caused a frequency drop much faster than the load shedding scheme was able to react [7].

Despite all the research with regard to the real-time management and stability of MGs [3, 7-19], none provides a comprehensive real-time power management solution which addresses issues, such as the impact of reference change fluctuation, impact of time delays in the system and network condition changes. The most relevant works are briefly discussed below to show the gap in the existing literature in this area, which this thesis aims to fill; however, it is recommended that readers also go through the other references mentioned above. For instance, [3] investigates MG stability through eigenvalue analysis when wind speed fluctuates in the range of a metre per second without considering real-time constraints related to time delays in the system.

Reference [8] also introduces an energy storage system to remove the oscillation caused by wind speed changes with no consideration of time delays when the model will be implemented in a real-life platform. Reference [9] models the stability of a DC MG using a small-signal model and also investigates the stability of the MG utilising eigenvalue analysis without considering time delays within the system. Neglecting time delays in the system also occurs in references [10-14] and many others for both centralised and decentralised schemes. Reference [15] reviews the frequency stability of an MV MG and indicates the necessity of fast communication in emergency operation mode; however, the later chapters of this thesis highlights the benefit of access to fast communication in real-time power management in normal operating modes as well as emergency conditions.

Reference [16] proposes a control architecture with real-time consideration of the stability of the decentralised system, but the power references, which are used in the case studies, are constant values and equal. In the real-time operation of a power plant, however, the power plant setpoint can change and this can send a stable system into an oscillatory zone or make it unstable.

Reference [18] uses Modbus TCP/IP communication protocol and proposes virtual droop control for the MG control under constant voltage and frequency; however, the communication time delay between control elements such as gas generator measurement devices and multiple controllers such as PLCs are not considered. In a later chapter, it will be observed that the lack of the full consideration of a time delay, in which the system can vary from time to time, can make a big difference.

The authors of [19] have investigated the stability of decentralised inverter control using wireless communications between MG control components. Their results have indicated that the increase in the time delay in the MG control systems can shift the eigenvalues of the system from the left side of the imaginary axis to the right half plane, which means the system is unstable. The proposed method enhances the stability by bringing the eigenvalues to a power sharing method. However, the considered solution only addresses a single scenario of instability and there is no solution for dealing with dynamic changes in the system such as power reference changes.

Reference [20] proposes an approach in this thesis to improve the communication performance in the microgrid. However, this proposed solution does not customise the IEC 61850 data class model for renewable purposes. Second, the protocol still needs to be converted to another conventional communication CAN bus. Third, the research does not explore the main contribution of a faster communication protocol. Lastly, and most importantly, the whole platform, including the stability, power quality and voltage control of the microgrid are not considered in their small signal model to be able to show under what exact time delay, the system will be unstable to justify the communication design.

Reference [21] presents a new control method in the DC microgrid and considers the time delay in the system while two main components are not discussed. First, the interoperability factor is not considered between different DGs. Second, the allowable time delay for the system to remain stable is not taken into account. Additionally, the communication protocol proposed in this thesis can improve the considered reasonable time delay used in [21]. The authors of [22-23] highlight the importance of the time delay in the stability of the system.

2.1.1 Power Management

Real-time power management for a renewable microgrid must have the following aspects to be able to be considered as a practical comprehensive real-time power management scheme.

2.1.1.1 Top level management scheme

The top-level management scheme used for high-level monitoring needs to be simple and understandable for any level of knowledge in a real system. It should also be implementable in any monitoring or supervisory platform, such as SCADA. Moreover, a high-level power management scheme should be able to show the status of the whole system at any given time including during normal operations, when stopped and in recovery considering minimum cost. Therefore, a Petri Net has been selected to present the system status in this thesis. The Petri Net is discussed in section 4.1.2.

2.1.1.2 Mid-level Control - Optimisation algorithm

A good power management also needs an optimisation algorithm that can adaptively find the most optimal operating point and adjustable parameters of the system. This

optimisation is considered a mid-level control tool, which updates the parameters of the system in accordance with system condition changes. Within several reliable optimisation algorithms, due to having a balanced trade-off between the speed and accuracy of the results, PSO was chosen for the management platform. However, as the optimisation is required to work within certain limits, the Co-evolutionary PSO known as CPSO has been utilised in this thesis. CPSO and its integration to the Petri Net is discussed in section 4.1.4.

It should be noted that every grid-connected MG needs to consider voltage control at the POC due to recent requirements from market operators; this can be at a normal operating point or in fault ride through a range. Therefore, this thesis includes a study of different scenarios to cover normal and ride through scenarios for both conventional and proposed platforms.

2.1.1.3 Modelling the system

Modelling the system is primarily dependent on the dynamic of the system and this varies from one power system to the next. For instance, the dynamic of the system in a pure renewable DC microgrid is significantly different to a hybrid microgrid with fuel-based generators. Therefore, it is expected that when the proposed real-time power management is used, the dynamic modelling of the system is well known. For example, the dynamic of the case study considered in this chapter is a small-signal model of an inverter-based microgrid containing three sources.

2.1.1.4 Communication

All the abovementioned key elements of the real-time management platform need to have a data exchange platform. This data exchange must be fast enough to increase the power quality and keep the system stable in terms of frequency and voltage. Chapter 2 reviews how time delays caused by slow and conventional communication protocols can affect the functionality of the power system. Therefore, a reliable communication protocol is necessary, which has been previously used for substation automation in a new format and application. Therefore, as Chapter 3 below explains, a renewable data class model is proposed for the IEC 61850 to be used in the real-time power management platform.

2.2 Components of Proposed Power Management Platform

2.2.1.1 Petri Net

A Petri Net is a tool that can embed the high-level supervision and control of a system, in which it can also visualise the real-time status. A PN dynamically does this using four key groups of elements such as “places”, “tokens”,” transitions” and “arcs”. “Places” and “transitions” are denoted as $p \in P$, $t \in T$ and “tokens” and “arcs” are typically represented by ball and arrow symbols respectively [8].

Places represent the status of the system at each given moment, and transitions carry the condition of status change. When a real system moves from ith to (i+1)th the token goes from p_i to p_{i+1} in respect to all the conditions being met in the transition element between the two places. Therefore, considering the simplicity and adaptability of the Petri Net, it is a proper graphical supervisory and management tool for stochastic systems. This thesis proposes a PN to run the real-time power management while a CPSO algorithm is proposed for cost optimisation [23-25].

2.2.1.2 PSO

For many years Particle Swarm Optimisations were used as a computation method to find the optimal answer of a system because of its simplicity of implementation and fast convergence. However, this is only practical when used for unconstrained problems. The system that this thesis is dealing with has constraints that shall always be monitored during the optimisation. For instance, the optimisation for power management shall find the most beneficial set of power references while the total power generated by all sources shall meet the power demand. In addition, according to the proposed control scheme of this thesis, the combination of power references between all power sources shall be selected so that the stability of the microgrid is maintained [22].

The inability of a basic PSO in dealing with multiple constraints necessitates the idea of a Co-evolutionary PSO to be able to take all linear and non-linear constraints into account. Conventionally, the dispatching optimisation issues the microgrid a power reference which minimises the cost and does not take the stability of the microgrid into account. In this situation, the microgrid controller comes up with the most beneficial

combination reference of power sources. What the proposed CPSO includes, in addition to conventional dispatching, is adding the non-linear stability condition of the microgrid into the optimisation algorithm. This is done using one group of swarms in the PSO. Additionally, the second group of swarms in the proposed CPSO looks for the solutions that provide the whole demand of the load or grid.

In simpler terms, the proposed CPSO only generates the power references that guarantee the stability of the microgrid while meeting demand. According to these two constraints, the PSO finds the power references that minimise system cost. The details of the main objective and the constraints will be discussed further in Chapter 4.

It should be noted that the optimisation method itself is not a contribution of the thesis; however, it was needed. Due to the flexibility of the Petri Net, the PSO can potentially be replaced with any optimisation which might work better for the system. It is believed though, that the PSO appears to be simplest and fastest for the accuracy needed for the application discussed in this thesis.

2.2.1.3 Proposed Petri PSO

The Petri PSO is proposed in this thesis in such a way that the Petri Net handles all the high-level supervision and the PSO embarks on the optimisation under one of the places in the Petri Net. This combination provides the opportunity for the power management scheme to: first, operate around the normal operation point while the system is operating optimally; second, make sure all system constraints are considered [26]; and third, provide the freedom to bypass the estimation in emergency conditions, while in normal operation, the system can run critical and non-critical pathways of control in parallel while one is not impacting the other.

This thesis proposes a Petri PSO in such a way that segregates active power management in response to demand, and voltage control in response to reactive power demand. However, this requires the power management system be facilitated by a fast communication system, so it can respond to both forms of demand as quick as possible. This fast communication is not only needed to provide the reference signals to the generating units, but also for updating the measured values and system statuses of each of the generating units.

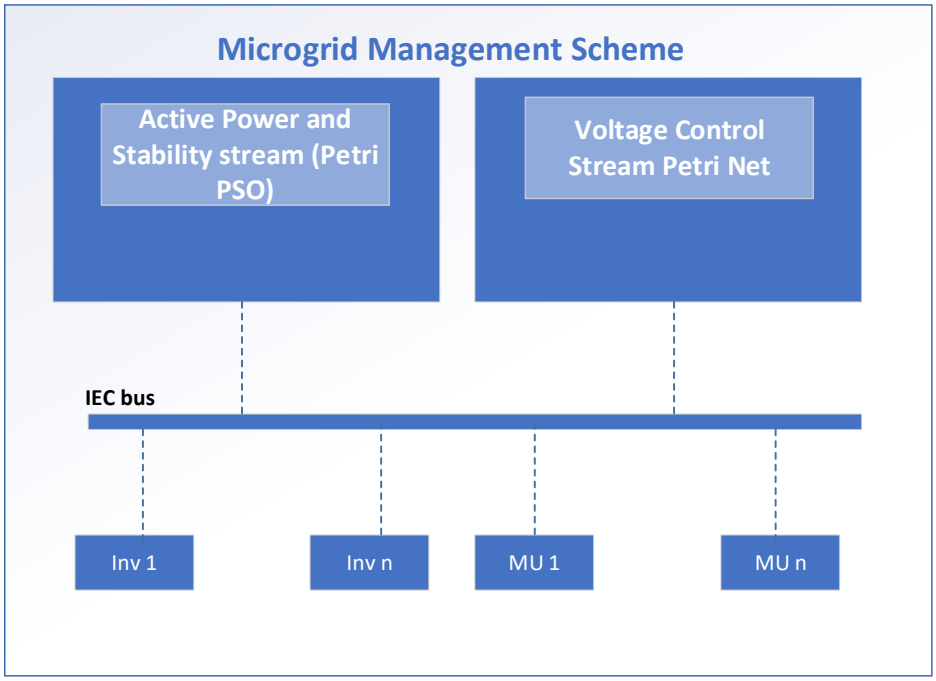

Figure 2.1 Power Management Overall Scheme Including Control and Communication Layout

In this thesis the "Active Power and Stability Stream" using a Petri PSO is explored and modelled in the case study in Chapter 4; the "Voltage Control Stream" using a Petri Net is explored and modelled in Chapter 5. The IEC bus and how the platform is being proposed to sit on OSI layers are discussed in Chapter 3; however, it is simulated and implemented for both case studies in Chapter 4 and 5. Figure 2.1 indicates the proposed power management scheme at a high level with the corresponding active power, voltage control and the proposed communication layout, which is discussed in section 2.2.1.4.

2.2.1.4 Fast communication Platform

The thesis has allocated section 3.2 to describe this new data class model due to the importance of this communication platform introduced as a new data class model in accordance with IEC 61850 supported by GOOSE and the SV basic model.

2.3 References

[1] F. Nejabatkhah and Y. W. Li, "Overview of power management strategies of hybrid AC/DC microgrid," *IEEE Trans. on Power Electronics*, vol. 30, no. 12, pp. 7072-7089, 2015.

[2] L. Meng, T. Dragicevic, J. Roldán-Pérez, J. C. Vasquez and J. M. Guerrero, "Modeling and sensitivity study of consensus algorithm-based distributed hierarchical control for DC microgrids," *IEEE Trans. on Smart Grid*, vol. 7, no. 3, pp. 1504-1515, 2016.

[3] X. Tang, W. Deng and Z. Qi, "Investigation of the dynamic stability of microgrid," *IEEE Trans. on Power Systems*, vol. 29, no. 2, 2014.

[4] A. Bengochea & O. Faet (2012) Renewable Energies and CO2 Emissions in the European Union,Energy Sources, Part B: Economics, Planning, and Policy, 7:2, 121-130, DOI: 10.1080/15567240902744635

[5] Chiu, Chien-Liang ; Chang, Ting-Huan, "Renewable Energy ; CO 2 Emissions ; Real GDP ; Energy Price ; Panel Threshold Regression Model," in *Renewable and Sustainable Energy Reviews,* Vol.13, no. 6, pp.1669-1674, 2009.

[6] M. A. Setiawan, A. Abu-Siada and F. Shahnia, "A New Technique for Simultaneous Load Current Sharing and Voltage Regulation in DC Microgrids," in *IEEE Transactions on Industrial Informatics*, vol. 14, no. 4, pp. 1403-1414, April 2018.

[7] C. Uhlmann, "South Australia's storm caused Transmission Faults, But That's Not The Whole Story," ABC NEWS, NSW. [Online]. http://www.abc.net.au/news/2016-10-19/wind-power-loss-key-event-in-sa-blackout-report-finds/7947478.

[8] X. Lu, M. Zhou, A. C. Ammari and J. Ji, "Hybrid Petri nets for modeling and analysis of microgrid systems," in *IEEE/CAA Journal of Automatica Sinica*, vol. 3, no. 4, pp. 349-356, Oct. 2016.

[9] J. A. P. Lopes, C. L. Moreira, and A. G.Madureira, "Defining control strategies for microgri ESS islanded operation," *IEEE Trans. Power Systems*, vol. 21, no. 2, pp. 916–924, 2006.

[10] S. Anand and B. G. Fernandes, "Reduced-order model and stability analysis of low-voltage DC microgrid," *IEEE Trans. on Industrial Electronics*, vol. 60, no. 11, pp. 5040-5049, 2013.

[11] X. Guo, Z. Lu, B. Wang, X. Sun, L. Wang and J. M. Guerrero, "Dynamic phasors-based modeling and stability analysis of droop-controlled inverters for microgrid applications," *IEEE Trans. on Smart Grid*, vol. 5, no. 6, pp. 2980-2987, 2014.

[12] A. Haddadi, B. Boulet, A. Yazdani and G. Joós, "A μ-based approach to small-signal stability analysis of an interconnected distributed energy resource unit and load," *IEEE Trans. on Power Delivery*, vol. 30, no. 4, pp. 1715-1726, 2015.

[13] R. Majumder, "Some Aspects of Stability in Microgrids," *IEEE Trans. on Power Systems*, vol. 28, no. 3, pp. 3243-3252, 2013.

[14] I. P. Nikolakakos, H. H. Zeineldin, M. S. El-Moursi and N. D. Hatziargyriou, “Stability evaluation of interconnected multi-inverter microgrids through critical clusters,” *IEEE Trans. on Power Systems*, vol. 31, no. 4, pp. 3060-3072, 2016.

[15] Z. Zhao, P. Yang, J. M. Guerrero, Z. Xu and T. C. Green, “Multiple-time-scales hierarchical frequency stability control strategy of medium-voltage isolated microgrid,” *IEEE Trans. on Power Electronics*, vol. 31, no. 8, pp. 5974-5991, 2016.

[16] Hongxia Wu, K. S. Tsakalis and G. T. Heydt, “Evaluation of time delay effects to wide-area power system stabilizer design,” *IEEE Trans. on Power Systems*, vol. 19, no. 4, pp. 1935-1941, 2004.

[17] C. M. Colson and M. H. Nehrir, “Comprehensive real-time microgrid power management and control with distributed agents,” *IEEE Trans.on Smart Grid*, vol. 4, no. 1, pp. 617-627, 2013.

[18] A. Solanki, A. Nasiri, V. Bhavaraju, Y. L. Familiant and Q. Fu, “A new framework for microgrid management: virtual droop control,” *IEEE Trans. on Smart Grid*, vol. 7, no. 2, pp. 554-566, 2016.

[19] H. Liang, B. J. Choi, W. Zhuang and X. Shen, "Stability enhancement of decentralized inverter control through wireless communications in microgrids,” *IEEE Trans. on Smart Grid*, vol. 4, no. 1, 2013.

[20] X. Pan, L. Zhang, J. Xiao, F. H. Choo, A. K. Rathore and P. Wang, "Design and implementation of a communication network and operating system for an adaptive integrated hybrid AC/DC microgrid module," in *CSEE Journal of Power and Energy Systems*, vol. 4, no. 1, pp. 19-28, March 2018.

[21] D. Kumar, F. Zare and A. Ghosh, "DC Microgrid Technology: System Architectures, AC Grid Interfaces, Grounding Schemes, Power Quality, Communication Networks, Applications, and Standardizations Aspects," in *IEEE Access*, vol. 5, pp. 12230-12256, 2017.

[22] G. Lou, W. Gu, Y. Xu, W. Jin and X. Du, "Stability Robustness for Secondary Voltage Control in Autonomous Microgrids With Consideration of Communication Delays," in *IEEE Transactions on Power Systems*, vol. 33, no. 4, pp. 4164-4178, July 2018.

[23] “Real-Time Power Management and Seamless Stability of Microgrid using Co-evolutionary Particle Swarm Optimization Supported by IEC 61850” Submitted to *IET Generation Transmission and Distribution*

[24] T. Murata, “Petri nets: Properties, analysis and applications,” in *Proceedings of the IEEE*, vol. 77, no. 4, pp. 541-580, April 1989.

[25] X. Lu, M. Zhou, A. C. Ammari and J. Ji, “Hybrid Petri nets for modeling and analysis of microgrid systems,” in *IEEE/CAA Journal of Automatica Sinica*, vol. 3, no. 4, pp. 349-356, Oct. 2016.

[26] Q. He, L. Wang and F. z. Huang, "Nonlinear constrained optimization by enhanced co-evolutionary PSO," *IEEE Congress on Evolutionary Computation*, Hong Kong, pp. 83-89, 2008.

3 CHAPTER THREE: The Impact of Time Delays on System Performance

As discussed in chapter two, chapter three aims to explore the problem that time delays can cause for a microgrid. This chapter also proposes a solution to the time delays caused by the usage of conventional time delays as well as the lack of proper interoperability between control elements in a system.

The results of this chapter have been published at an IEEE conference and presented in an article in Appendix B.

3.1 The Problem

The stability of a grid-connected microgrid is investigated from the early stages of the development of a power plant. For instance, in Australia prior to a power plant being signed off for development, the Australian Energy Market Operator (AEMO) reviews the stability of the plant by running different case studies on the plant model within the network. The model of the plant is issued with its Generator Performance Standard (GPS) that dictates the power quality criteria such as harmonic distortion, voltage unbalanced level and voltage flicker level [1].

Time delays can have a significant impact on the power system in several respects. This section of the thesis explores the impact of time delays on the *stability* and *power quality* of a selection of renewable microgrids because, in recent years, the power industry has spent significant amounts of money meeting the requirements for grids and microgrids from these two perspectives [2-4].

In addition, grid-connected microgrids must comply with the grid standards in the event of various disturbances caused by the grid or other power elements in the grid. These disturbances include voltage and frequency, which can be minor or major. Depending on the magnitude of the grid disturbance, the microgrids need to assist the grid for a certain period, and to achieve this the plant first needs to remain connected and second, during the fault, provide the agreed active and reactive power to the grid. For some levels of voltage and frequency fault, there are only 100 to 200 milliseconds

in which to respond. Therefore, the communication network must be designed to minimise time delays within the system otherwise a significant margin of response time is consumed on signal delivery, which could be used by the control system to provide a better response.

The author of this thesis also investigated the behaviour of a wind farm located in the neighbourhood of a hydro station. The simulation results discussed in the paper in Appendix B, have shown that the wind farm could potentially ride through the fault with the assistance of the hydro station. These simulations were run with the assumption that the hydro station control system could communicate with the wind farm POC otherwise the wind farm will trip. This is another case study that shows the criticality of having access to fast communication between the controllers of the plants.

3.1.1 Control Model for a Grid-connected Microgrid

This section reviews the impact of time delays on a grid-connected microgrid's stability using phase and gain margin, while also indicating the impact on the voltage and the current of the connection point before a fault, during a fault and after a fault.

In this model microgrid, all the power sources feed a DC bus, which is connected to a grid through a shunt voltage source inverter. As shown in figure 3.1, there is a series inverter connected to the DC bus and feeder of the POC to regulate the current of the feeder when needed. The feeder which connects the microgrid has R and L impedances indicated in figure 3.1. The local load in this case study is a critical load and needs to be protected against fault while it needs to remain supplied as much as is practical [4].

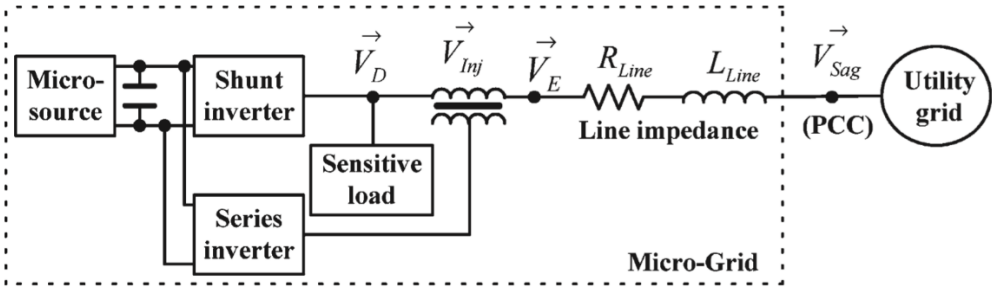

Figure 3.1 Single-phase representation of microgrid system under study with specific voltage phasors indicated [4,5]

Table 3.1 System Parameters

Parameters	Value
Nominal Line-Line Voltage	120kV
Frequency	50 Hz
DC Supply Voltage	250
Switching Frequency for both Inverters	10 kHz
Series Inverter Filter Capacitance	10 µF
Series Inverter Filter Inductance	3.9 mH
RL Feedforward Impedance{ R_{Inj}, L_{Inj}}	7.8 Ω, 26 mH
Flux-Charged Model Inductance {L_0}	38 mH
Shunt Inverter Filter Capacitance	30 µF
Shunt Inverter Filter Inductance	5 mH
Line Resistance R_{Line}	3Ω
Line Inductance L_{Line}	10 mH
Sensitive Load In Microgrid	120 W, 90 Var

3.1.1.1 Microgrid Operation During Voltage Drop at POC

During a voltage sag occurrence at the POC (shown as PCC), a large current will pass through the line impedance. This over current is generated by the voltage difference between the POC and point D. The overcurrent will continue until the fault clears or the protection relays trip the microgrid on the over current or low voltage. This microgrid has been modelled as a DC bus; however, it connects to the grid and its local load is via a DC-AC converter (inverter).

In this situation the formula below presents the voltage across point D and POC.

$$\Delta V = V_D - V_{PCC} \quad (1)$$

The authors of [5] propose two algorithms to be implemented in the series inverter. These algorithms are intended to protect the critical load that is local to the microgrid. These algorithms are feedforward current-limiting and flux-charges methods. Since the flux-charged control strategy appears to be advantaged base on the results of [4], this thesis only implements this method; however, both methods are briefly explained.

3.1.1.2 Feed forward current-limiting Algorithm

This method uses a series inverter to locate a virtual impedance and determine the voltage references which can avoid an over current at the sensitive load connection to the feeder. Figure 3.2 shows the control of the voltage proposed by this approach.

Once the voltage of the POC exceeds the normal limit, the current will exceed its limits determined by the system designer. The series inverter will apply voltage V_{inj} to raise the voltage of point E. The series inverter also adds a large impedance to assist in reducing the voltage of the POC and V_E. Consequently, the voltage reduction will reduce the overcurrent going to the sensitive load. Applying this voltage and impedance will also help the POC during recovery by avoiding any spike or overshoot.

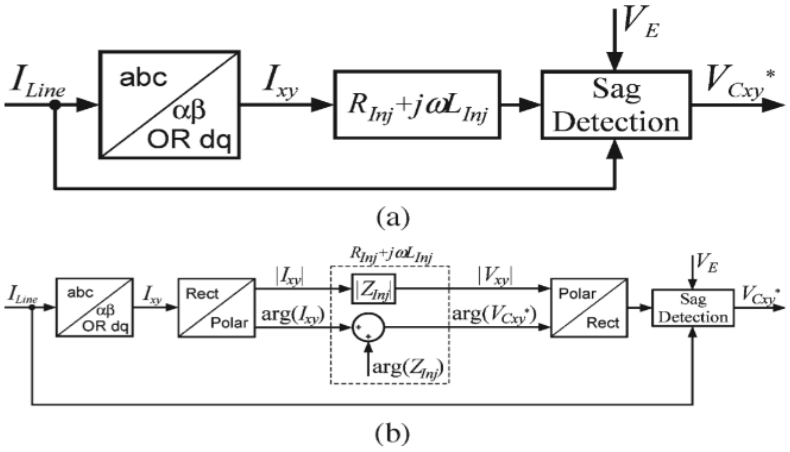

Figure 3.2 The RL feedforward current-limiting algorithm [4,5]: (a) control block diagram, (b) implementation.

This control approach has two disadvantages. First, it does not provide proper damping as it is a feedforward based control. To overcome this issue, the R value needs to be optimally calculated but, considering the limitation of the system, some undesired power circulation might appear in some fault scenarios.

In this control method as seen in figure 3.2, there is an S operant equivalent representing a derivative component for inductive current calculation, which can amplify the noise in the control. This also complicates the control system design.

The block diagram in figure 3.2 represents the RL feedforward control scheme, which explores how virtual impedance is inserted once the voltage sag is detected when $I_{Line} > I_T$. In this control scheme, the algorithm measures the current of the line and times it on the basis of $R_{Inj} + sL_{Inj}$ ("s" is Laplace Operator). Using this calculation, the suitable voltage injection has been calculated and selected as the reference of the voltage regulator, which generates the reference of the PWM for the series inverter. When the fault is cleared, terminal voltage, which is approximately equal to voltage sag at the time of the fault, is raised to normal voltage. RL control is inhibited in this post fault condition and the plant moves to its normal operation.

3.1.1.3 Flux-Charge-model Control Modes

To overcome the power circulation between the two inverters in the system, FCMC proposes a closed-loop algorithm which injects a virtual inductor in series with DF. This algorithm addresses the damping of the current-limiting method with no resistive component. FCMC uses the controller gains to achieve the proper damping of the controller. The FCMC algorithm develops its control model presented in [6,7]. In this method the flux is to be:

$$\varphi_{ref} = -L_0\, i_{line} \tag{2}$$

$$\varphi = \int V_c\, dt \tag{3}$$

where V_C and i_{Line} represent the filter-capacitor voltage and the inverter output current of series inverter, respectively.

The flux error is calculated from the difference between the flux variable and the setpoint. $k_{inv} = \frac{2}{V_{dc}}$ represents the PWM modulator and received the flux error. Figure

3.3 shows the final layout of the control method while figure 3.4 is the simplified version of the control algorithm.

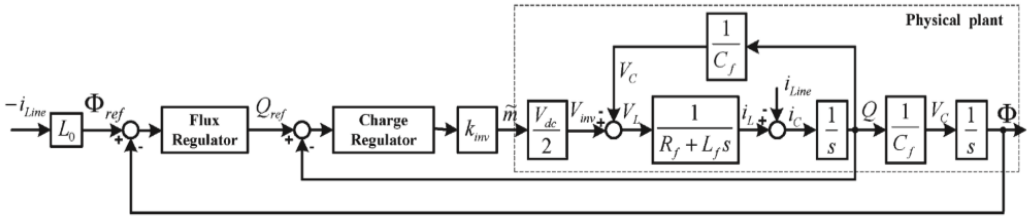

Figure 3.3 Control Block representation of flux-charge model algorithm [4,5].

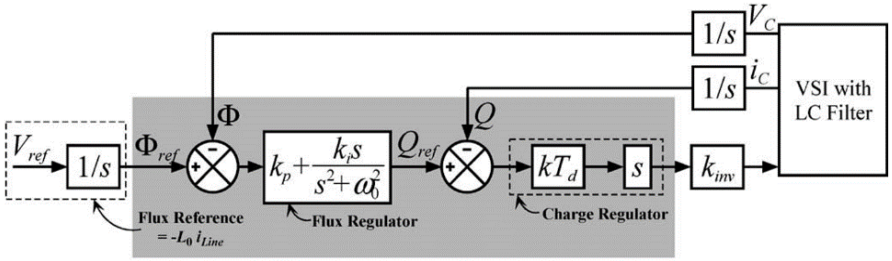

Figure 3.4 Modification of flux-charge-model control [4,5].

Figures 3.3 indicates the outer loop control for filter capacitance voltage and the inner control loop for filter capacitor current. In order to improve the tracking of the voltage in the outer loop, the resonant compensator has been added. This resonant compensator has been represented as $G_{Flux} = K_p + \frac{k_i S}{S^2+\omega_0^2}$ where k_p and k_i are the constant gains and ω_0 is the resonant frequency set at 50 Hz for this application. This compensator adds significant gain at the positive-sequence and negative-sequence input errors to zero. Unlike the outer loop, the inner loop control only utilises the proportional gain controller denoted as kT_d.This minimizes the impact on the accuracy of the setpoint tracking carried out by the outer loop controller. This controller uses the filter capacitor current as the feedback of the control loop.

The "s" and "1/s" operands can be added to the feedforward path of the control without compromising the voltage regulation performance. The integrator "1/s" can be shifted to the back shaded box shown in figure 3.4, where there is the control scheme of figure

3.3. In the modified block diagram as it is seen, the outer loop control is built using the P-resonant compensator and the inner loop control using the derivative controller. The derivative controller can be modelled as $kT_d s \approx {kT_d s}/{(1 + {T_d s}/{N})}$. This change has been proposed to add a pole to limit the regulator gain to Nk, at high frequency to prevent noise amplification [4].

To observe the impact of time delays in this considered system, a time delay is added in the voltage measurement path, which is shown in figure 3.5. The rest of the control components will remain as they are in figure 3.5 to provide the pure effect of this time delay in the feedback loop.

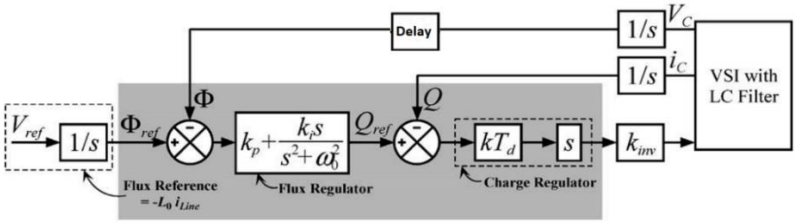

Figure 3.5 Flux-charge model control with time delay [4,5]

3.1.2 Simulation and Results in Relation to the Effect of Time Delays

The model proposed in figure 3.1 with the embedded time delay has been developed in the MATLAB Simulink environment and the results of the model's behaviour are compared for different time delays. The operation of the plant is compared in terms of voltage and current stability.

In relation to stability, section 2.3.1 explores the output voltage and current of the microgrid while comparing the stability margins of the system using bode plot.

Three cases are presented in section 2.3.1 and 2.3.2 to demonstrate the impact of time delays on the stability margins including phase margin and gain margin. The current and voltage of a sensitive load in each case study are illustrated for a 50% voltage drop at the POC as the worst-case scenario. The time delays are considered as 1 µs, 1 ms and 5 ms in the event of grid voltage disturbance. The 50% voltage drop is used as it is the worst-case scenario that AEMO considers in the grid connection assessment in an Australian renewable grid connected plant. The voltage control strategy is aimed to

ride through the fault to avoid the current of a sensitive load exceeding 10 Amps for longer than 200 milliseconds.

3.1.2.1.1 Case A

This case considers an arbitrary time delay of 1 μs; however, it is understood that 1 μs is not practical and hard to achieve in the real network. This delay has been indicated in figure 3.5 in the feedback loop of V-Φ control. As seen in figure 3.6, voltage and current are responded to post fault with a smaller spike compared to the other cases with larger time delays. The steady-state response of the microgrid is also greatly controlled with good rise and settling times. The overshoot in this case is generating a current of less than 8 amperes, which is less than other cases, which will be seen in case B and case C. Figure 3.7 also indicates the bode plot of the microgrid with the time delay of 1 μs.

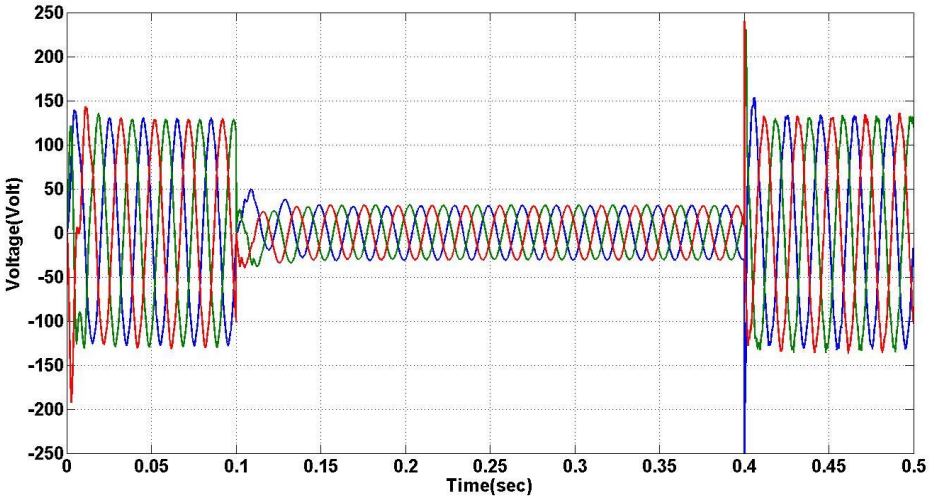

(a)

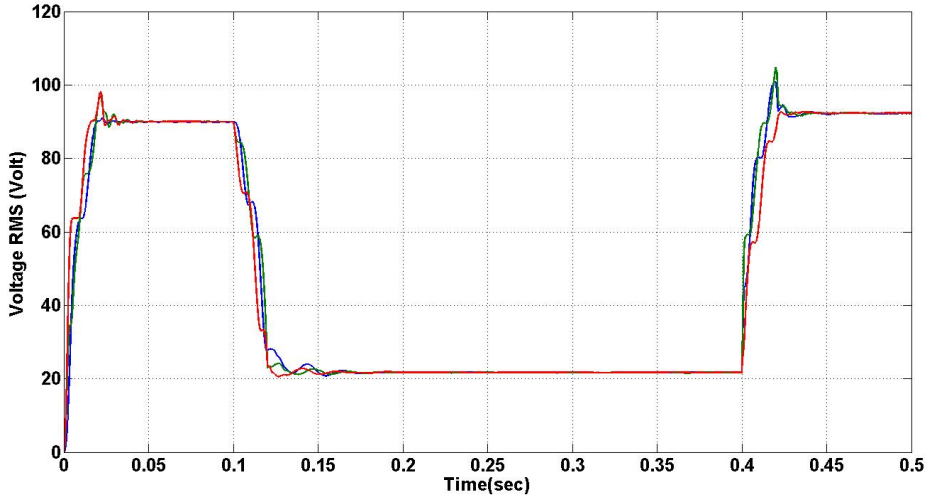
Voltage RMS (Volt)
Time(sec)
0
20
40
60
80
100
120
0
0.05
0.1
0.15
0.2
0.25
0.3
0.35
0.4
0.45
0.5

(b)

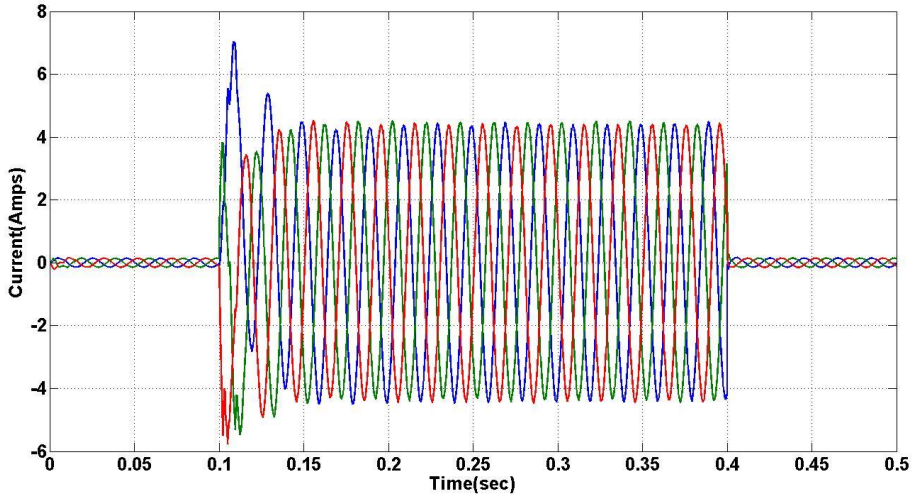
Current(Amps)
Time(sec)
-6
-4
-2
0
2
4
6
8
0
0.05
0.1
0.15
0.2
0.25
0.3
0.35
0.4
0.45
0.5

(c)

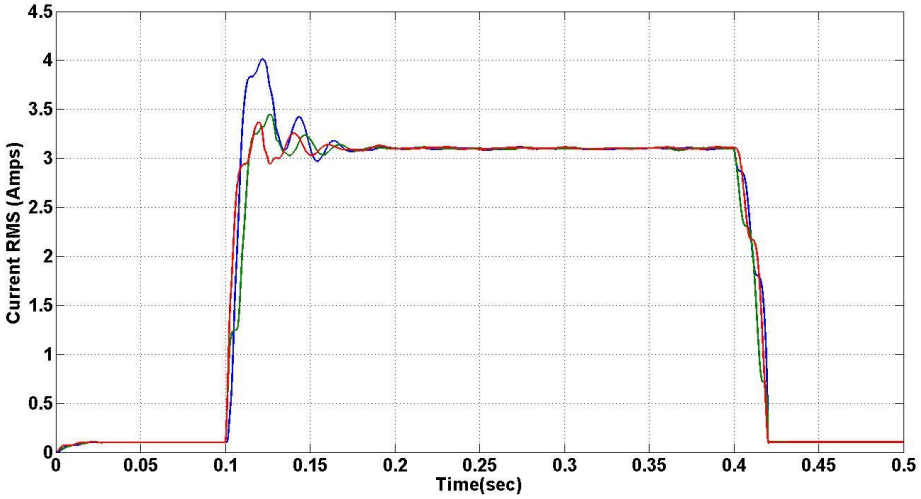

(d)

Figure 3.6 (a) Critical load voltage, (b) Critical load RMS voltage, (c) Critical load current, (d) Critical load RMS current for time delay = 1 μs [5]

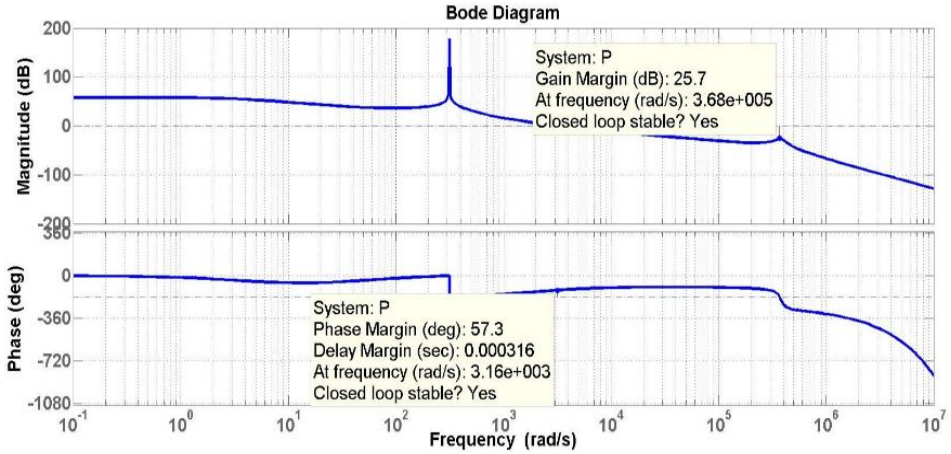

Figure 3.7 Bode Plot of the Open Loop Control System of Microgrid Transfer Function with a time delay of 1 μs [5]

3.1.2.1.2 Case B

Case B refers to a time delay of 1 millisecond. This delay has been indicated in figure 3.5 in the feedback loop of V-Φ control. As seen, a 1 second time delay has generated a spike in current up to 8 amperes, which still is within the limits of the system. The steady state of the microgrid in this case study is acceptable. Figures 3.8 (b) and 3.8

(d) also show the voltage RMS and current RMS of the instantaneous voltage and current illustrated in figure 3.8 (a) and 3.8 (c).

Figure 3.8 shows the voltage and current of the sensitive load pre, during and post fault, while figure 3.9 shows the bode plot of the system with updated phase and gain margins for the transfer function of the system with respect to the voltage at POC. It should be noted that the bode plot is the bode plot of the open loop system transfer function, which has been selected to observe the direct impact of the time delay only in the feedforward path of the considered system.

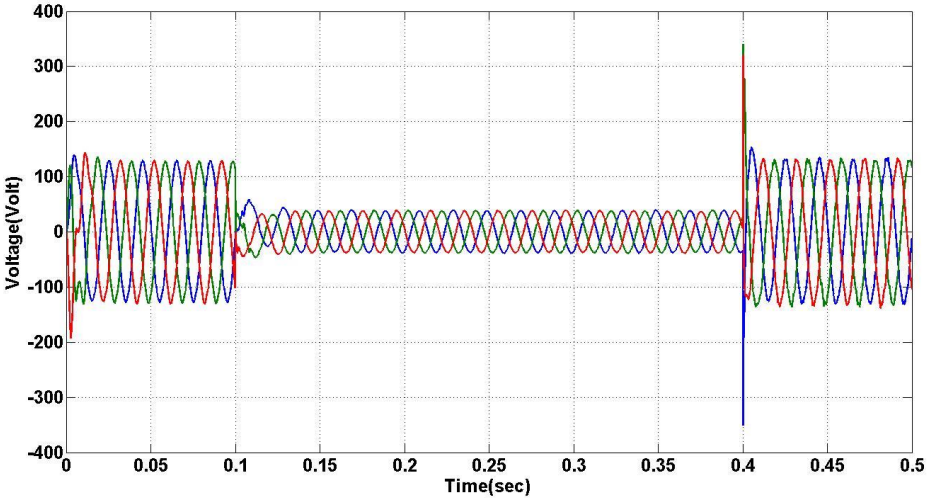

(a)

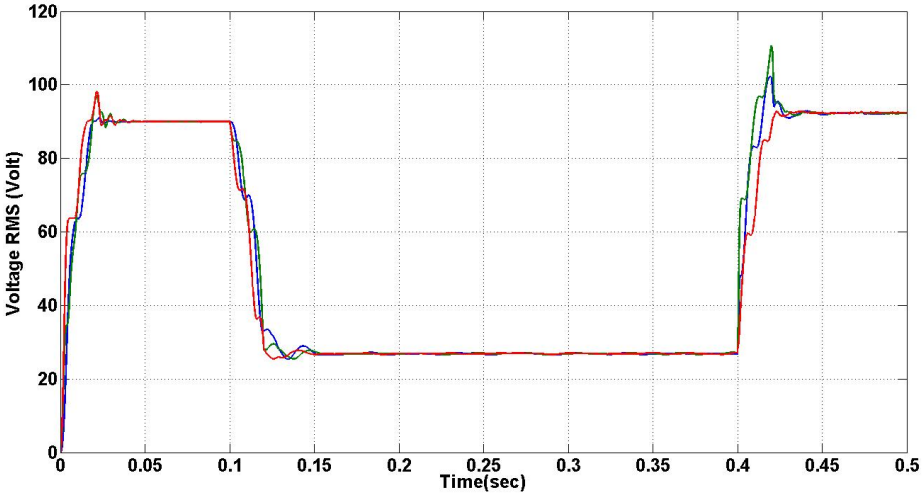

(b)

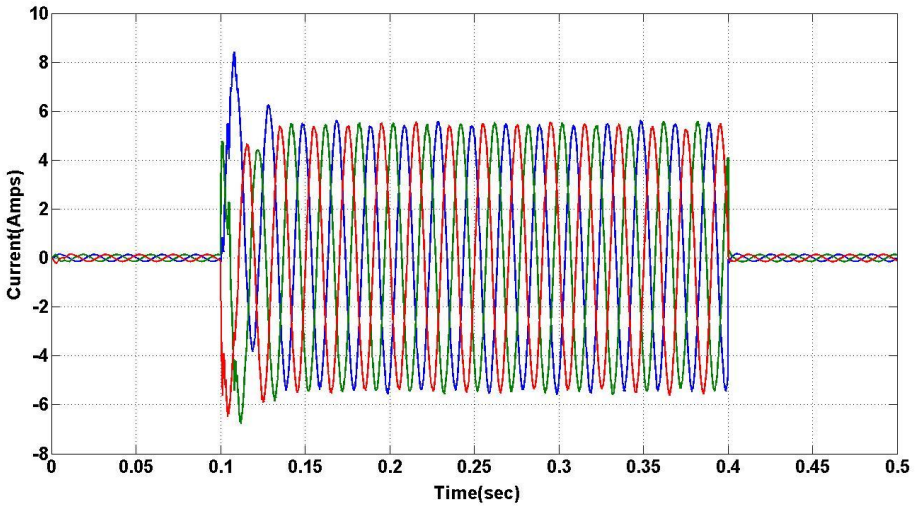

(c)

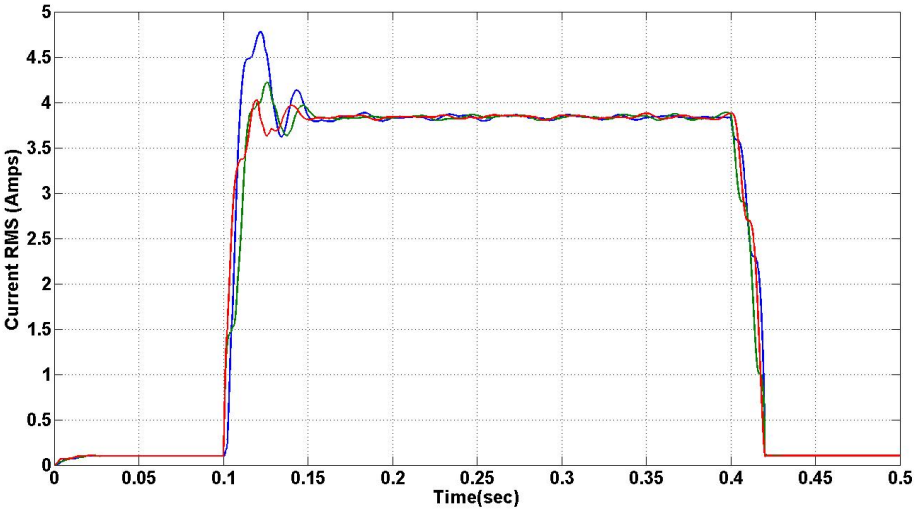

(d)

Figure 3.8 (a) Critical load voltage, (b) Critical load RMS voltage, (c) Critical load current, (d) Critical load RMS current for time delay = 1 ms

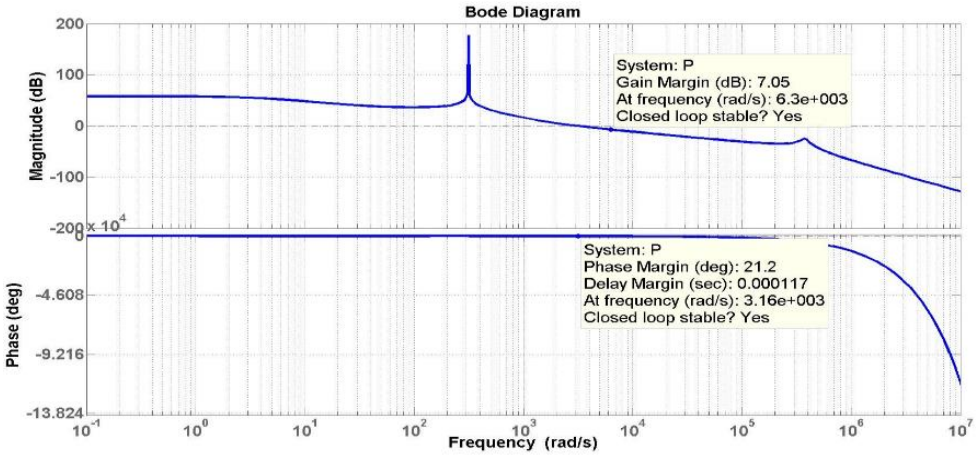

Figure 3.9 Bode Plot of the Open Loop Control System of Microgrid Transfer Function with time delay = 1 ms [5]

3.1.2.1.3 Case C

The time delay of the feedback loop of V-Φ increased to 5 milliseconds for case C. The results show a major change in the voltage and current post fault. This time delay also makes the stability margin smaller relative to two other cases. Figure 3.10 and 3.11 show the voltage and the current sensitive load and bode plot of the system respectively. It is understood that in the practical case, the system designer fixes the oscillations using other tools. These tools sometime can be inexpensive but complex, such as retuning the controllers which can be limited, or can be expensive, such as additional hardware including stabilisers, STATCOMs etc.

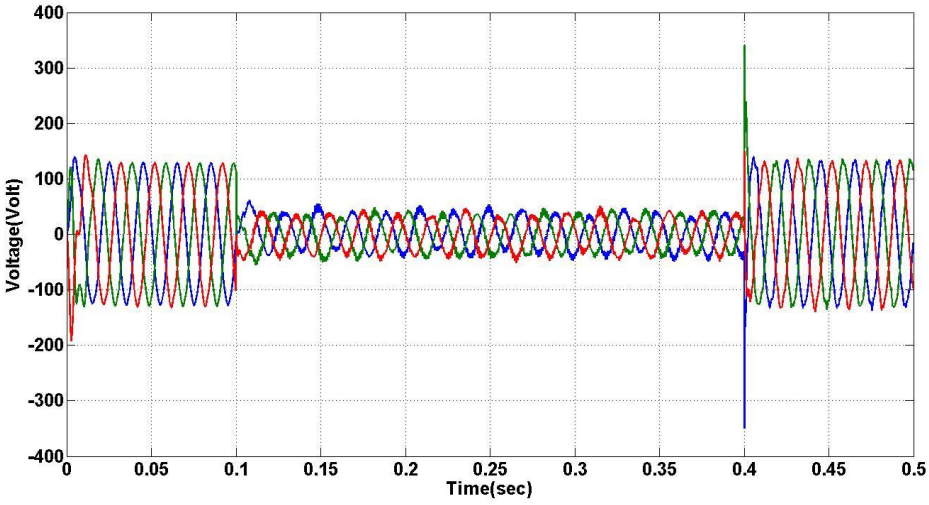

(a)

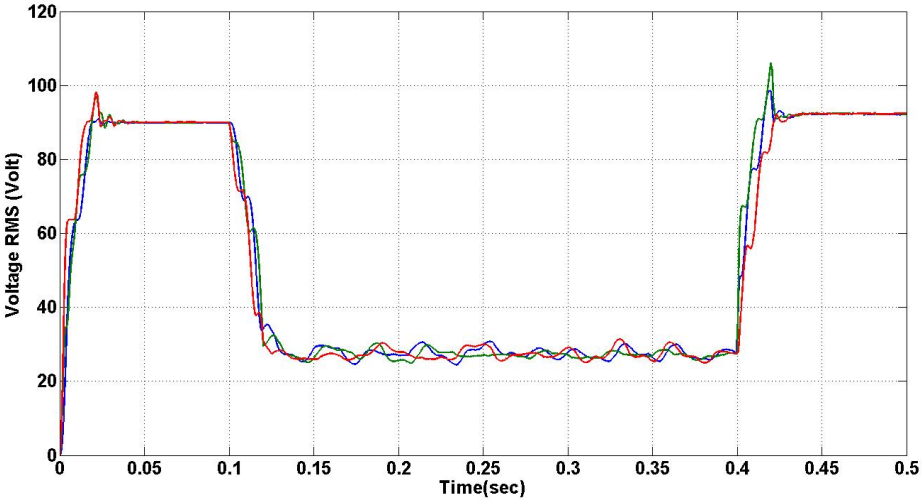
Voltage RMS (Volt)
Time(sec)
0
20
40
60
80
100
120
0.05
0.1
0.15
0.2
0.25
0.3
0.35
0.4
0.45
0.5

(b)

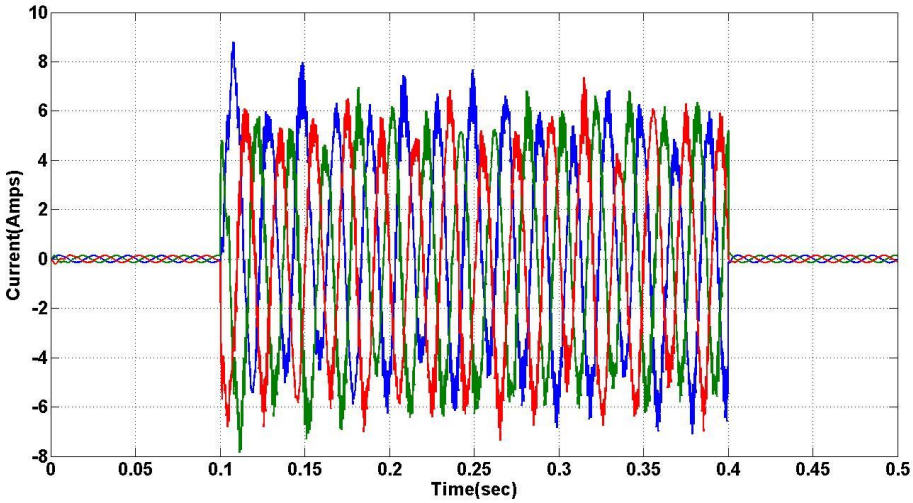
Current(Amps)
Time(sec)
10
8
6
4
2
0
-2
-4
-6
-8
0.05
0.1
0.15
0.2
0.25
0.3
0.35
0.4
0.45
0.5

(c)

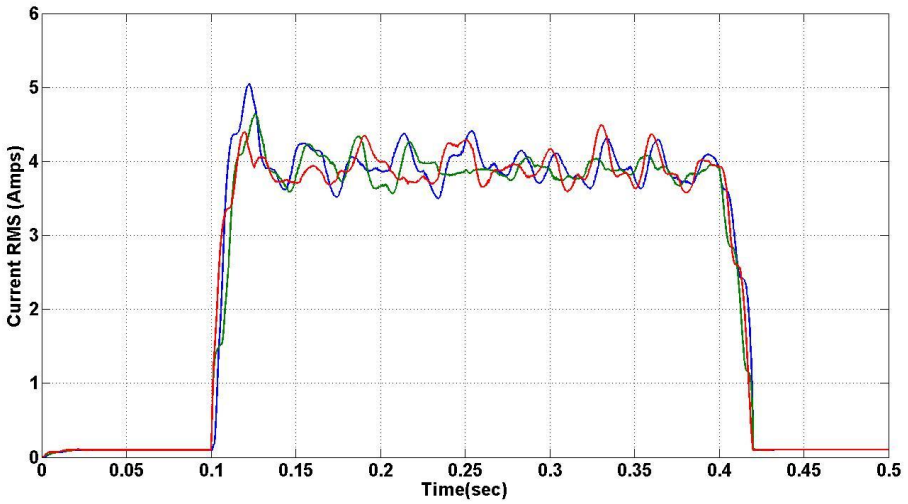

(d)

Figure 3.10 (a) Critical load voltage, (b) Critical load RMS voltage, (c) Critical load current, (d) Critical load RMS current for time delay = 5 ms [5]

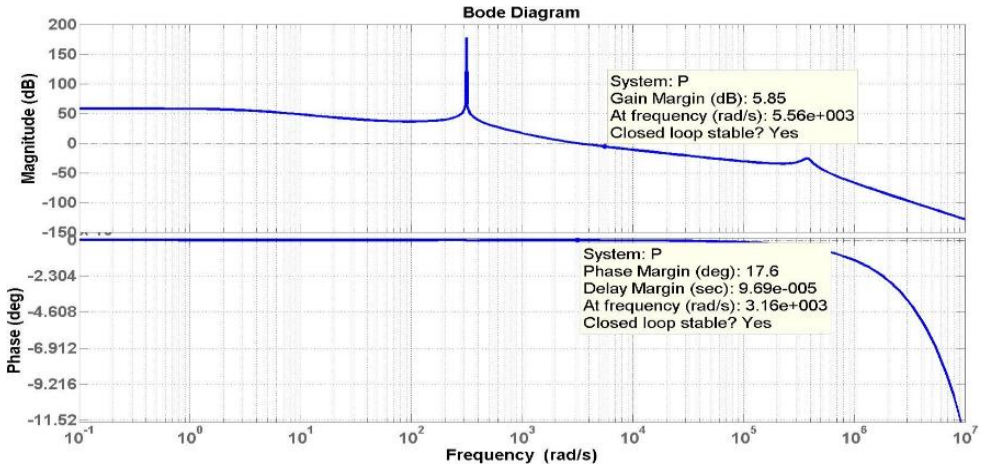

Figure 3.11 Bode Plot of the Open Loop Control System of Microgrid Transfer Function with time delay = 5 ms [5]

It should be noted that the bode plot is the bode plot of the open loop system, which has been selected to observe the direct impact of the time delay only in the feedforward path of the considered system.

3.2 Proposed Communication Platform Solution

3.2.1 Introduction of IEC 61850

As discussed in section 2 of this thesis, the time delay has a significant impact on the performance and stability of the power system. Therefore, this section focuses on the proposed solution to reduce the time delay as much as is practical.

The International Electrotechnical Commission (IEC) has published the IEC 61850 standard for substation automation [8]. This standard includes all the features of the communication structures of the substation automation devices and how they integrate. These devices include substation protection relays, measurement units, circuit breakers, IEDs and transformers. This standard brings the interoperability capability into the communication platform of the microgrid such that all microgrid components can simply communicate with the equipment from different manufacturers without using media converters. The main elements of this standard are intelligent electronic devices (IEDs).

Committee 57 of the IEC published the IEC 61850-7, which provides more detail of the standards in relation to the power system and all other related communication parts, including but not limited to logical nodes (LN), data transferred method and the data classes supported by this standard. In this chapter of the thesis, a new application of this standard and a new data class model is proposed to be included into the standard in order to be utilised in all measurement and control elements in renewable power systems.

IEDs which play key roles in substation automations from the protection perspective handle most of the duties of the IEC 61850 standard. These are Logical Nodes (LN) which are in fact physical components in the substation such as circuit breakers. LDs have their own specific naming conventions in IEC 61850. For instance, circuit breakers in the IEC 61850 are noted as XCBR. This naming convention is used to bring simplicity in developing the configuration files developed in the IEDs. Followed by LNs, the configuration of an IED has data and data-attributes which are assigned to each LN. For example, in the circuit breaker (CB) example mentioned above, the data of the XCBR can be the position that the CB holds.

Similarly, this data can refer to a different data-attribute at a lower level, such as current position known as stVal or if the CB has a current transformer (CT) in the same feeder

the value of the current can be another data-attribute which is coded as ctVal. Figure 3.12 indicates an example of CB control and protection on a single device [5].

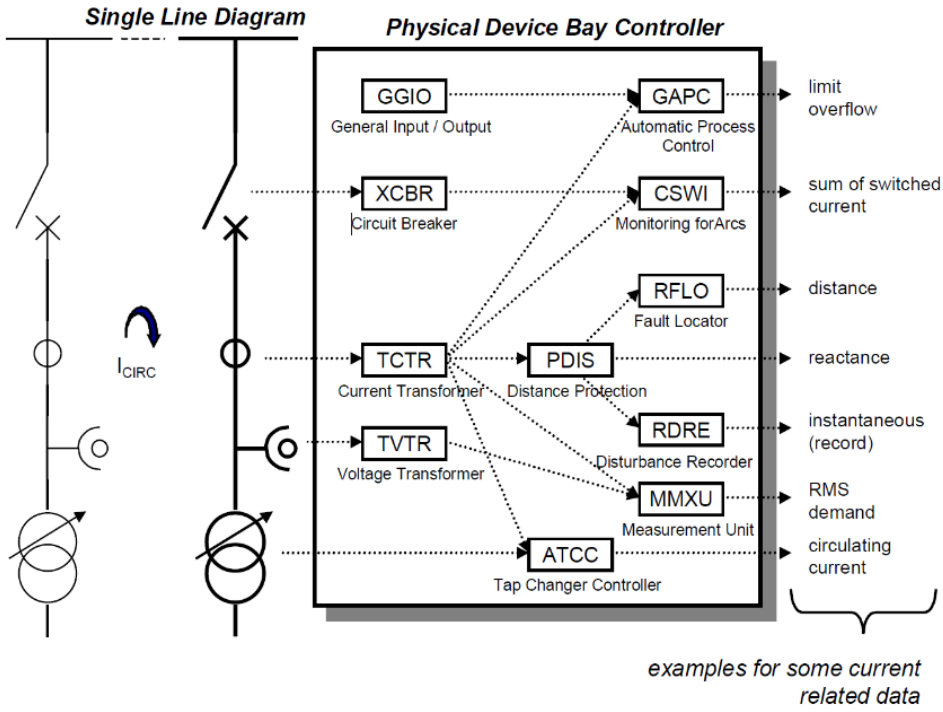

Figure 3.12 Control and protection LNs combined in one physical device [5,8]

In a later section of this thesis, a new data class model of the IEC 61850 is presented to be added to the IEC standard purely for renewable centralised and decentralised control. The data class model and data attributes are selected based on a review of multiple renewable plants such as wind farms, solar farms, wind-solar farms and small microgrids. The proposed data classes are based on Sampled Value (SV) and Generic Object-Oriented Substation Event (GOOSE) message; however, these are proposed to be customised for renewable utility size microgrids.

3.2.2 Proposed New Data Class Model

In this section GOOSE and SV data are discussed to provide basic knowledge of the proposed IEC 61850 new data class model.

3.2.2.1 GOOSE

GOOSE messaging as one of the most commonly used data models of the IEC 61850 platform. This platform is a publisher-subscriber based fast communication which transfers data from one IED to another. GOOSE is an event-based communication which can have various speeds of packet delivery. For instance, when a predefined event occurs, GOOSE messages start being published and transferred every 3ms and sometimes before another event takes place the data transfer speed changes to a 250 ms sample rate. Both the 3 millisecond and 250 millisecond rates are arbitrary up to a certain level and can vary according to the design engineer based on the detailed design of the system. It is worth noting that the GOOSE message keeps transferring the same value as triggered the event and it does not update the value unless a second event is triggered.

The new scheme utilises the existing elements of the existing typical IEC 61850 platform and in addition an IED is added to the renewable inverters; however, the main idea of this part of the thesis is to add the feature of IEDs in the inverter controllers so that inverters will be independent of an additional IED. Therefore, inverters from any manufacturer will be directly communicating to measurement devices such as meters or IEDs.

Figure 3.13 shows the overall layout of the conceptual scheme of the peer-to-peer data publish pathway in the proposed scheme. While on the other peer of this communication an inverter shall be equipped with the same communication infrastructure to be able to receive such multicast packets. Therefore, a new class of data model, logical device, logical nodes, data and data attributes shall be created to complete the communication loop for the purpose of power system control for renewable plants and, for the purpose of this thesis, renewable microgrids.

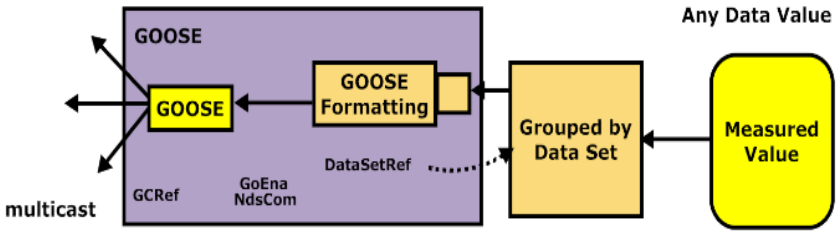

Figure 3.13 Peer-to-peer data value publishing model (conceptual) [8]

A summarised version of proposed data for microgrid control has been indicated in figure 3.14 to indicate the overall structure of the proposed data class in the scheme. The proposed data are comprehensively presented in Appendix A. This brief version of the proposed data class is used for the instance that will be discussed in Chapter four of this thesis, which is an inverter-based microgrid equipped with three inverters. Only one inverter has been illustrated in this example.

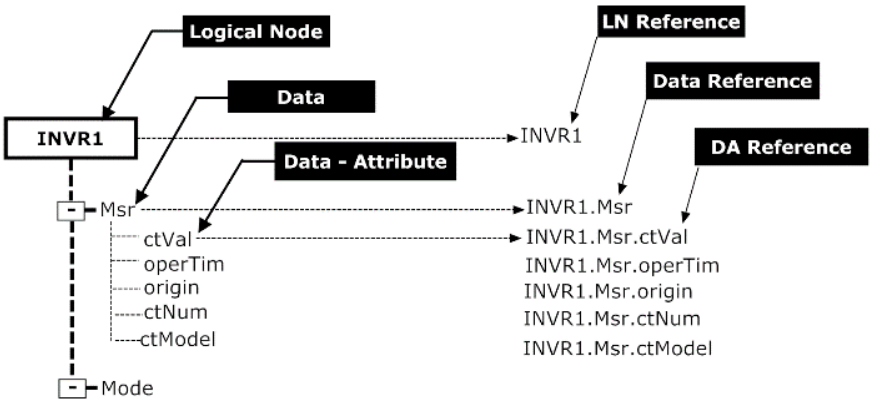

Figure 3.14 MG inverter and controller information proposed structure

The illustrated structure in the tree in figure 3.14 refers to the instance of current value measured by a CT shown in figure 3.14.

3.2.2.2 Sampled Value

Sampled values are the other type of data that provide fast communication between the components of the IEC 61850. The major difference between SVs and GOOSE message are in their sampling rates scheme.

As noted above, the transfer speed of GOOSE message data varies after the event occurs, and if no other event takes place, a GOOSE message moves towards the maximum that has been configured by the system designer. As mentioned in section

3.2.1, a GOOSE message is a data exchange that is repeated once the event has been triggered. This is while SVs can be updating the measured value on a fixed sampling rate independent of any event determination. Therefore, for the measurement application when the traffic of the network is not a major concern, the SV is preferred to the GOOSE based data model.

3.2.2.3 Proposed platform on OSI

The proposed data type as a new data class model for the IEC 61850 is proposed according to figure 3.14. Similar to the Sample Value and GOOSE data types, the proposed data type is proposed to bypass all OSI stack layers and embark on ethernet. Figure 3.15 shows the stack layer proposed for the new data type.

It is worth noting that for all the IEC 61850 simulation and field tests, the author did not have the facility to develop the new data class and had to use existing GOOSE and SV to prove the speed and improvement.

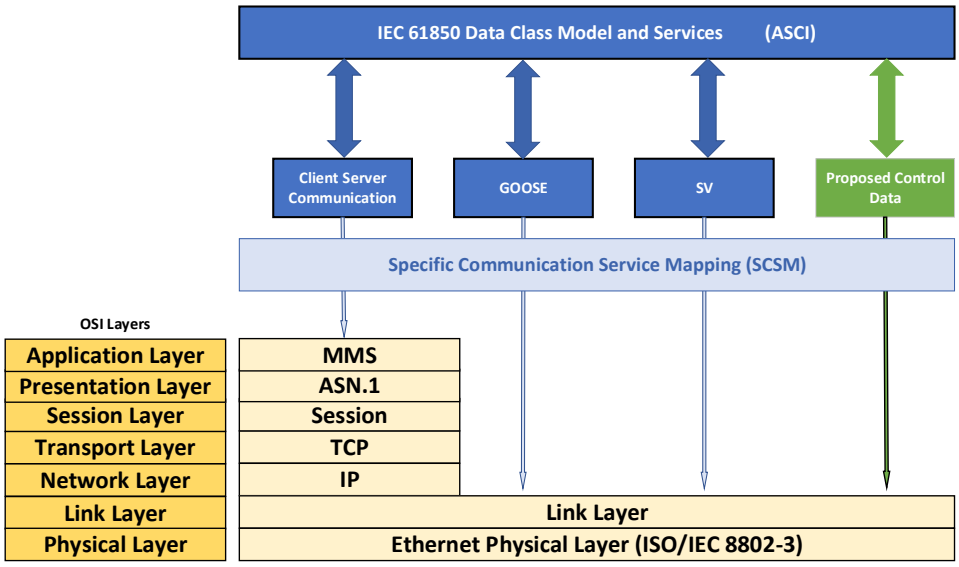

Figure 3.15 GOOSE, SV, Proposed Data class and Client Server Communication on OSI layer

GOOSE, which normally carries protection data, such as blocking and tripping signals, needs to be fast and reliable. Therefore, this is a time critical data class. Sample value and the new data class model proposed in the thesis are required to be accurately synchronised. So, the sampling data which feeds these two data types, must be

precisely synchronised with the highest demand of 1 μs. In case that sampling is not synchronised, the samples have to be tagged with a time of the same accuracy for the purpose of comparing the sinusoidal wave. This might also be needed for phasor calculation.

Therefore, GOOSE, SV and the proposed renewable data class model need to bypass the five top layers of OSI to be transferred very fast from one device to another. The proposed data are based on IEEE 802.3 supporting VLAN, which has tag prioritizing to be sent on the Ethernet. A virtual server client setup is developed as a case study in Chapter four of the thesis, which shows what communication time delay is possible to achieve using the new data class model. In this setup SV and GOOSE is customised to be used as a conceptual model of the proposed data.

Appendix A shows all the data and formatting of the proposed data base, which is proposed for a renewable generating unit within a microgrid.

3.2.3 IEC 61850 Versus Industrial Communication Protocols

This chapter presents a comparison of the IEC 61850 and the most commonly used protocols such as Modbus, DNP3 and IEC 60870-104. These protocols are common in power and utility industries for SCADA and control data transmission depending on the application. All the communication protocols discussed in this section, including DNP3, IEC 870, Modbus and Profibus, can to some extent be used in utility and power control applications. However, time delays caused by them and their guaranteed performances differ.

As discussed in a previous section of this chapter, improving the time delay in sampling section, setpoint delivery and feedback command can largely improve important features of the control system. Table 3.2 shows a quick comparison between the most commonly used protocols.

As it is seen, IEC 61850 can deliver a large amount of data with a short time delay through some of its data class models such as GOOSE, SV and MMS. In fact, IEC 61850 is the only protocol that has guaranteed performance for such short time delivery and others can only transmit the data delivery at their maximum speed, which is lower than the IEC 61850's fastest capability depending on some factors such as CPU scan capability, network architecture and data types.

Table 3.2 Protocol Comparison [9-12]

Protocol	Standardisation	Adjustable Frequency	Fast Guaranteed Data Delivery (less than 5 ms)	Is there a cost for protocol conversion to other vendors
DNP3	Open industry standard (1993)- DNP user‘s group	Yes	No	Yes
IEC 870	IEC Standard (1995)- IEC TC 57 WG 03	No	No	Yes
Modbus	Modicon Inc	Yes	No	Yes
Profibus	BMBF(German department of education &research1989)		No	Yes
IEC 61850	Currently all the vendors which support IEC 61850	Yes	Yes	No

There have also been studies that show that the IEC 61850 can even provide raw data measurement such as on current and voltage in less than 1 millisecond [12].

Reference [13] also runs several cases using IEC 61850 GOOSE messaging; however, only for protection purposes – but it proves that this protocol is minimally impacted by heavy background traffic in the network, which is something all the other network protocols suffer from. This study provides real-time measured data for background traffic from 5% to 85% within the network.

Communication protocols by nature reduce the cost of installation compare to hardwire cabling. One of the advantages of the IEC 61850 in respect to protection, which is outside the scope of this thesis, was the major reduction of cabling, engineering hours and installation. Therefore, in most power plants, IEDs already exist in the substations performing substation bays and transformer protection. However, this proposed

method requires an additional cost when adding the IEC 61850 in the inverters to be able to directly communicate to other IEDs and control elements. This cost is a one-off cost, and once the driver is developed by all inverter manufacturers, there is no additional cost for the usage of the IEC 61850 base communication.

A fast communication protocol can reduce the other costs associated with unnecessary tripping due to slow responses from power plants and load controls, media converters (hardware, software and installation) used between various vendors and related engineering costs.

In addition to the abovementioned literature, reference [14] provides the benefits of using GOOSE messaging for inter substation communication and proves the stability improvement via fault clearance. This research also indicates that improving time delays in the system can fix power quality issues to some extent.

3.2.4 Conclusion

3.2.4.1 Power System Improvement Using a Fast Communication Platform in the Control System

The simulation results indicate substantial impact on the stability margins including phase and gain margins. Figure 3.9 shows that to change the time delay from 1μs to 1ms the gain margin reduces by 72% and phase margin by 63%. Similarly, if the time delay increases to 5ms, the system will be operating within smaller stability margins by another 18% in gain margin and 12% in phase margin.

The impact of time delay has also been illustrated in the voltage and current of the sensitive load for three different time delays in the feedback path of the voltage. The results show a noticeable change in the voltage and current by increasing the time delay from 1 μs to 1ms and the more significant change of from 1ms to 5ms.

The waveform of voltage and current also represent more significant THD for the system with a larger time delay.

3.2.4.2 Communication Advantages of Using the Proposed Platform

When using the proposed data class, any renewable control and measurement device from any manufacturer can be interoperable and communicating with others. This significantly reduces time delays.

This will also eliminate all the media conversion required between conventional protocols which reduces the complexity of the system engineering.

The proposed data can provide the time delay value as part of the data packet, which can adaptively update the modelled time delay. This can facilitate the model to be able to update all other control parameters accordingly. This is currently not provided with any of the conventional communication protocols used in control systems and only protocols used for protection can access this information.

3.3 References

[1] Australian Energy Market Operator (2016 Sep). Generator Performance Standard. Available at https://www.aemo.com.au/-/media/Files/Doc/0110-0163.

[2] M. S. Manikandan, S. R. Samantaray and I. Kamwa, "Detection and Classification of Power Quality Disturbances Using Sparse Signal Decomposition on Hybrid Dictionaries," in *IEEE Transactions on Instrumentation and Measurement*, vol. 64, no. 1, pp. 27-38, Jan. 2015.

[3] M. Kallamadi and V. Sarkar, "Enhanced real-time power balancing of an AC microgrid through transiently coupled droop control," in *IET Generation, Transmission & Distribution*, vol. 11, no. 8, pp. 1933-1942, 2017.

[4] Y. W. Li, D. M. Vilathgamuwa, and P. C. Loh, "Design, analysis and realtime testing of controllers for multi-bus micro-grid system," *IEEE Trans. Power Electron.*, vol. 19, no. 5, pp. 1195–1204, Sep. 2004.

[5] N. Aghanoori, M. A. S. Masoum, S. Islam and S. Nethery, "Investigation of microgrid instability caused by time delay," *2017 10th International Conference on Electrical and Electronics Engineering (ELECO)*, Bursa, 2017, pp. 105-110.

[6] H. Funato, K. Kamiyama, and A. Kawamura, "Transient performance of power circuit including virtual inductance realized by fully digital controlled variable active–passive reactance (VAPAR)," in *Proc. IEEE PESC*, pp. 1195–1200.

[7] H. Funato, T. Ishikawa, and K. Kamiyama, "Transient response of three phase variable inductance realized by variable active–passive reactance (VAPAR)," in Proc. *IEEE APEC*, pp. 1281–1286, 2001.

[8] IEC for basic communication structure for substation and feeder equipment Principles and models, IEC 61850-7-1, 2003.

[9] Comparison of protocols used in remote monitoring: DNP 3.0, IEC 870-5-101 & Modbus Jay Makhija (03307905), Supervisor: Prof. L.R.Subramanyan

[10] A.Ortega, Ailton A. Shinoda, Christiane M. Schweitzer, Fabrizio Granelli, Aleciana V. Ortega, and Fabiola Bonvecchio "Performance Evaluation of the DNP3 Protocol for Smart Grid Applications over IEEE 802.3/802.11 Networks and Heterogeneous Traffic" ResearchGate 2015

[11] A. Bonetti and R. Douib, "Transfer time measurement for protection relay applications with the IEC 61850 standard," *2010 IEEE International Symposium on Electrical Insulation*, San Diego, CA, 2010, pp. 1-5.

[12] N. Das, W. Ma and S. Islam, "Comparison study of various factors affecting end-to-end delay in IEC 61850 substation communications using OPNET," *2012 22nd Australasian Universities Power Engineering Conference (AUPEC)*, Bali, 2012, pp. 1-5

[13] M. Hosny Tawfeek Essa and P. Crossley, "GOOSE performance assessment on an IEC 61850 redundant network," in *The Journal of Engineering*, vol. 2018, no. 15, pp. 841-845, 10 2018. doi: 10.1049/joe.2018.0208

[14] M. A. Aftab, S. Roostaee, S. M. Suhail Hussain, I. Ali, M. S. Thomas and S. Mehfuz, "Performance evaluation of IEC 61850 GOOSE-based inter-substation communication for accelerated distance protection scheme," in *IET Generation, Transmission & Distribution*, vol. 12, no. 18, pp. 4089-4098, 16 10 2018.

4 CHAPTER FOUR: Power Management Implementation

This chapter applies the solutions presented in chapters two and three for a microgrid with three sources of power and implements the real-time power management for this microgrid based on the adaptive Petri PSO equipped with IEC 61850 communication platform. This chapter also explores how in a cascaded manner, communication time delay impacts MG system stability and MG system stability impacts optimal power management.

4.1 Three-Source Standalone Microgrid

The microgrid model considered here has been previously presented in references [1-2] and in this chapter, this microgrid is enhanced using the proposed method. Figure 4.1 shows the overall layout of this microgrid [1]. In [1–2], as previously mentioned in Chapter 2, there was no power-sharing reference update; however, in the practical application, the power reference can change continuously. Therefore, the Petri PSO proposed by this thesis monitors the references at all time and in the event of any change, the new set of power references are transmitted to the inverters using the proposed renewable IEC 61850 data class. The control in this case study is a centralised control and the power sources are a solar farm, fuel cell generator and micro-generator. However, the real-time management is proposed in such a way that it can be applied to any microgrid by adjusting the dynamic model of the power system. The dynamic of the system has been considered using small signal in state space format. The dynamic of the microgrid is expressed in equations 1–34. Therefore, this chapter models the microgrid with n DG units, H number of loads, L number of feeders and a single centralised control platform which communicates to the individual inverters. The DGs are connected to the loads through feeders. The power management must be monitoring load demand and providing proper power references to the inverters.

The power system equations are all formatted in state-space based on the modular structure of the microgrid. The loads in this example have been noted as local loads, while in grid-connected microgrids they can be the total demand from the utility grid [1].

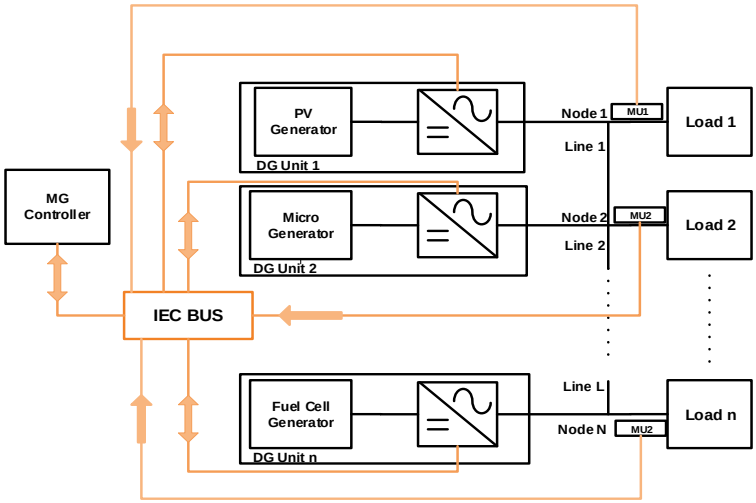

Figure 4.1 The isolated MG under consideration with the addition of IEC 61850 GOOSE Messaging (similar to the MG in [1] with PV, micro-turbine and fuel cell generators)

4.2 State Space Modelling of the MG

4.2.1 Microgrid Control Layout

The power sharing strategy presented in reference [1] was the base of the discussed MG control mode. In this thesis, decentralised control is replaced by centralised real-time power management using an adaptive Petri PSO, as centralised controls appear to be more practical in the renewable microgrid industry. Therefore, centralised power management can seamlessly monitor the operational conditions and update the optimisation algorithm. This thesis considers the stability of the microgrid as a part of the dispatch signal calculation based on the small-signal model, which is one of its main contributions. The stability is assessed on a continuous basis using eigenvalue analysis.

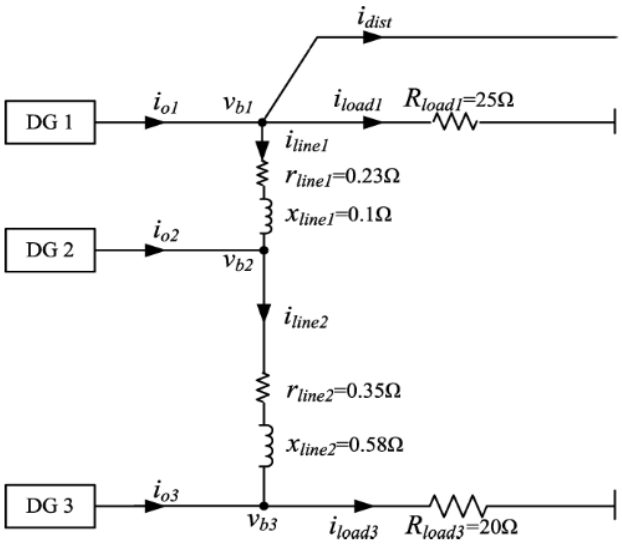

Figure 4.2 Considered Microgrid Single Line Diagram

The single line diagram of the specific microgrid has been shown in figure 4.2 to illustrate the electrical details of the system. The system parameters and the initial values of the modelling are shown in table 4.1 and 4.2 respectively.

Table 4.1 Inverter Detailed Parameters

Inverter Rating (10 kVA)	
Parameters	**Value**
f_s	8 kHz
L_f	1.35 mH
C_s	50 µF
r_f	0.1 Ω
L_c	0.35 mH
r_{LC}	0.03Ω
ω_s	31.41
m_p	9.4e-5
n_q	1.3e-3
K_{pv}	390
K_{iv}	10.5
K_{ic}	16e3
F	0.75

Table 4.2 Initial Modelling Values

Parameters	Value
V_{od}	[380.8 381.8 380.4]
V_{oq}	[0 0 0]
I_{od}	[11.4 11.4 11.4]
I_{oq}	[0.4 -1.45 1.25]
I_{ld}	[11.4 11.4 11.4]
I_{lq}	[-5.5 -7.3 -4.6]
V_{bd}	[379.5 380.5 379]
V_{bq}	[-6 -6 -5]
ω_0	[314]
δ_0	[0 1.9e-3 -0.0113]
I_{line1d}	[-3.8]
I_{line1q}	[0.4]
I_{line2d}	[7.6]
I_{line2d}	[-1.3]

Figure 4.3 is the block diagram for the single inverter control block diagram, which includes the connection to the load and IEC bus. The control is subdivided into two levels of inner and outer control. The inner control includes voltage and current control loops, while the outer control performs the high-level power management, stability analysis and optimal operation. The outputs of the outer controller are the voltage and frequency reference. As can be seen, the inner control then converts the references d-q frame reference for simplicity.

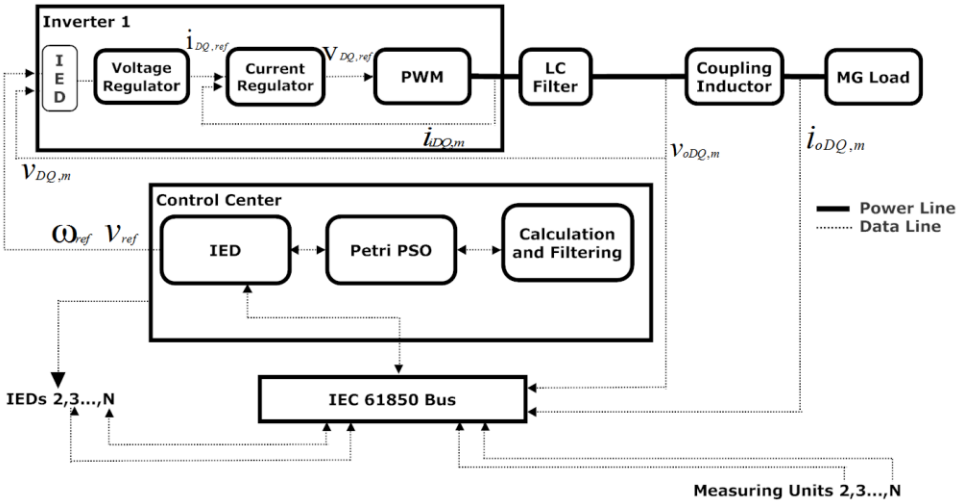

Figure 4.3 Inverter control, central controller and IEC 61850 bus block diagram

Figure 4.3 demonstrates measurement from the field, data transmission to the IEC bus and data loop from controller IED to Inverter IED. Voltage and current d-q components are measured and transmitted to the IEC bus while decentralised IEDs or IEC 61850 drivers of the inverter can access these measurements directly, the controller uses these values and updates the references based on the adaptive Petri PSO. Once the references are generated, they are sent to the inverters on the IEC 61850. It should be noted that the stability analysis utilises the time delay shown in equations (1–7). More details of the droop control and power sharing management are available in [1–3].

4.2.2 State Space Model of DG Inverters

The equations below explain the small signal model of the inverters in the microgrid in the d-q frame. The d-axis and q-axis used in the equations are the states of the state space model rotated with the reference frequency.

The input of the power controller, which is also shown in figure 4.3, has real and reactive components. These components are filtered through a low pass filter with a cut off frequency of ω_c. The real and reactive power are calculated using equation 1 and 2.

$$P^{inv} = v_{od}^{inv} i_{od}^{inv} + v_{oq}^{inv} i_{oq}^{inv} \quad (1)$$

$$q^{inv} = v_{od}^{inv} i_{oq}^{inv} - v_{oq}^{inv} i_{od}^{inv} \quad (2)$$

Then, the output of the voltage controller using the power plant controllers are calculated as equations 3 and 4 and followed by that, the output of the current controller referring to the power references are given by equations 5 and 6.

$$i_{R,id}^{inv} = K_{pv}\left(v_{R,od}^{inv} - v_{od}^{inv}\right) + K_{iv}\int(v_{R,od}^{inv} - v_{od}^{inv})dt - \omega_0 C_f v_{oq}^{inv} + F i_{od}^{inv} \quad (3)$$

$$i_{R,iq}^{inv} = K_{pv}\left(v_{R,oq}^{inv} - v_{oq}^{inv}\right) + K_{iv}\int(v_{R,oq}^{inv} - v_{oq}^{inv})dt + \omega_0 C_f v_{od}^{inv} + F i_{oq}^{inv} \quad (4)$$

$$v_{R,id}^{inv} = K_{pi}\left(i_{R,id}^{inv} - i_{id}^{inv}\right) + K_{ii}\int(i_{R,id}^{inv} - i_{id}^{inv})dt - \omega_0 L_f i_{iq}^{inv} \quad (5)$$

$$v_{R,iq}^{inv} = K_{pi}\left(i_{R,iq}^{inv} - i_{iq}^{inv}\right) + K_{ii}\int(i_{R,iq}^{inv} - i_{iq}^{inv})dt + \omega_0 L_f v_{oq}^{inv} \quad (6)$$

Where K_{pv} and K_{iv} are the proportional and integral gains of the voltage controller and K_{pi} and K_{ii} are the proportional and integral coefficients of the current controller. C_f, L_f and F are the capacitance of the LC filter, inductance of the filter and feedforward gains.

For the traditional droop control and the power sharing method between all the inverters equations 7–12 explain the relationships of the voltages and frequencies in a very simple formula.

$$\omega_{R\_dr}^{inv} = \omega_0 - K_{P-dr}^{inv} P^{inv} \quad (7)$$

$$v_{R\_dr}^{inv} = v_{0,od} - K_{Q\_dr}^{inv} Q^{inv} \quad (8)$$

$$v_{R-dr}^{inv} = 0 \quad (9)$$

K_{P-dr}^{inv} and $K_{Q\_dr}^{inv}$ are the frequency and voltage gains with respect to a specific range of voltage and frequency accepted by the system the MG is connected to.

It should also be noted that the summation of the power provided by the inverters in the microgrid must be 1. In a simpler term $\sum_{inv=1}^{g} \alpha_P^{inv} = 1$ and $\sum_{inv=1}^{g} \alpha_Q^{inv} = 1$. It will be seen that these conditions are two important constraints of the PSO used in the cost objective function and the most optimal combination of α set is achieved to ensure a complete response to the active and reactive demand. The responses to the demanded active and reactive power are also shown and considered in the calculations as shown in equations 10 and 11.

$$P_{tot} = \int_{inv=1}^{g} P^{inv} \quad (10)$$

$$Q_{tot} = \int_{inv=1}^{g} Q^{inv} \quad (11)$$

Therefore, using power sharing between the inverters, the voltage and frequencies are given by:

$$\omega_R^{inv} = \omega_{R\_dr}^{inv} + K_{P-sh}^{inv}[\alpha_p^{inv} P_{tot} - P^{inv}] \quad (10)$$

$$v_{R\_od}^{inv} = v_{R_{dr},od}^{inv} + K_{Q-sh}^{inv} \int \alpha_Q^{inv}\, Q_{tot} - Q^{inv} dt \quad (11)$$

$$v_{R-oq}^{inv} = 0 \quad (12)$$

Where K_{P-sh}^{inv} and K_{Q-sh}^{inv} are the control gains with respect to the active and reactive power sharing between the inverters of the considered microgrid.

An integral operator has been added to the default droop formula of the power sharing to minimise the inaccuracy, which can be seen in the reactive power droop formula.

Once the communication time delay is considered in the above formula, the frequency and voltage are given by:

$$\omega_R^{inv} = \omega(t)_{R\_dr}^{inv} + K_{P-sh}^{inv}[\alpha_p^{inv} P(t-\tau)_{tot} - P(t-\tau)^{inv}] \quad (13)$$

$$v_{R\_od}^{inv} = v(t)_{R_{dr},od}^{inv} + K_{Q-sh}^{inv} \int \alpha_Q^{inv}\, Q(t-\tau)_{tot} - Q(t-\tau)^{inv} dt \quad (14)$$

$$v_{R-oq}^{inv} = 0 \quad (15)$$

Where $\omega(t)_{R\_dr}^{inv}$ and $v(t)_{R_{dr},od}^{inv}$ are calculated using equations (1) and (2).

Similarly, the power controller shown in figure 4.3, which incorporates the total value of the active and reactive power of all the inverters, and the generation in the microgrid are given as:

$$\dot{\Delta\delta}^{inv} = \left[-K_{P_{dr}}^{inv} + K_{P_{sh}}^{inv}\alpha_P^{inv} - K_{P_{sh}}^{inv}\right]\Delta P^{inv} + \sum_{\substack{i=0 \\ i\neq g}}^{g} [K_{P\_sh}^{inv}\alpha_P^{inv}\Delta P^{inv}] - \Delta\omega_{com} \quad (16)$$

$$\dot{\Delta P}^{inv} = -\omega_c \Delta P^{inv} + \omega_c I_{od}^{inv}\Delta v_{od}^{inv} + \omega_c I_{oq}^{inv} v_{oq}^{inv} + \omega_c V_{od}^{inv}\Delta i_{od}^{inv} + \omega_c V_{oq}^{inv} i_{oq}^{inv} \quad (17)$$

$$\dot{\Delta Q}^{inv} = -\omega_c \Delta Q^{inv} + \omega_c I_{oq}^{inv}\Delta v_{od}^{inv} - \omega_c I_{od}^{inv}\Delta v_{oq}^{inv} - \omega_c V_{oq}^{inv}\Delta i_{od}^{inv} + \omega_c V_{od}^{inv}\Delta i_{oq}^{inv} \quad (18)$$

In the above formula, the initial values of voltage and current for both d and q components are given in Table 4.2., the integrator state of power controller elements is denoted as S_Q^{inv} and the state is summarised in equation 19 below.

$$\dot{\Delta S}^{inv} = \alpha_Q^{inv} \sum_{inv=1}^{g} \Delta Q^{inv} - \Delta Q^{inv} = \left[\alpha_Q^{inv} - 1\right]\Delta Q^{inv} + \alpha_Q^{inv} \sum_{\substack{inv=1 \\ inv\neq g}}^{g} \Delta Q^{inv} \quad (19)$$

Then the small signal model for the voltage reference, which is the output of the power controller, is equal to:

$$\Delta v_{R\_dr}^{inv} = -K_{Q\_dr}^{inv}\Delta Q^{inv} + K_{Q\_sh}^{inv}\Delta S_{Q}^{inv} \quad (20)$$

$$v_{R-oq}^{inv} = 0 \quad (21)$$

Among all the inverters, inverter g is selected as the common reference frame, therefore the small signal model of it with respect to the common frequency will be:

$$\Delta\omega_{com} = \Delta\omega_{R}^{g} \quad (22)$$

$$\Delta\omega_{com} = \left[-K_{P\_dr}^{g} + K_{P\_sh}^{g}\alpha_{P}^{g} - K_{P\_sh}^{g}\right]\Delta P^{g} + \sum_{\substack{i=1 \\ i\neq g}}^{G}[K_{P\_sh}^{g}\alpha_{P}^{g}\Delta P^{i}] \quad (23)$$

As seen in the equations above, conventional PI controllers regulate the voltage and current of the inverters setpoints. Taking these outputs into the state-space model adds additional states of $\Delta S_{V,D}^{(g)}$ $\Delta S_{V,Q}^{(g)}$ $\Delta S_{I,Q}^{(g)}$ and $\Delta S_{I,Q}^{(g)}$.

Once the inverters are added to the plant control system, their output currents and voltages require a conversion based on the reference frame. More comprehensive explanations are found in [18].

The state space model of each inverter within the MG is [1]:

$$\Delta\dot{x} = A_1\Delta x + B_1 M_1'\Delta v_{bDQ} \quad (24)$$

$$\Delta I_{oDQ} = C_1\Delta x \quad (25)$$

$$\Delta\omega_{com} = C_{com}\Delta x \quad (26)$$

$$\Delta x = \Big[\Delta\delta^{(g)}\ \Delta P^{(g)}\Delta Q^{(g)}\Delta S_{Q}^{(g)}\Delta S_{V,D}^{(g)}\ \Delta S_{V,Q}^{(g)}\ \Delta S_{I,Q}^{(g)}\ \Delta S_{I,Q}^{(g)}$$
$$\Delta i_{iD}^{(g)}\ \Delta i_{iQ}^{(g)}\ \Delta v_{oD}^{(g)}\ \Delta v_{oQ}^{(g)}\ \Delta i_{oD}^{(g)}\ \Delta i_{oQ}^{(g)}\Big] \quad (27)$$

Where x is a 14-element vector containing states of the inverter's voltage and current regulators, coupling inductance and an LCL filter.

Additionally, the states of the model have the inputs of $\Delta P^{i}, \Delta Q^{i}, \Delta v_{bDQ}$ and $\Delta\omega_{com}$. Therefore $\Delta\dot{x}$ are given by:

$$\Delta\dot{x}^{inv} = A_1^{inv}\Delta x^{inv} + B_1^{inv}\Delta v_{b,DQ}^{n} + B_{com}^{inv}\Delta\omega_{com} + \sum_{inv=1}^{g} B_{P,inv}^{g}\Delta x^{inv} +$$
$$\sum_{inv=1}^{g} B_{Q,inv}^{inv}\,\Delta x^{inv} \quad (28)$$

Where A_1^{inv} is given by the equations discussed above and shown in matrices of $A_{11}^{inv}$and A_{12}^{inv}.

$$A_{11}^{inv} = \begin{bmatrix} 0 & -K_{p\_dr}^{inv} & 0 & 0 & 0 & 0 \\ 0 & -\omega_c & 0 & 0 & 0 & 0 \\ 0 & 0 & -\omega_c & 0 & 0 & 0 \\ 0 & 0 & 0 & 0 & 0 & 0 \\ 0 & 0 & -K_{Q\_dr}^{inv} & K_{Q\_sh}^{inv} & 0 & 0 \\ 0 & 0 & 0 & 0 & 0 & 0 \\ 0 & 0 & -K_{pv}K_{Q\_dr}^{inv} & K_{pv}K_{Q\_sh}^{inv} & K_{iv} & 0 \\ 0 & 0 & 0 & 0 & 0 & K_{iv} \\ 0 & -K_{P\_dr}^{inv} I_{iq}^{inv} & \frac{-K_{Q\_dr}^{inv} K_{pv} K_{pi}}{L_f} & \frac{K_{Q\_sh}^{inv} K_{pv} K_{pi}}{L_f} & \frac{K_{pv} K_{pi}}{L_f} & 0 \\ 0 & K_{P\_dr}^{inv} I_{id}^{inv} & 0 & 0 & 0 & \frac{K_{pv} K_{pi}}{L_f} \\ 0 & -K_{P\_dr}^{inv} V_{oq}^{inv} & 0 & 0 & 0 & 0 \\ 0 & K_{P\_dr}^{inv} V_{od}^{inv} & 0 & 0 & 0 & 0 \\ -\frac{-V_{bd}^{n} \sin \delta_0^{inv} + V_{b,Q}^{n} \cos \delta_0^{inv}}{L_c} & -K_{P\_dr}^{inv} I_{oq}^{inv} & 0 & 0 & 0 & 0 \\ \frac{-V_{bd}^{n} \cos \delta_0^{inv} - V_{b,Q}^{n} \sin \delta_0^{inv}}{L_c} & K_{P\_dr}^{inv} I_{od}^{inv} & 0 & 0 & 0 & 0 \end{bmatrix}$$

$$A_{12}^{inv} = \begin{bmatrix} 0 & 0 & 0 & 0 & 0 & 0 & 0 & 0 \\ 0 & 0 & 0 & 0 & \omega_c I_{od}^{inv} & \omega_c I_{oq}^{inv} & \omega_c V_{od}^{inv} & \omega_c v_{oq}^{inv} \\ 0 & 0 & 0 & 0 & \omega_c I_{oq}^{inv} & -\omega_c I_{od}^{inv} & -\omega_c V_{oq}^{inv} & \omega_c V_{od}^{inv} \\ 0 & 0 & 0 & 0 & 0 & 0 & 0 & 0 \\ 0 & 0 & 0 & 0 & -1 & 0 & 0 & 0 \\ 0 & 0 & 0 & 0 & 0 & -1 & 0 & 0 \\ 0 & 0 & -1 & 0 & -K_{pv} & -\omega_0 C_f & F & 0 \\ \frac{K_{ii}}{L_f} & 0 & 0 & -1 & \omega_0 C_f & -K_{pv} & 0 & F \\ -\frac{R_f + K_{pi}}{L_f} & \omega_{sys} - \omega_0 & \frac{1 + K_{pv} K_{pi}}{L_f} & \frac{-\omega_0 C_f K_{pi}}{L_f} & \frac{F K_{pi}}{L_f} & 0 & \frac{1}{L_c} & 0 \\ 0 & \frac{K_{ii}}{L_f} & -\omega_{sys} + \omega_0 & -\frac{R_f + K_{pi}}{L_f} & \frac{\omega_0 C_f K_{pi}}{L_f} & -\frac{1 + K_{pv} K_{pi}}{L_f} & 0 & \frac{F K_{pi}}{L_f} \\ 0 & 0 & \frac{1}{C_f} & 0 & 0 & -\omega_{sys} & -\frac{1}{C_f} & 0 \\ 0 & 0 & 0 & \frac{1}{C_f} & -\omega_{sys} & 0 & 0 & -\frac{1}{C_f} \\ 0 & 0 & 0 & 0 & \frac{1}{L_c} & 0 & -\frac{R_c}{L_c} & \omega_{sys} \\ 0 & 0 & 0 & 0 & 0 & \frac{1}{L_c} & -\omega_{sys} & -\frac{R_c}{L_c} \end{bmatrix}$$

For simplicity in presenting the equations, the matrices of $B_{Q,i}$, $B_{P,i}$ and C_{com} are presented in the format below from [1]. This format also helps the programming in MATLAB to be simplified.

$$B_{Q,i}^{g} = [b(j,k)_{Q,i}^{g}]_{14\times 14} \tag{29}$$

$$b_{Q,i=g}^{g}(j,k) = \begin{cases} \alpha_Q^g - 1, & if\ j = 4\ and\ k = 3 \\ 0, & otherwise \end{cases} \tag{30}$$

$$b_{Q,i\neq g}^{(g)}(j,k) = \begin{cases} \alpha_Q^g, & if\ j = 4\ and\ k = 3 \\ 0, & otherwise \end{cases} \tag{31}$$

$$b(j,k)_{P,i=g}^{(g)} = \begin{cases} K_{P\_sh}^{g}\alpha_P^g - K_{P\_sh}^{g}, & if\ j = 1, k = 2 \\ I_{iq}^{g}\left[K_{P\_sh}^{g}\alpha_P^g - K_{P\_sh}^{g}\right], & if\ j = 9, k = 2 \\ -I_{id}^{g}\left[K_{P_{sh}}^{g}\alpha_P^g - K_{P_{sh}}^{g}\right], & if\ j = 10, k = 2 \\ V_{oq}^{g}\left[K_{P_{sh}}^{g}\alpha_P^g - K_{P_{sh}}^{g}\right], & if\ j = 11, k = 2 \\ -V_{od}^{g}\left[K_{P_{sh}}^{g}\alpha_P^g - K_{P_{sh}}^{g}\right], & if\ j = 12, k = 2 \\ I_{oq}^{g}\left[K_{P_{sh}}^{g}\alpha_P^g - K_{P_{sh}}^{g}\right], & if\ j = 13, k = 3 \\ -I_{od}^{g}\left[K_{P_{sh}}^{g}\alpha_P^g - K_{P_{sh}}^{g}\right], & if\ j = 14, k = 2 \\ 0, & otherwise \end{cases}$$

$$b(j,k)_{P,i\neq inv}^{g} = \begin{cases} K_{P\_sh}^{g}\alpha_P^g, & ifj = 1, k = 2 \\ I_{iq}^{g}K_{P\_sh}^{g}\alpha_P^g, & if\ j = 9, k = 2 \\ -I_{id}^{g}K_{P\_sh}^{g}\alpha_P^g, & if\ j = 10, k = 2 \\ V_{oq}^{g}K_{P\_sh}^{g}\alpha_P^g, & if\ j = 11, k = 2 \\ -V_{od}^{g}K_{P\_sh}^{g}\alpha_P^g, & if\ j = 12, k = 2 \\ I_{oq}^{g}K_{P\_sh}^{g}\alpha_P^g, & if\ j = 13, k = 2 \\ -I_{od}^{g}K_{P\_sh}^{g}\alpha_P^g, & if\ j = 14, k = 2 \\ 0, & otherwise \end{cases}$$

4.2.3 MG State Space Model Considering Dispatch and Communication

4.2.4 Impact of Power Reference Upgrading

Including the communication time delay in the transmission of power reference affects the overall stability of the MG. The time delay is introduced to the dynamic matrices of the MG's state space model as variable τ. It is expected that in adding this parameter to the system, the determinant's roots and consequently the eigenvalues of the system change. The location of the eigenvalues represents the general stability of the system; therefore, it is critical to inspect the eigenvalue analysis of the system as a function of the time delay [1].

$$\Omega(\lambda, \tau) = \lambda I_0 - A_{MG-dr} - A_{MG-sh} e^{-\lambda\tau} \quad (32)$$

"In building matrices $A_{grid-dr}$ and $A_{grid-sh}$ (Eqs. 5-7), variables α are defined to represent the desired levels of DG active and reactive power sharing. The α for DGi is calculated using [1–2]":

$$\alpha_i = P_{DGi}/P_{load}. \quad (33)$$

Since the summation of all the contributed power from the DGs in the MG shall equal the total requested power from loads or grid demand, therefore [1]:

$$\sum_1^n \alpha_{DGi} = 1. \quad (34)$$

The α values for DG inverters are included in the MG's dynamic matrices in the small-signal state space model [1, 3].

By solving equation 7, the zeros of this equation are gained, which can provide the MG eigenvalues (λ) and as discussed before, the stability of the MG can be analysed. Thus, it is crucial to screen the effect of α_{DGi} on the stability, when they are changed by the real-time management platform for the purpose of cost minimisation.

To prevent instability in the MG, the proposed adaptive Petri PSO analyses the stability through equation 7 prior to the references being sent to the inverters and this is done as a part of the optimisation process in such a way that the answers achieved by the CPOS optimisation are only acceptable subject to providing a stable system based on the location of the eigenvalues. In addition to this contribution, the time delay has been significantly reduced from the conventional communication protocol from an average of 100–200 milliseconds to a few milliseconds. Moreover, as each renewable IEC packet gets to the inverter according to a time stamp, the optimisation can always

review the time delay as they are all connected to a GPS clock. Therefore, the time delay τ is no longer an estimated value used in the system dynamic based on previous experiences but is an accurate value instead. Detailed equations of each inverter are discussed in reference [1].

4.3 Proposed Real-Time Power Management and Stability Control Scheme

4.3.1 Adaptive Petri PSO

Conventional cost optimisations for MGs provide the dispatch signals to minimize the cost with no stability consideration in terms of frequency and voltage [4–9]. The proposed adaptive Petri PSO mathematically establishes a relationship between the stability and cost function in such a way that while the plant is operating, it moves the system away from the power references, which situate the MG in a zone of poor stability. Thus, while the cost is optimized the stability criteria is also met.

This adaptive Petri PSO can handle two levels of control and monitoring:

- ***Top Control Layer*** – PN is implemented at this level of control to monitor the overall condition of the system
- ***Lower Control Layer*** – This level includes the logic, system modelling, system dynamic, optimisation and the detailed calculations. Each one of these details is located in the Petri Net places and shows the system operator the current system status.

The MG in this case study has seven places p1 to p7 and these seven statuses of the MG. These statuses change from one to the other when transitions t1 to t8 are met. Equations 7–10 explain the rules for the system status change.

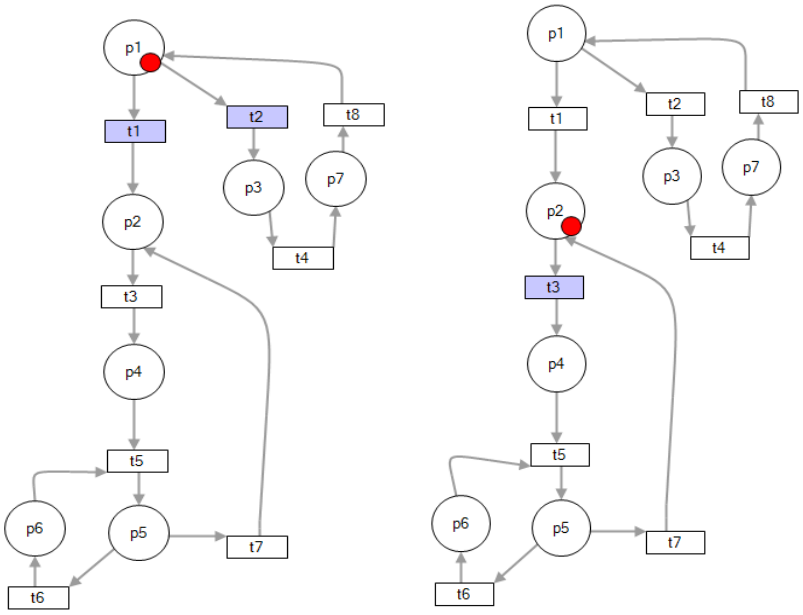

Figure 4.4 Proposed MG Petri Net simulated using HIPS software with the system status (a) at place 1, and (b) at place 2

Table 4.3 Petri Net Configuration Elements [2]

Symbol	Definition
p_1	Starting the process and turning the inverter on
p_2, p_3, p_4	Running PSO, Resetting the fault, Sending references
p_5	Reading network data and comparing the cost
p_6	Keeping the references unchanged
p_7	Informing the operator or restarting the device
t_1, t_2	Inverters are healthy, Inverters are not healthy
t_3, t_4	Communication is okay, Inverters are still faulty
t_5	Power measured values and time delay are received
t_6	Cost is within ±5% of optimal references
t_7, t_8	Cost is not within ±5%, Alarm is acknowledged

4.3.2 Petri PSO Cost Objective Function

Figure 4.4 (b) shows the adaptive Petri PSO snapshot while the system is at p_2. This seamlessly sends the power reference signals while the objective is to work out the references that provide the minimum cost of the system and maintain system stability. Therefore, p_2 represents the objective function as being achieved by the CPSO and as the outcome of this stage the individual inverter references (α_{DGi}) are calculated.

The cost objective function has the constraint which is stability analysis, which can be found in equations 37–40.

The selected MG cost objective function is:

$$Min\ C_{MG}(t) = \sum_{i}^{n} C_{DGi}(t) = \sum_{i=1}^{n} LC_{DGi} P_{DGi}(t) \quad (35)$$

where LCDGi is the levelized cost of DG unit i in $/kWh. Three power sources are then considered in the equation below, as the summation of the cost for all units will be the total cost of the system. Note this does not include the capital cost of installation in this example; however, in the real-life example it can potentially include that too if it is required by the financial model of the microgrid.

$$Min\ C_{MG}(t) = C_{solar}(t) + C_{MT}(t) + C_{FC} = LC_{solar} P_{solar}(t) + LC_{MT} P_{MT}(t) + LC_{FC} P_{FC} \quad (36)$$

where selected levelized costs are LC_{solar}= 0 $/kWh, $LC_{MT=}$ 0.06$/kWh and LC_{FC} = 0.04$/kWh [3,16]; however, these values are dependent on the MG type and some other factors including but not limited to thermal energy requirement and location. These factors can affect the cost and contribution of the FCs. In this research it is assumed fuel cells satisfy the minimum demand for thermal energy usage.

4.3.3 Petri PSO Constraints

The full list of the constraints of the CPSO optimisation are discussed here. At P_2 under the optimisation formula there are 5 constraints and in different applications there can be more or less depending on the application that the Petri PSO will be implemented for.

1) Total Power Demand: this constraint is to ensure the total power supply meets the

condition of the load or grid. This constraint needs the PSO particles to approach solutions that satisfy the total required power. In simpler terms:

$$P_{load}(t) = \sum_{i=1}^{n} P_{DGi}(t) \quad (37)$$

$$P_{DGi}^{min} < P_{DGi}(t) < P_{DGi}^{max} \quad (38)$$

2) Frequency and Voltage Constraint: requiring MG frequency and voltage to be maintained within acceptable limits of $[\omega_{min}^{i}, \omega_{max}^{i}]$ and $[v_{min}^{i}, v_{max}^{i}]$. The proportional coefficients of droop control for the active and reactive power control of DG unit i are calculated as follows:

$$K_{P-dr}^{i} = (\omega_{max}^{i} - \omega_{min}^{i})/P_{max}^{i} \quad (39)$$

$$K_{Q-dr}^{i} = (v_{max}^{i} - v_{min}^{i})/Q_{max}^{i} \quad (40)$$

3) Stability Constraint: this is considered to maintain the stability of the microgrid when due to any reason the inverter reference signals need to change. Eigenvalue analysis has been considered to check the stability of the MG at each given time. Therefore, when the cost objective function dictates the optimal $P_{DGi}(t)$, the inverter can simply provide the reference with the assurance that these values will keep the MG stable with enough stability margin. The main target of the CPSO is to keep the eigenvalue as far left as possible of the imaginary axis of the state-space plant, while the cost function is at a minimum (Equ. 36).

4.3.4 Adaptive Petri PSO

The Petri PSO also monitors the time delay within the system in a similar way as it monitors all other parameters of the system. If the time delay within the system, which is calculated based on the carried time stamp of the proposed renewable IEC 61850 data class model, exceeds the acceptable margin, it will adapt the control value using the CPSO. For instance, if the time delay exceeds the normal range expected from IEC 61850 SV or GOOSE then it updates the power sharing coefficient or control parameters to make the controller more aggressive. This is while the offered values are still assessed by the stability constraint to maintain system stability. Providing all these updates, receiving the data from the measurement devices (perhaps from difference

vendors), all controllers and inverters will bring inherent time delays in the control system.

4.4 Implemented Fast Data Exchange Communication MG Based on IEC 61850

In a laboratory facility, two laptops with high specifications were setup to be an IEC 61850 server and client (publisher and subscriber). These two laptops were connected via an ethernet switch. This lab test has been configured to demonstrate that the proposed renewable microgrid data class for the IEC 61850 presented in Chapter 3 can be transmitted within the claimed time frame and can also meet the criteria of 20 milliseconds for the stability condition of the considered microgrid in reference [1].

The laboratory setup is captured in figure 4.5 with two laptops running Xelas Energy software used to perform the simulation of the IEC 61850 network and monitoring of the proposed data exchange between the publisher and subscriber. Both GOOSE and SV were tested to carry the data in the proposed format between the two virtual IEDs. The data are digitalised using the Xelas software, while in the reality it is expected that the real data would be digitalised by the merging unit, which receives the measured value from analogue measurement devices. In return, the calculated dispatch signals in the format of power sharing references (α_{DGi}; Eqs. 8-9) are sent to each virtual IED developed in the inverters. In the screen shots captured in Fig. 4.5, the righthand workstation is the virtual IEC 61850 server and the lefthand workstation runs the client. The communication is over an ethernet. A packet sniffer software called Wireshark has been used to monitor and measure the packet delivery time between the two virtual IEDs.

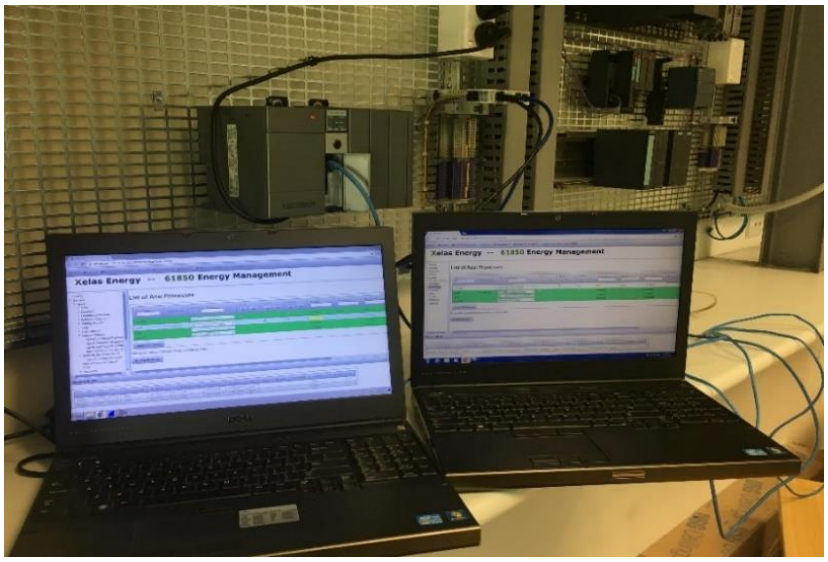

Figure 4.5 Laboratory setup for communication test of the proposed new class of IEC 61850 GOOSE messaging

4.5 Results and Discussion

To analyse the functionality of the real-time power management proposed by the adaptive Petri PSO equipped with fast communication protocol, the MG indicated in figure 4.1 and has been simulated using the MATLAB Simulink platform. The MG has been subjected to real-time power management (power sharing) reference updates with practical time delays. The results of this Petri PSO facilitated with the IEC 61850 standard time delay are illustrated in section 4.5.1.

Some laboratory test results are also presented in section 4.5.2 to prove the time delay provided by the proposed protocol is achievable for the considered MG application.

4.5.1 Real-time Power Management and Stability Analysis of an MG

4.5.1.1 Case A: Impacts of Time Delays on MG Stability

The effect on the MG's stability of time delays as a consequence of using conventional industrial communication protocols between the inverters, controller and measurement devices is investigated in this case scenario. In this control scenario, the third constraints of the CPSO have not be considered. The resulting calculated optimal cost was 0.026946 $/kWh independent of time delays. In this case, the power references

sent to the power sources are 0.7212, 0.2683 and 0.01505 pu for the solar farm, fuel cell and micro turbine in turn.

The results of the MG simulation are presented in figure 4.6. This figure shows the eigenvalues of the MG on the z-plan for time delays of 1 millisecond to 30 milliseconds. The resolution of the time delay increase is 1 millisecond in order to indicate the effect of the time delay for every millisecond that the time delay is increased. In this control scenario, the power sharing references remain constant.

Regarding Fig. 4.6:

- There are different branches of the eigenvalues and each one is a single mode of the system which has been plotted for time delays in the range of 1 to 30 milliseconds for every 1 millisecond time delay increase.
- It can be seen how increasing the time delay by 10 milliseconds can situate some of the eigenvalues in the unstable zone by moving the eigenvalues from the left to the right side of the imaginary axis.
- It is also clear that there are some eigenvalues representing some modes which are stable but as they are located very close to the imaginary axis, they can either put the system in an oscillatory mode or even make it unstable. These are the modes that will be attempted to be maintained as far as possible from the imaginary axis while the Petri PSO is running the optimisation.
- This figure only shows the eigenvalues which can be fitted within the range of the figure. The remaining eigenvalues are on the far-left side, which carry no stability risk. According to the results, increasing the time delay does not move those hidden eigenvalues to the unstable zone under any circumstances using practical time delays from conventional industrial communication protocols such as Modbus Serial, Modbus TCP, Profibus, ProfiNet and all other known protocols in the automation industry.

According to the results gained using the Xelas simulation of the proposed new IEC 61850 data type, both the new IEC 61850 GOOSE and the new SV can provide fast data exchange in such a way that the time delay for this MG is less than 20 milliseconds. This means that when using this fast communication tool, all the eigenvalues are in the left-hand plane and the system is stable.

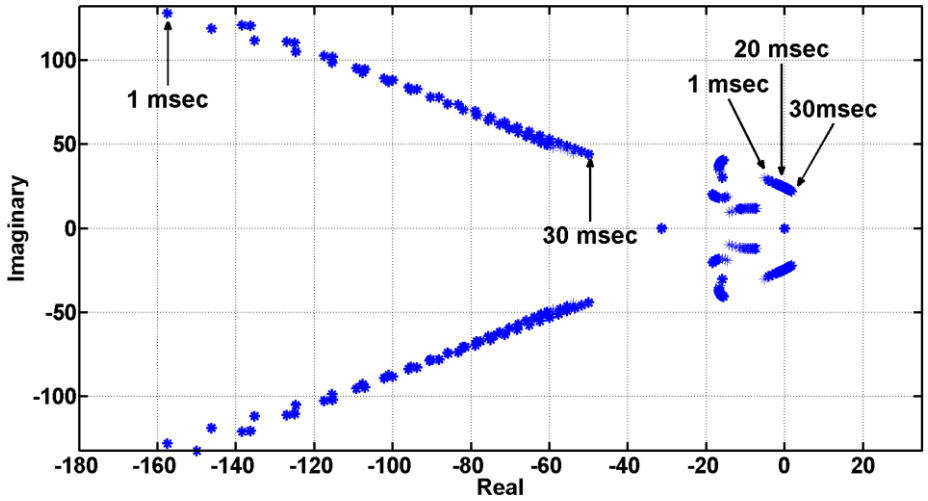

Figure 4.6 Low frequency MG eigenvalues plotted for τ=1 msec and τ=30 msec

4.5.1.2 *Case B: Performance of the MG with the Proposed Real-Time Power Management and Stability Control Scheme Equipped with IEC 61850*

In this case study, full real-time power management with stability control is applied to the MG with the three inverters shown in figure 4.1 with communication time delays of 5 milliseconds and 15 milliseconds. Table 4.4 shows a summary of the case studies with time delays associated with each test.

Both the 5 and 15 millisecond time delays are achievable using the proposed IEC 61850 data class with either GOOSE or SV. Figure 4.7 runs a comparison with a low frequency mode by indicating the location of the eigenvalues close to the imaginary axis. As expected, two pairs of eigenvalues have been moved significantly towards the unstable zone by increasing the 5-millisecond communication time delay to 15 milliseconds.

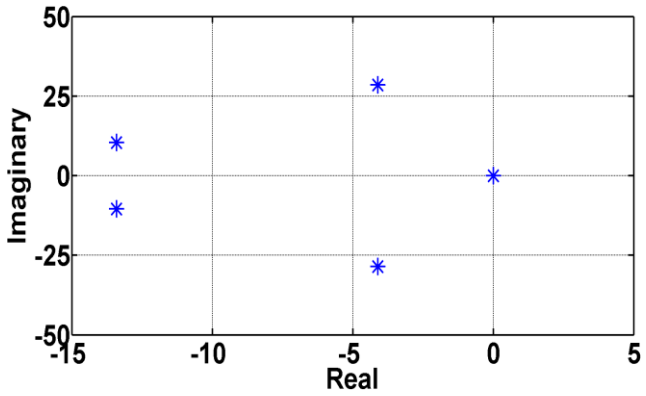

(a)

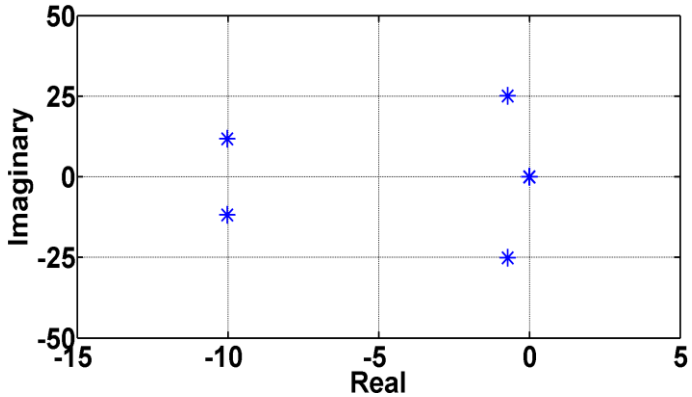

(b)

Figure 4.7 Low frequency eigenvalues of the MG for: (a) τ=5 msec, (b) τ=15 msec.

Figure 8 and figure 9 indicate the DC bus voltage and power output for each inverter along with the total power generated by the MG with time delays of 5 and 15 milliseconds. Changing the 5-millisecond time delay to 15 milliseconds created considerable oscillation in the power output and DC bus voltage. As a result, deteriorated MG power quality and higher THD of current and voltage can also be observed. Under more severe conditions, these could either cause a trip, a constraint on MG production in network connected cases, or damage to the equipment. The simulation time frame is 1.8 seconds and at t= 0.4, 1 pu of power demand is requested of the MG where the step reposes can be seen in part "a" of figures 4.8 and 4.9.

Table 4.4 Summary of the simulation results

Case	Stability Constraint	τ [msec]	α_{DGi} [pu] for			Cost [$/kWh]	Stable
			P_{Solar}	P_{FC}	P_{MT}		
A1	Not Considered	τ>20	0.721	0.268	0.010	0.0269	No (Fig. 10)
A2	Not Considered	0<τ<19	0.721	0.268	0.010	0.0269	Yes (Fig. 10)
B1	Considered	τ=5	0.624	0.278	0.098	0.0366	Yes (Figs. 11a,12)
B2	Considered	τ=15	0.577	0.348	0.074	0.0418	Yes (Figs. 11b,13)

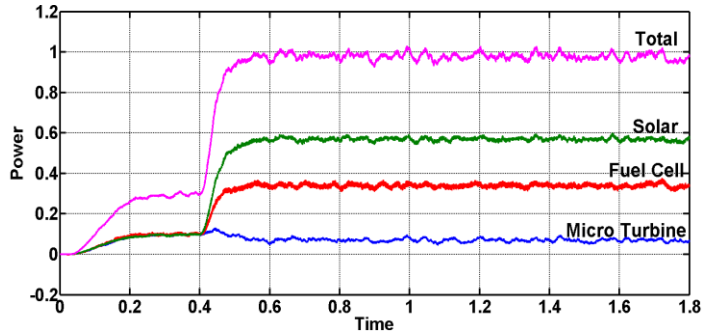

(a)

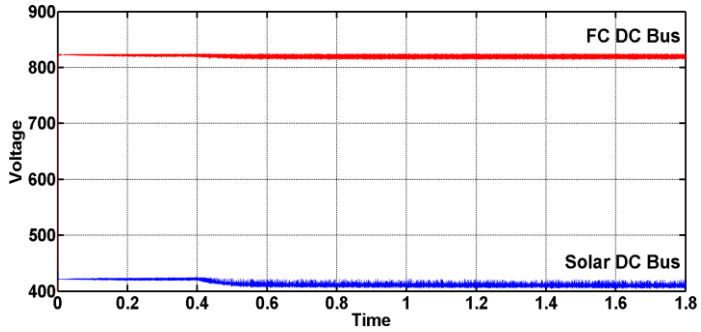

(b)

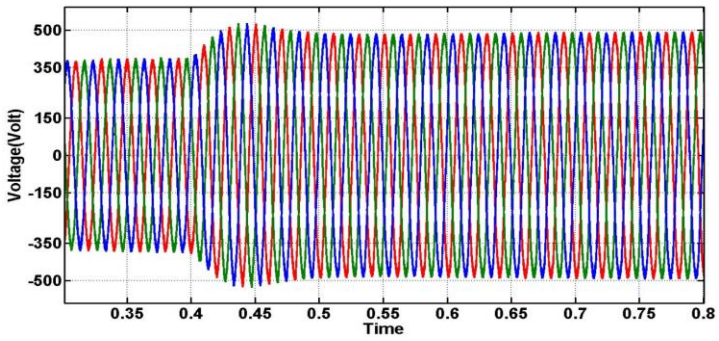

(c)

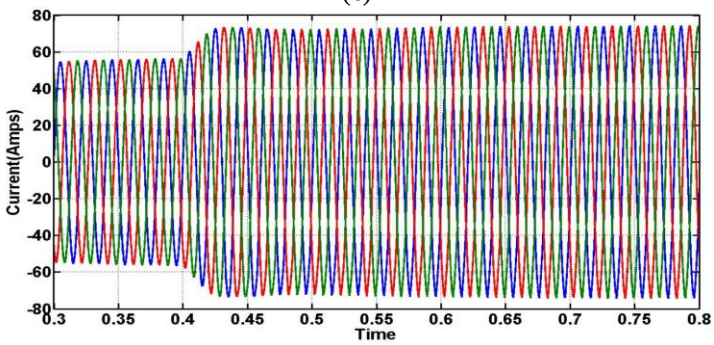

(d)

Figure 4.8 (a) Power output from each inverter with τ=5 msec, (b) DC voltage of Solar and FC inverters with τ=5 msec, (c) Load Voltage (d) Load Current

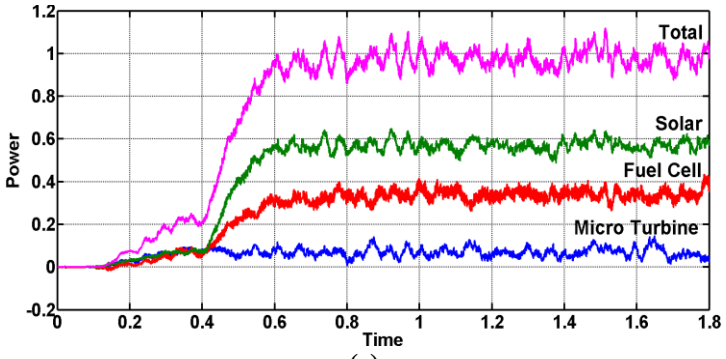

(a)

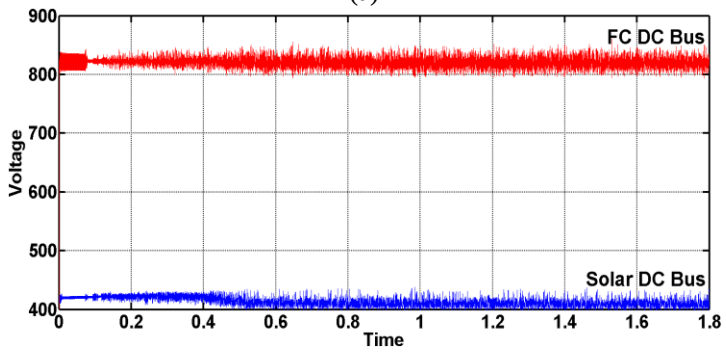

(b)

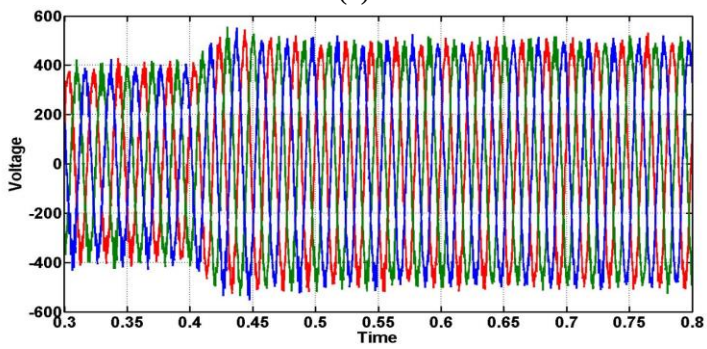

(c)

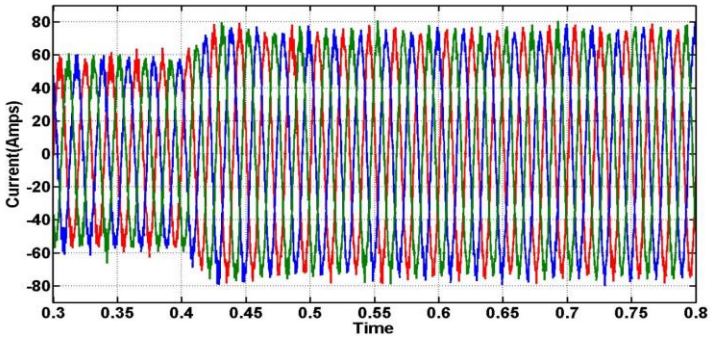

(d)

Figure 4.9 (a) Power output from each inverter with τ=15 msec, (b) DC voltage of solar and FC inverters with τ=15 msec, (c) Load Voltage (d) Load Current

It should be noted that in both case studies of A and B, the weighting factors are calculated by the CPSO. The CPSO code, which can be found in appendix D, ensures the frequency and voltages are within the acceptable range, the combination of the total power generated by the microgrid respond to the power demand, and the combination also satisfies the stability of the microgrid. The main objective of the optimisation is the total cost of the demanded power while this cost will be sacrificed if stability is endangered.

In the meantime, it can be seen that the shorter time delay within the control system shows a better response in terms of power quality and, more importantly, stability. The trajectory of the peak points of the current and voltage signals in figure 4.9, shows that the system experiences oscillations, while in figure 4.8 after t=0.4, the system has adequately damped responses when the new setpoint is applied.

This management of the power system through the PSO considered each power plant at its maximum capacity at the time of the optimisation iteration. This value has been considered the plant nameplate and all case studies assume the solar farm is fully available because these studies have all been conducted using a small signal model, which is unlikely to indicate changes of solar irradiance. However, the CPSO has been developed as a modular program and the size of the solar farm can be dynamically adjusted using a formula which captures the solar farm availability at any given time. Using this, the formula will automatically exclude the solar farm from the available sources of power and the optimisation will consider only two sources of power.

4.5.2 IEC 61850 GOOSE and SV Test in the MG

As indicated in figure 4.10, the IEC client and IEC server are running on the IP address 192.168.0.120 and 192.168.0.131 on the laboratory network. The reason that these two IP addresses were selected was because the others were occupied for other purposes in the laboratory.

Figure 4.11 shows the IEC packages were delivered on the IEC client. As expected, the delivery time of GOOSE messages has changed from 2 milliseconds to 4 milliseconds and packet delivery has remained constant at 2 milliseconds for the SV.

Both delivery times are configurable in the SCL file (shown in Fig. 4.11), while they are developed in the IEC 61850/IEC 61400 Model Designer software platform.

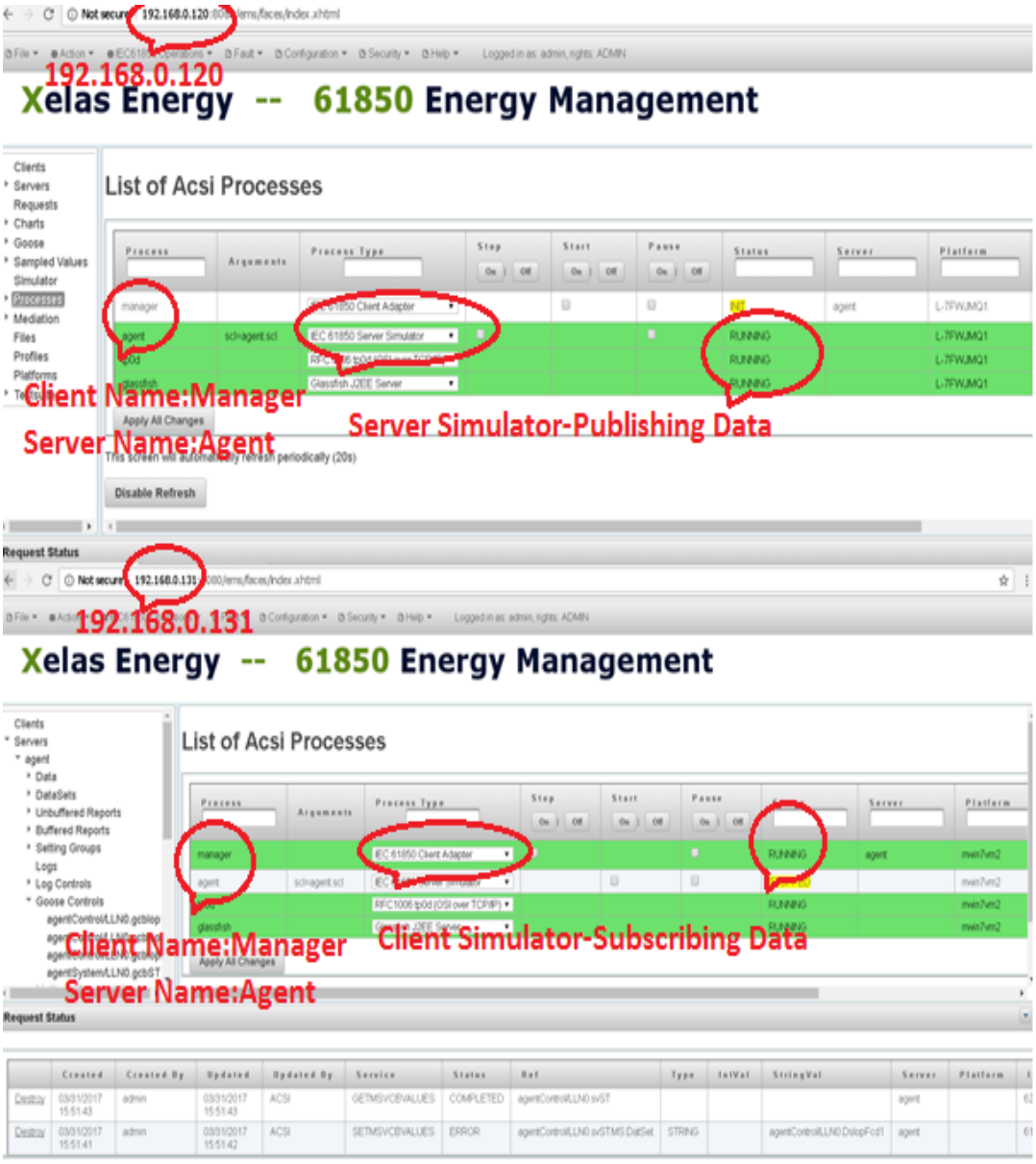

Figure 4.10 IEC 61850 Server and Client Running on the Xelas Energy Management Graphic User Interface (GUI)

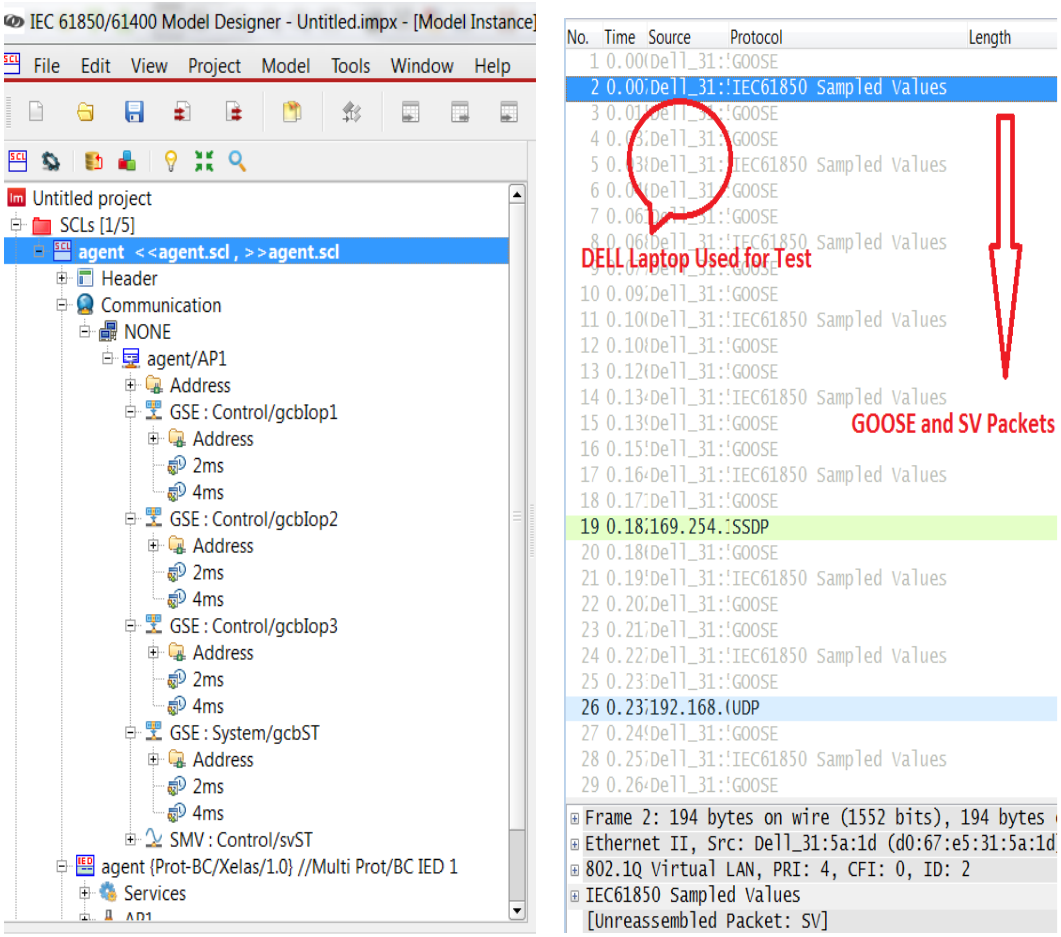

(a) (b)

Figure 4.11 (a) Server SCL file in the Xelas Energy model designer software package, (b) Wireshark IEC 61850 captured SVs at the Client End

4.6 Conclusion

4.6.1 Power Management and Stability Modelling

Simultaneous real-time power management and continuous stability analysis of MGs can significantly assist with renewable penetration and renewable DG contribution within the utility network. However, this requires a wider range of data exchange within a short period of time along with a sophisticated power management platform which not only minimises cost but also reviews the stability of the MG.

The main conclusions according to the simulation implemented in MATLAB and the experimental measurement of the MG shown in figure 4.1 are as follows:

- A Real-time Power Management Petri PSO equipped with fast communication, not only minimized the overall cost of the MG but also maintained the stability of the MG. The proposed method provided better DC bus voltage and less fluctuation and oscillation at the power output which represent better power quality.
- The significant impact of time delays on the stability of the MG, especially in lower frequency mode, has been witnessed in the results of the simulations. The eigenvalues of the low frequency mode shifted to the right half z plane by increasing the communication time delay (figures. 4.6 – 4.7).
- Increasing the time delay even in the stable zone caused considerable fluctuations and oscillation in the inverter DC bus and power output (figures. 4.8– 4.9).
- A 20-millisecond time delay was calculated as the limit for the communication time delay with optimal control parameters. Therefore, a laboratory test was setup to prove the practicality of the proposed new IEC data class model. Both Sampled Value and GOOSE messages were able to deliver the data a lot faster than 20 milliseconds. However, SV appeared to be a better data type as it can maintain a consistent sampling rate and there is no need for event determination. GOOSE messages needed to have a customised even definition in the configuration, which involves some difficulty. In summary, the new data type is proposed to be a customised SV. It is worth mentioning that the 20-millisecond time delay is not achievable using conventional communication protocols for such a system.

- The conventional dispatch method has been enhanced by considering stability analysis. The stability analysis is facilitated by the fast communication, which results in reasonable cost and maintains system stability. Existing dispatch (Table 4.4, columns 7–8) methods managed to run the system at insignificantly lower cost but without consideration of stability or power quality factors in the real-time scheme.

4.6.2 IEC 61850 GOOSE and SV Modelling

The results of communication field tests and simulations shows that:

- SV performs sampling every 2 milliseconds as set in the SCL file and sends the value to the client, while GOOSE only takes the sample when an event occurs based on the maximum speed setting in the SCL file, which eventually slows down to the minimum speed.
- GOOSE messages do not send updated values unless a new event is triggered, and keeps repeating the same value till the next event happens, whereas the SV takes the sample and sends it through regardless.
- SV messages generate significantly more traffic in the network. These experimental results show that the communication scheme of Section IV based on IEC 61850 with GOOSE and SV data types can meet the minimum time delay requirement of 20 milliseconds for the MG in figure. 4.1.

4.7 References

[1] H. Liang, B. J. Choi, W. Zhuang and X. Shen, "Stability enhancement of decentralized inverter control through wireless communications in microgrids," *IEEE Trans. on Smart Grid*, vol. 4, no. 1, 2013.

[2] N. Pogaku, M. Prodanovic and T. C. Green, "Modelling, analysis and testing of autonomous operation of an inverter-based microgrid," *IEEE Trans. on Power Electronics*, vol. 22, no. 2, pp. 613-625, March 2007

[3] C. Dou, M. Lv, T. Zhao, Y. Ji and H. Li, "Decentralised coordinated control of microgrid based on multi-agent system," in *IET Generation, Transmission & Distribution*, vol. 9, no. 16, pp. 2474-2484, 2015.

[4] T. Murata, "Petri nets: Properties, analysis and applications," in *Proceedings of the IEEE*, vol. 77, no. 4, pp. 541-580, April 1989.

[5] Q. He, L. Wang and F. z. Huang, "Nonlinear constrained optimization by enhanced co-evolutionary PSO," *IEEE Congress on Evolutionary Computation*, Hong Kong, pp. 83-89, 2008.

[6] C. C. Thompson, P. E. Konstantinos Oikonomou, A. H. Etemadi and V. J. Sorger, "Optimization of data center battery storage investments for microgrid cost savings, emissions reduction, and reliability enhancement," *IEEE Trans.* on Industry Appli., vol. 52, no. 3, 2016.

[7] T. A. Nguyen and M. L. Crow, "Stochastic optimization of renewable-based microgrid operation incorporating battery operating cost," *IEEE Trans. on Power Systems*, vol. 31, no. 3, pp. 2289-2296, May 2016.

[8] C. Li, F. de Bosio, F. Chen, S. K. Chaudhary, J. C. Vasquez and J. M. Guerrero, "Economic dispatch for operating cost minimization under real-time pricing in droop-controlled DC microgrid," *IEEE Journal of Emerging and Selected Topics in Power Electronics*, vol. 5, no. 1, pp. 587-595, March 2017.

[9] M. Zachar and P. Daoutidis, "Microgrid/Macrogrid energy exchange: A novel market structure and stochastic scheduling," *IEEE Trans. on Smart Grid*, vol. 8, no. 1, pp. 178-189, Jan. 2017.

5 CHAPTER FIVE: Grid-Connected Voltage and Reactive Power Control Improvement Using Fast Communication and Virtual Impedance

5.1 Introduction

As previously discussed, the number of renewable microgrids has been growing in recent years; however, they have also brought some complexity to power grid operation and control. Wind and solar farms are not exempt from this. Some instability issues due to wind speed and direction fluctuations are the most common discussions in this field. However, some governments still encourage the renewable industry to increase renewable generation by providing assistance such as subsidies for power energy bills [1–4]. Utility size microgrids are one of the best methods to increase renewable penetration.

A co-located wind-solar farm in the format of a microgrid, which has some local loads, is one of the solutions that has been proposed to increase renewable power. Such microgrids can operate in both large utility scale grid-connected and small-scale islanded formats. Increasing renewable plants and microgrids in the grid has raised expectations of utility operators with respect to voltage and frequency support. In this chapter, the proposed real-time management is developed and investigated for a co-located wind-solar farm, which is assumed to be a part of a future microgrid to indicate performance improvement in terms of voltage-reactive power control for a remote point of a grid. For this example, a Petri Net without PSO optimisation is used for the purpose of voltage control, while the effect of the Petri Net and the new data class model is investigated in the same example. The wind-solar farm has been selected as there were no real microgrids available to implement the model. The wind-solar farm can be assumed to be part of a utility size MG.

5.2 Problem

The compliance of reactive power support from grid-connected microgrid and wind-solar farms have become very strict. For instance, the Australian Energy Market Operator (AEMO) needs some plants to respond to a voltage change with a settling time of five seconds and a rise time of two seconds. This is a short time for a microgrid

to respond, and to achieve this, the controllers such as the PI controller have to be tuned to be very aggressive. In some networks, which are strong enough, this over-tuning might cause oscillations. Meanwhile, a large proportion of these settling times of two or five seconds are consumed by measurement or communication between the control elements.

Normally, a microgrid with a wind farm, such as MW utility size plants, are required to be controlled in droop control mode at the Point of Connection. This conventional control strategy was primarily developed for remote points on the grid, where there was no access to communication facilities. These days utility and transmission companies still use voltage droop as the main control method, even though there communication links to the majority of the power plants do exist.

Conventional droop control brings some advantages and drawbacks. These have been discussed in previous research, but this chapter attempts to explore it in more detail using field implementations.

The authors of [5] have conducted analysis to match a curve that can fit the Q-V model to be able to control the voltage of a wind farm at a POC. They investigated two wind farms located in Canada, and accordingly found that reactive power and voltage at the POC can be nonlinear. The matching curves followed different trajectories at different voltage levels. Despite investigating in depth [5], the reason for this nonlinearity was not discussed, and a solution not proposed.

Chia- Tse Lee et al. in reference [6] considered various impedances for each feeder line and proposed Q-$\dot{V}$ with V restoration [6, 20]. This new approach is proposed by reference [6] because the conventional droop strategy does not consider the different impedances of the line or POC, and at each voltage the same amount of reactive power is requested by the grid of the microgrids or wind-solar farms [6, 20]. The authors of references [7] and [8] review the effect of the adaptive virtual impedances for enhancing reactive power dispatch between sources, as this method can enhance the voltage control more accurately at the POC.

Many other studies have also been published on the control method utilising communication links between the power system control elements such as the Power Plant Controller (PPC), inverters and the dispatch centre [7–16], and a few of them have been successful in presenting an effective method. For example, the proposed strategy in reference [11] and [12] shows improvement on reactive power sharing;

however, it specifies that fast communication be established between the control elements within 16 ms. This time delay for control elements, which are physically distant from each other is not practical using the existing industrial control communication protocols.

On the other hand, the majority of the control methods considered in the extended literature of this thesis, were considered as a decentralised droop control strategy. While the control scheme of the utility scales in renewable microgrids [17–19], which is the area of this thesis, are centralised. In utility size renewable MGs, the network operators communicate to a single plant controller, which is responsible for all the control aspects. Therefore, there is a lack of comprehensive research in the literature integrating large renewable microgrids.

This chapter develops, simulates and analyses the advantages and disadvantages of the conventional voltage droop control for a real wind-solar farm located in NSW, Australia. This wind-solar farm is selected as the size is appropriate for a utility size MG investigation. It should be noted that as there is no need for a PSO in this case study; the optimisation part is disabled for this example and only the Petri Net and new communication data exchange are applied for this wind farm. In addition, a new voltage control method is proposed, and it is considered as the dynamic of the system. The proposed strategy and platform are simulated in MATLAB and are implemented to expand the contribution of renewable microgrids (wind-solar farm in this study) in the voltage control of remote points in utility grids. The results of the study, along with the limitations of both the conventional droop and the proposed methods from theory and perspectives, are then discussed.

5.3 Voltage Control of a Wind-Solar farm in or outside a Microgrid

5.3.1 Droop Control Strategy

Conventional V-Q droop control is discussed in detail in [5, 20–21]; however, the simplified version of it is equation (1). In this formula, the transmission line is assumed to be lossless, or in simpler terms, resistance of the line is equal to zero. Therefore, for the mainly inductive line:

$$V_{ref}^{t} = V_{rated} - K_{dr}\,(Q_{rated} - Q_{measured}^{t}) \quad (1)$$

"Where K_{dr} is the droop magnitude coefficient, V_{rated} and Q_{rated} are the rated voltage and reactive power, $Q^{t}_{measured}$ is the measured reactive power at time *t*, and V^{t}_{ref} is the voltage reference at time *t* [5]" [28].

It should be noted that K_{dr} plays a significant role in this equation and most of the time displays a relationship with the impedance of the power line and POC transformers. As can be seen, this formula has a droop coefficient as a constant number; however, this value shall be updated in different conditions of the network or the generation plant such as the current reactive consumption of the grid or current apparent power flow at the POC.

The formula in equation (1) is the most common way of writing the droop control; however, this chapter uses equation (2) as it is exactly how it has been implemented in the case study wind-solar farm located in NSW, Australia. This formula is the relationship that is typically requested by AEMO for Australian renewable plants such as MGs with independent wind or wind-solar farms [17–19]:

$$Q^{t}_{ref} = \frac{1}{Z\%} \times \frac{\left(V^{t}_{ref} - V^{t}_{m}\right)}{V^{PoC}_{wf}} \times S^{PoC}_{wfsf} \quad (2)$$

…where V^{PoC}_{wf} is the nominal voltage of the POC for the wind-solar farm, Q^{t}_{ref} is the reactive power required at the POC, S^{PoC}_{wfsf} is the size of the plant on the basis of the plant's nameplate, V^{t}_{ref} is the voltage reference dictated by the NSP and V^{t}_{m} is the voltage measured at the POC. In this formula, Z% is the transformer impedance in the percentage, which is provided by the transformer manufacturer data sheet. The droop gain can be set to be more or less aggressive depending on the network characteristics, wind farm characteristics and POC system strength.

Typically, the renewable MGs have two levels of control. One is the MG, which in this case is called the park controller or farm controller, and the other is at the turbine and/or inverter level. Both controllers are usually PI-based controllers such that the higher-level control loop is the outer loop and the turbine/inverters are called inner loops. Since the focus of this study is at the MG or farm level, the inner loop control is explored less and is assumed to be the same for the conventional droop controller and the proposed real-time management platform.

Figure 5.1 indicates the control BD of the droop control for the wind-solar farm considered in the case studies in this thesis.

Figure 5.1 shows that there are two time delays in the control system of the Wind-Solar farm. The feedforward time delays is represented by z^{-n}, which causes late delivery of the reference command from the out-loop controller to the inner loop control inverters in the wind-solar farm.

The feedback time delay of the control loop is z^{-m}, which generates an unwanted delay in the delivery of the measured variables, including but not limited to the availability of the inverters/turbines, active-reactive power and voltage. These time delays are indicated in the time domain because the programming of the PLCs is all discrete based.

The consequences of time delays in a power system are discussed here to highlight the importance of considering these delays and enhancing them using a real-time adaptive management platform:

- z^{-n} which is the time delay in the feedforward path has direct consequences on the control of the plant. For example, if z^{-n} is 200 milliseconds, the same time delay of 200 ms will be seen in the data exchange from the main controller to the individual inverter controllers of the MG of, in this instance, the wind turbine and solar farm. When this time delay is embedded in the system, the controllers have to become more aggressive to be able to compensate for the signals that are lagged. Designing the controllers to be more aggressive can potentially increase the chance of instability, especially in smaller networks or remote networks, which are the focus of this chapter. For instance, aggressive tuning can increase overshoot or create oscillation [23–14, 28].
- Time delays in the feedback loop can also cause oscillatory behaviour or in more severe cases makes the system unstable [23–24].
- Power quality can also be affected by time delays in the feedback of the controller. For example, the harmonic distortions can increase when the time delay in the feedback is increased [25–26, 28].

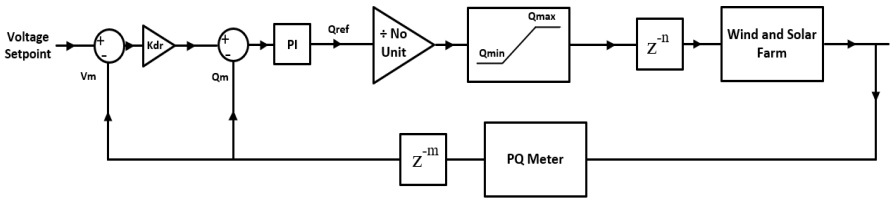

Figure 5.1 Conventional Voltage Control Block Diagram [20]

Figure 5.1 shows the overall layout of the conventional droop control, which is dictated to the MGs or renewable wind-solar plant. This layout appears as a voltage control; however, considering equation (2), the functionality of the droop controller as a control method practically works as reactive power. Please note that:

- As previously noted, the conventional droop control was initially proposed to assist in controlling the frequency and voltage of the power plants, which had no communication with the network operators or the dispatch centre. These days there it is possible to establish data exchange with all the power plants.
- Secondly, the industrial communication protocols currently used in the power industry are not fast enough in such way that MGs can use them to adaptively control the varying voltage setpoint for different levels of fault in the grid.
- More importantly, in the existing control method, some proportion of the reactive power capability of the plant is ignored due to an inappropriate droop ratio during the fault. The droop controller cannot tell how much reactive power is available and how much loss is expected at the time of the fault. This highlights the need for a more sophisticated real-time adaptive method of power management.
- As is seen in figure 5.1, the PI controller controls the reactive power while the outer loop is the voltage of the POC at the remote points in the network. Therefore, the reactive power PI controller can never be accurate for the purpose of voltage control. The simulation and the field data will be presented in later sections to explore the abovementioned issues. [28]
- If the voltage of the MG at the POC is not controlled accurately, it can affect the reactive power capability of the power sources such as the wind turbine or solar inverter, as they are significantly dependent on the voltage of their terminal connection point.

5.3.2 Wind-Solar White Rock Model

White Rock is a renewable plant located in NSW and connected to the Transgrid network at Inverell-Glen Innes, and is selected to be modelled in this study because it has two sources of renewable energy and some local loads. This plant has not been registered as an MG; however, from the perspective that this thesis, it can behave like an MG. White Rock has 70 wind turbine generators as well as 8 solar farm inverters connected to a 33kV bus. This 33kV bus is connected to the utility grid through a 33/132 kV transformer with a rating of 183 MVA. The single line diagram of the plant is shown in figure 5.2.

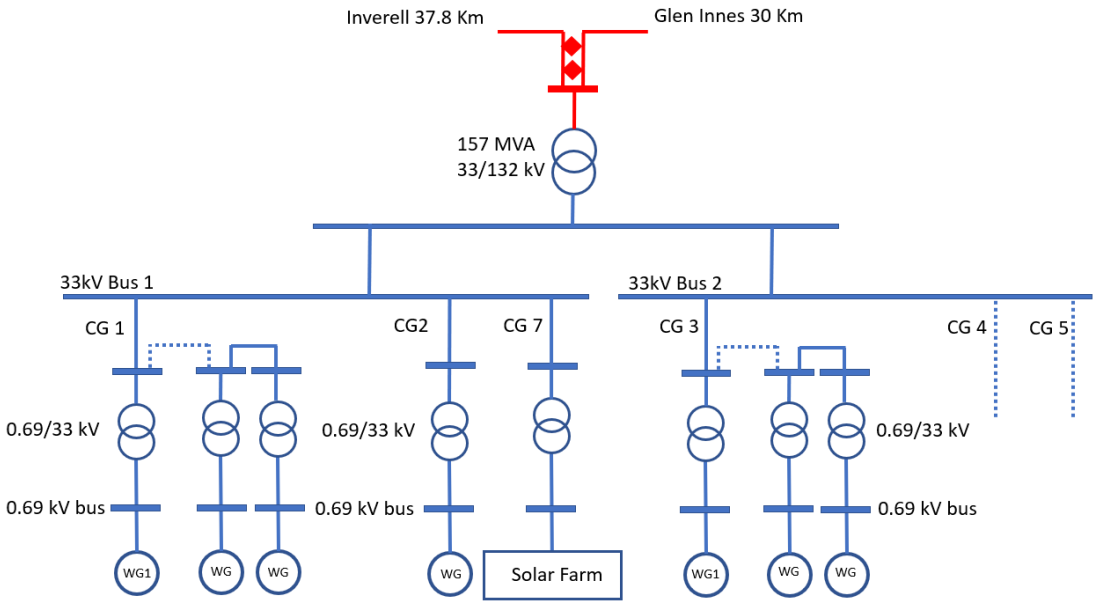

Figure 5.2 Simplified Single Line Diagram of White Rock Solar Wind Farm used for the Simulations and Field data Measurements

The 70 turbines are rated at 2.5 MW and 8 Solar inverters are 2.75 MW but operating at 2.5MVA in the White Rock Solar Wind Farm. This farm has a capacity of 172.5 MW power export at POC. The POC main transformer impedance percentage is approximately 12%. Therefore, the voltage droop coefficient is conservatively calculated in (3) [28].

$$K_{dr} = \frac{1}{Z\%} = 8.33 \quad (3)$$

$$\text{Droop Ratio} = K_{dr} = \frac{\%Q}{\%V} \quad (4)$$

Equations 3 and 4 indicate that droop gain is 8.33. This means that for every 1% step change in the voltage at the POC, there is an 8.33% change in reactive power to control the voltage. Droop gain is a constant number and does not take the reactive power consumption of the main transformer at different voltage levels into account, and is not adapted to the power flow of the POC.

The proposed adaptive method provides more accurate voltage control and it also makes the renewable plant able to control the voltage of a certain part of the network more precisely. This is a significant advantage for a remote utility connected MG. This method is proposed to the grid operator for improved coordination of the MG and renewable plants in the network. Currently, each power plant is responsible for its pro rata demand for reactive power to stabilise network voltage. Therefore, the voltage of the MG (or wind-solar farm) is highly dependent on the other power plants., This impact on the reactive power may also impact active power depending on the P-Q priority configuration of the power plant.. Additionally, if utility size plants including MGs are physically distant from the rest of the network, the reactive power support from other sources for this POC may be insufficient.

Moreover, the POC transformer has significant reactive power consumption. This reactive power consumption has two main components. One component is constant and independent of voltage and power flow at the POC, while the other component varies based on power flow and voltage at the POC. Also, when a plant is proposed as an MG it might have some local loads that can restrict operating specifications, which need to be facilitated by more accurate voltage control.

5.3.3 Adaptive Petri Net for Virtual Impedance Voltage Control Equipped with Fast Communication

A Petri Net with the structure explained in table 5.1 has been developed to show high-level voltage management. As explained previously, the places represent the status of the system which in this case are the voltage control status of the wind-solar farm. The transitions are the conditions programmed and arcs show the move from one status to

another. The example below shows the wind-solar farm just it had transition 2 (t2) met and has moved to p2. This simply means that the measurements and calculations of the system are done and the Voltage Management Platform (VMP) is comparing virtual impedance and voltage to see whether they have changed enough to be out of the dead band zone. In this case the dead band has been configured as 400 Volts at 132kV bus.

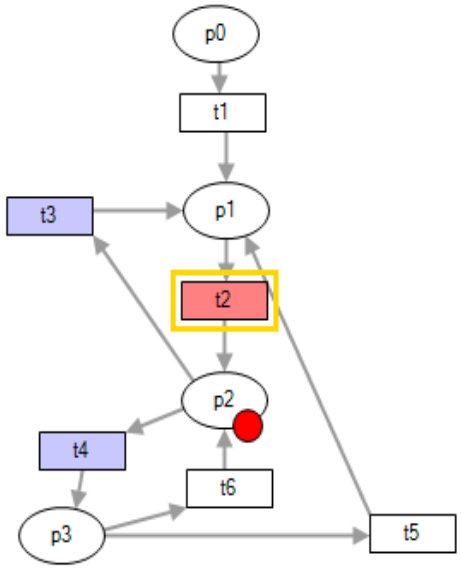

Figure 5.3 Voltage Management Platform Petri Net [28]

Table 5.1 Petri Net Configuration Elements [28]

Symbol	Definition
p_0	Starting the process and turning the inverter and controllers on
p_1	Measuring V&Q and Calculating X
p_2	Comparing Voltage and X to previous Value
p_3	Calculate Pref and send to Inverters
t_1	Elements are Healthy
t_2	Measurement and Calculation are completed
t_3	The Change is within DB
t_4	The Change is Not within DB
t_5	Pref is delivered to Inverters and Voltage is achieved
t_6	Pref is Not delivered to Inverters OR Voltage is Not achieved

5.4 Real-time Adaptive Petri Net Applied to Control the Voltage of the Wind-Solar Farm

5.4.1 Proposed Voltage Scheme

Conventional V-Q droop control does not provide accurate voltage control to the POC of an MG for few reasons, which are reviewed in section 5.4. Two of the discussed reasons were that it does not consider the current operating voltage and current power flow at the POC. This is expected to be addressed using the real-time management equipped with an adaptive Petri PSO and fast communication. The proposed voltage control equipped with fast communication has the following advantages.

"It proves that the utility scale renewable plant can be the master voltage controller of a certain part of the grid more accurately.

More significantly, it is proposed to bring independence to the renewable plant for voltage control of a certain part of the grid" [28].

In all the research in the literature presented in this thesis, only a limited number of them discuss Virtual Impedance in decentralised mode. Utility size MGs, wind farms or solar farms, need to be controlled in a centralised mode and the MG or farm controller is responsible for the whole plant performance [28].

Between every two parts of the power system network there is an impedance due to the nature of the elements of the power system. In the example considered in this case study the impedance between White Rock wind-solar farm at the POC and the Inverell network is shown in figure 5.2 in a simple format. This includes the impedance of all the transformers, feeders and all other power elements including LV and HV. This impedance can be different under different conditions of the grid both at load and generation ends. Moreover, when the generation of the farm varies, the reactive power consumption of the transformers changes because there are more losses in the full load transformer than non-full load transformer. Therefore, a dynamically changing virtual impedance is utilised to represent the value of the impedance when it changes.

It should be also mentioned that as the HV lines, which include the large transformers, show significantly more inductive behaviour than resistive (X>>R), the whole network is taken as inductive rather than resistive to simplify the modelling. The X component in figure 5.4 can change and represent the Virtual Impedance of the POC that the Wind-Solar farm faces at each given time of the operation.

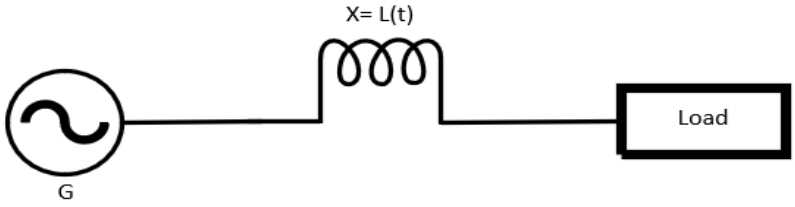

Figure 5.4 Simplified Network-Farm POC Model [28]

When the reactive power consumption of grid elements, such as transformers, change, the Petri Net updates the value of the virtual impedance. This virtual impedance is simply calculated based on the voltage and reactive power measured at the POC, which is provided on the IEC 61850 data exchange. This virtual value is calculated between every instance that the data is provided by the IEC 61850 protocol. Therefore, the accuracy and speed of sampling play a key role.

Virtual impedance is calculated between two times as:

$$X_{gr} = \frac{\Delta V}{\Delta I_q} = \frac{V_{t2} - V_{t1}}{\frac{Q_{t2}}{V_{t2}} - \frac{Q_{t1}}{V_{t1}}} \quad (5)$$

"Where X_{gr} is the equivalent virtual impedance of the network, I_q is the reactive current component, V_{t1} , V_{t2}, Q_{t1} and Q_{t2} are voltage and reactive power of the POC at time *t1* and *t2*.

From (5), when a new amount of reactive power is needed from the plant; the voltage, reactive power and impedance values are simply substituted into the same equation, which is expressed in (6)" [20].

$$Q_{ref,t3}^{PoC} = \left(\frac{V_{ref,t3} - V_{t2}}{X_{gr}} + \frac{Q_{t2}}{V_{t2}}\right) \times V_{ref,t3} \quad (6)$$

In equation (6), $Q_{ref,t3}^{PoC}$ is the reactive power required to provide the voltage of the POC, at t3. The value of this method is that if the network condition has changed between *t2* and *t3*, it will be captured through the voltage and reactive power measured at the POC. Should the impedance of the network change, the reactive power required also changes; however, fast communication is required for the data transmission between the control element and the supervisor of the plant [28].

5.4.2 Proposed IEC 61850 Data Exchange Layout

In the proposed model, every device supports IEC 61850 using a deriver that communicates with other IEDs or other devices which support IEC 61850. The communication between the control elements, such as farm controllers, turbine PLCs and inverters, are established between their IEC 61850 drivers rather than conventional industrial protocol ports. Using this layout, the time delays are reduced from the range of a couple of hundred milliseconds to a few milliseconds [28].

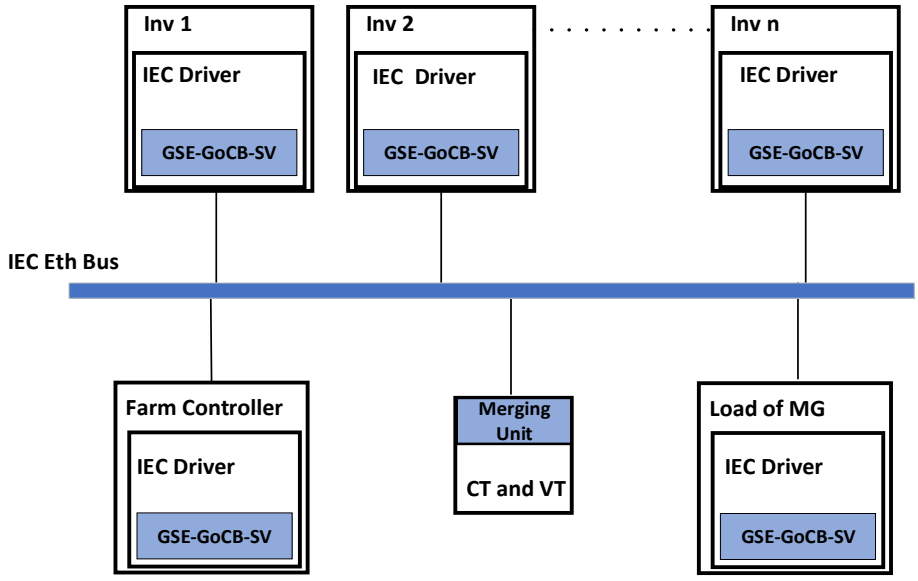

Figure 5.5 The Proposed Overall Communication Layout [28]

5.5 Simulation and Results

As the case study has been selected to be grid connected, and voltage support is critical for utility scale grid connected MGs and renewable plants, this chapter focuses on the real-time adaptive voltage control. Voltage step responses are also one of the biggest benchmarks of power plant commissioning in all Hold Point (HP) tests. Typically, for the negotiated access standard of wind-solar based microgrids or other MG plants the rise time and settling time in the event of a 5% voltage change at the POC are within 2 and 5 seconds. In practical applications, this is agreed in the plant's Generator Performance Standard (GPS). In the case study of this chapter, both simulation and

field case studies consider the cases for 5%, which require 2 seconds of rise time and 5 seconds of settling time.

The definition of the rise time and settling times can vary from one country to another; however, the Australian NER defines rise time as the time in which the voltage and reactive power change between 10% to 90% of its whole change range in a single step response, and settling time being the time between when the step change occurs and the voltage and reactive power is damped within 10% of steady state [27–28]

All the simulation case studies are performed in MATLAB and the model presented in figure 5.1 is used for all the simulation case studies [28].

5.5.1 Simulation Results

5.5.1.1 5% Voltage Drop control using Droop Control and Virtual Impedance in full load Transformer and normal R/X ratio

An infinite voltage bus at t=2 is configured to have a 5% voltage drop to indicate the performance of the conventional droop for this change. Figure 5.6 shows the voltage has recovered to approximately 3%. This is while only 0.85pu of each turbine reactive power capability has been requested by the droop controller. This calculation of the required reactive power does not consider the increase of the reactive power consumption by the transformer at a higher voltage, and greater power flow is not considered in the conventional droop strategy.

This section also reviews the performance of the proposed method using virtual impedance implemented on the Petri Net in the event of a 5% step change on the voltage at the POC at t=2.

The figures below show a comparison between the results achieved by conventional droop and virtual impedance for 5% step responses applied on the voltage of the POC.

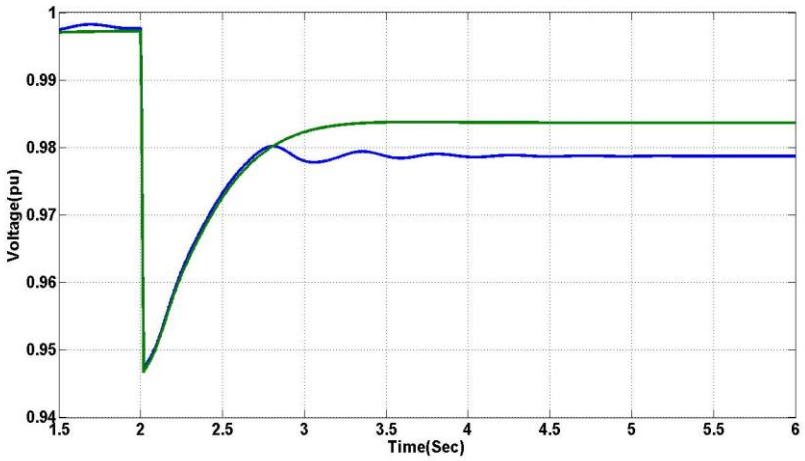

Figure 5.6 Plant Voltage Response using Droop ▮ and Virtual Impedance ▮

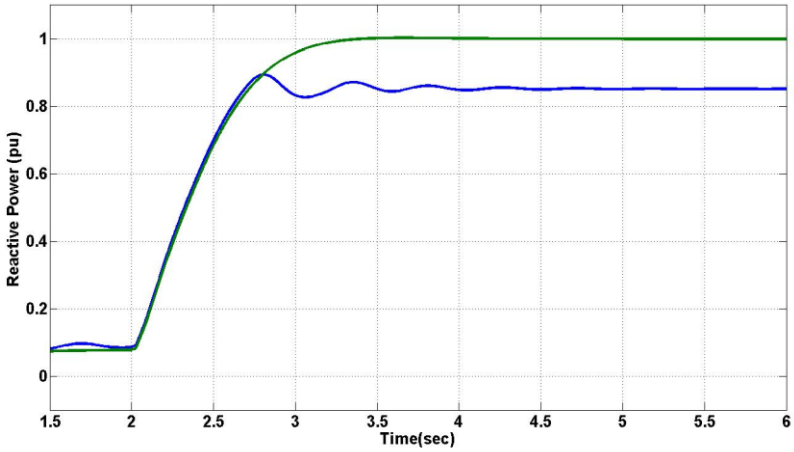

Figure 5.7 Turbine Reactive Power Response using Droop ▮ and Virtual Impedance ▮

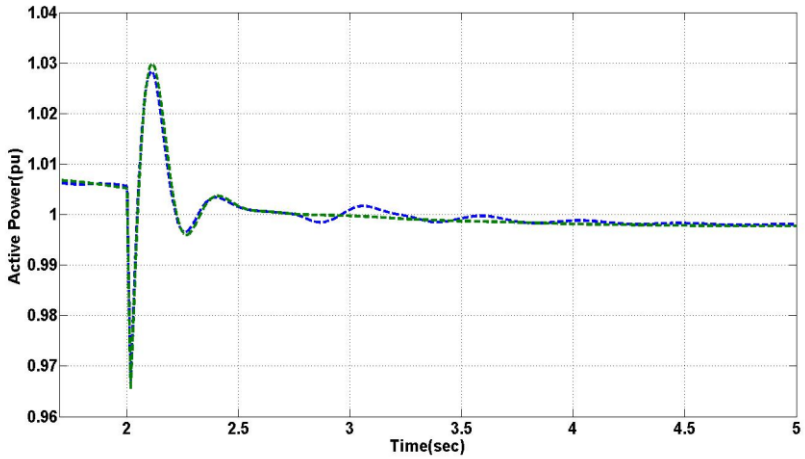

Figure 5.8 Plant Active Power at POC Droop ▮ Virtual Impedance ▮

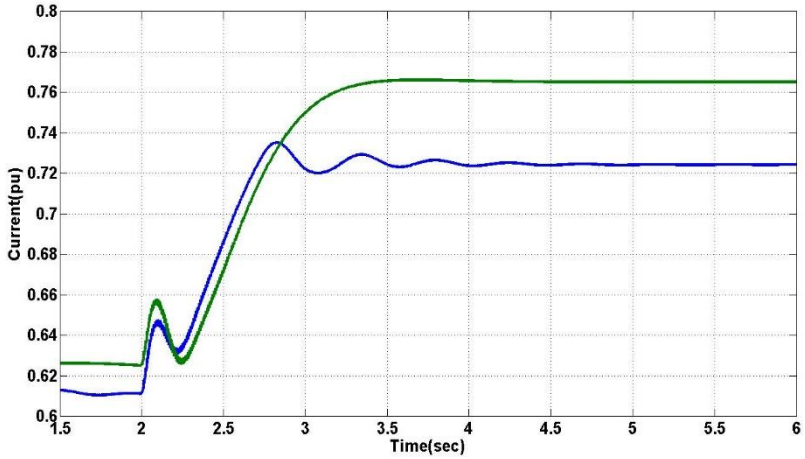

Figure 5.9 Turbine Current at Terminal Droop Control ▮ Virtual Impedance ▮

- While both figures indicate compliant behaviour with respect to the National Electricity Rules of Australia, the response to a 5% step change using the virtual impedance proposed method equipped with fast communication is faster than the result achieved by conventional droop control. This is while droop has been well tuned.
- It can also be seen that the steady-state error is smaller than that achieved by conventional droop control at 0.984 pu. As the 5% step response is a significant change

in the voltage of the farm, the impedance calculation requested the full reactive power capability of the wind turbines which is 1pu, whereas in the same condition the conventional droop control requested less reactive power.

- Figure 5.8 illustrates an instantaneous drop in the active power, which is caused by the significant drop in voltage. However, this is compensated by adjusting the active and reactive current of the turbines. The wind turbines are configured in the Q over P priority and as soon as a large gap is seen in the park controller, the reactive power commands are sent to the turbines for compensation.
- As can be seen in figure 5.9, the turbine needs to comply with the reactive power sent to the turbine controller (inverter controller); therefore, it increases the reactive current first to recover the voltage. However, as the DC bus of the turbines changes instantly, and it is prioritised to recover, it settles down to an acceptable level away from the nominal voltage (1050 V). Followed by the recovery, the turbine generates more reactive current. This is the phenomena seen in figure 5.9 from t=2 s to t=2.5 s.
- The internal control method of the turbines can be modified from one application to another and as the control method remains the same, it does not impact the comparison. It must be noted that the focus of this section is the farm level controller not the turbine level controller.
- Following a major voltage drop, the active power of the turbines drops instantaneously. This causes oscillations in the DC bus of the turbines; however, this DC bus voltage is quickly recovered simultaneous to the reactive power increase. It is observed that by using virtual impedance control, the farm controller demands a greater amount of reactive power from the aggregated turbine and as a result it provides a better compensation of voltage at the POC.

5.5.1.2 Phase to Ground Faults

When the turbines low voltage ride through (LVRT) modes are triggered, they do not follow the reactive power setpoints for the outer loop controllers; however, according to NER they are subject to tolerate the fault while they inject reactive power to recover their own terminal voltage until they exit LVRT mode. Therefore, it is critical to analyse the stability of the plant post fault clearance when the wind turbines switch from LVRT mode to normal farm control mode by exceeding the LVRT threshold.

In this section the behaviour of the wind farm using the aggregated turbine model is investigated in the event of a single phase (phase A) to ground fault. As illustrated in figure 5.10, this fault occurs at the system infinite bus and a shunt is applied to simulate the impedance change of the grid during the fault. The fault in this case study clears in 100 ms. The fault is selected to apply at t=3 s, when the model is completely initialised. The voltage has dropped to 0.6 pu and the turbine LVRT is enabled.

The voltage is almost fully recovered immediately post fault with clearance at t=3.1. The different behaviour of the reactive power is observed from the moment the voltage exits the LVRT threshold. At just after t=3.1, the droop method still exhibits a large error between the voltage measured and the voltage setpoint (1 pu); therefore, it overcompensates the reactive power. There is an undesired spike of reactive power, which can cause significant voltage swing in weak networks, which is the subject of this section and needs to be avoided as much as is practical. Unlike the droop control, the virtual impedance controller closely observes the network impedance and once that has recovered back to normal (after 100 ms), the controller decreases the reactive power of the turbines more precisely in a timely manner. The significant role of fast communication between control elements is clearly observed here.

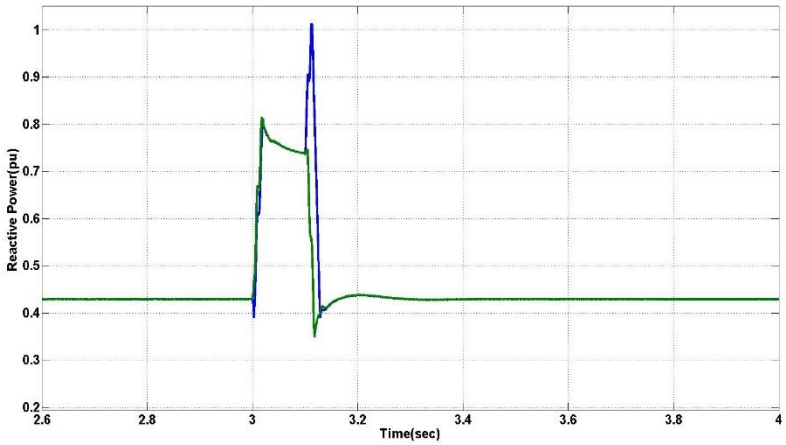
Reactive Power(pu)
Time(sec)
1
0.9
0.8
0.7
0.6
0.5
0.4
0.3
0.2
2.6
2.8
3
3.2
3.4
3.6
3.8
4

(a)

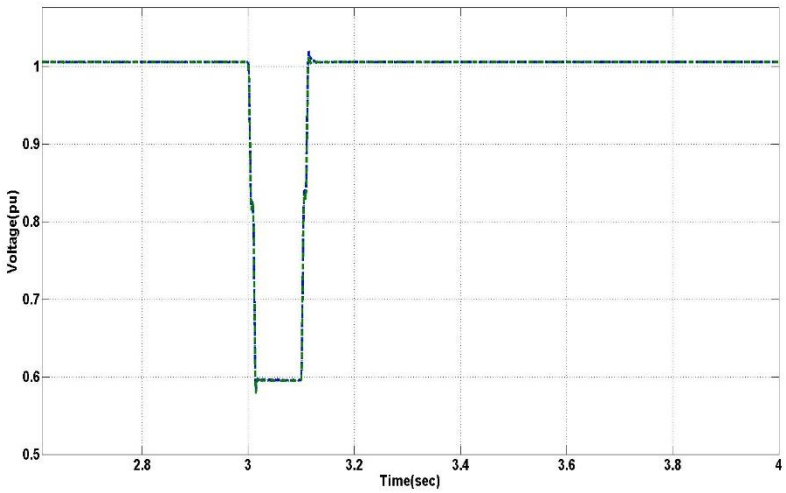
Voltage(pu)
Time(sec)
1
0.9
0.8
0.7
0.6
0.5
2.8
3
3.2
3.4
3.6
3.8
4

(b)

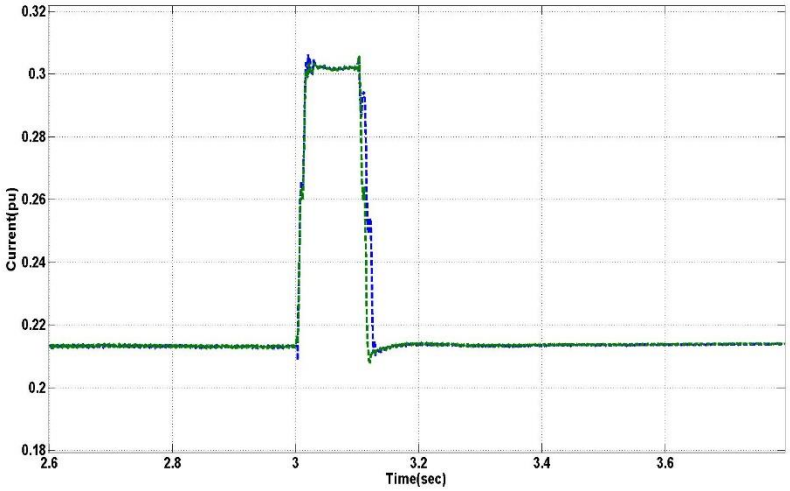

(c)

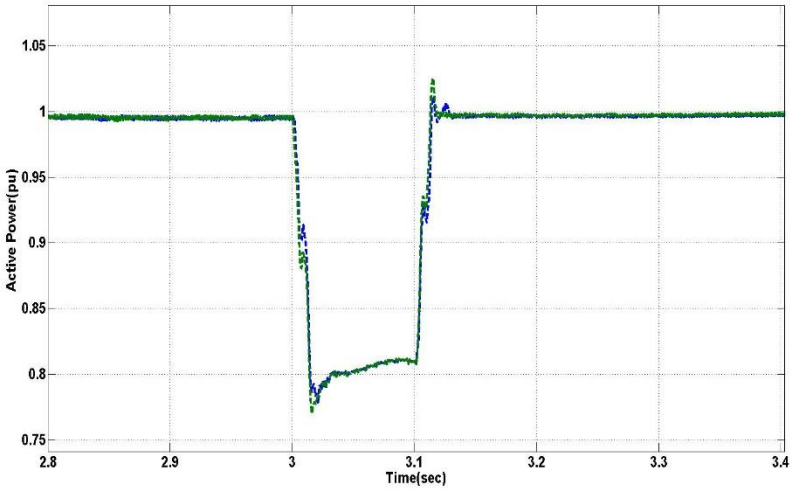

(d)

Figure 5.10 . a) Turbine Reactive Power, b) POC Voltage, c) Turbine Current, d) POC Active Power Droop ▮ Virtual Impedance ▮

5.5.2 Field Test Results

This section presents the results from the simulation and field study for a wind-solar power plant, which can represent a utility MG for this control method investigation. It is understood that an MG can have different features; however, no MG was available at the time of this test to benchmark the proposed Petri Net base control and IEC 61850 base communication protocol. Therefore, the wind-solar farm described above was selected for the test.

5.5.2.1 The 5% Step Response Test at White Rock at a 53MW limit using Conventional Droop Control

Based on industrial practice and the technical requirements of AEMO, all the wind-solar farms need to be commissioned in a few stages. In stage one, there are a few Hold Points, which refer to different levels of power production. The data from the test in this chapter are the farm HP1 when the farm was only allowed to operate at 53 MW. This was approximately a third of its capacity.

Figure 5.11 indicates the performance of the White Rock plant in response to a 5% voltage variation using the droop control method equipped with conventional communication protocols.

Clearly, there is a half a per unit overshoot and a settling time of about 4 seconds. Both features are compliant with the grid standard agreed in its GPS. Some voltage ripples are also noticed in the reactive power shown in figure 5.11, which will be discussed further.

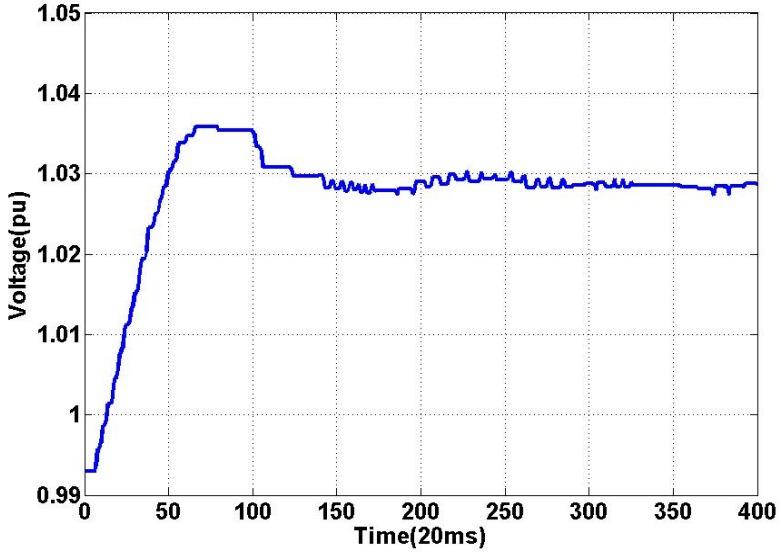

(a)

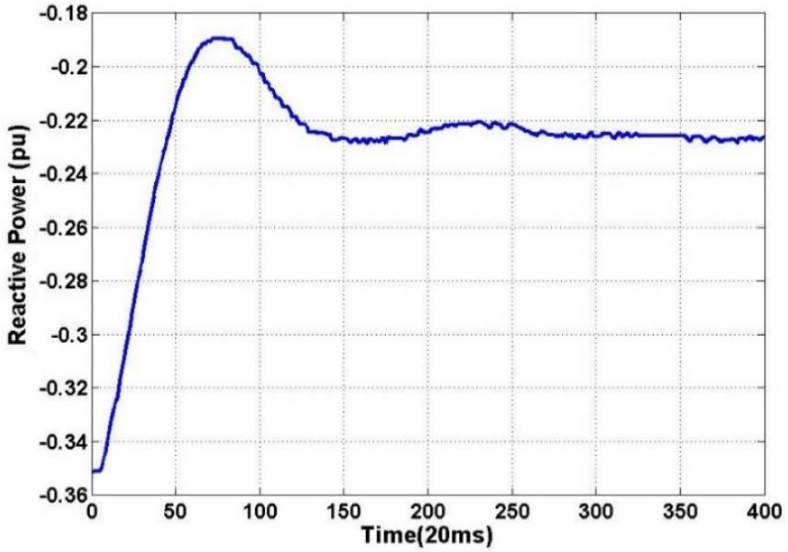

(b)

Figure 5.11 WRWSF plant response to a 5% voltage setpoint change using droop control (a) POC voltage, (b) individual wind turbine

5.5.2.2 The 5% Step Response test at White Rock at a 53 MW Limit using Virtual Impedance Control

Figure 5.12 illustrates the performance of the White Rock farm in response to a 5%

voltage setpoint increase at the POC at the HP1 (53 MW) range of production utilising the new control method. This 5% is applied to increase the voltage from approximately 1 pu to 1.05 pu and a faster response and significantly better transient response in terms of overshoot is observed.

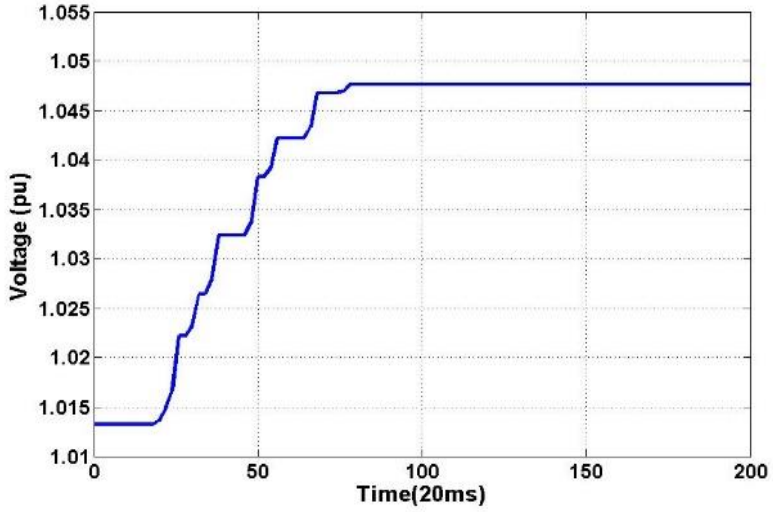

(a)

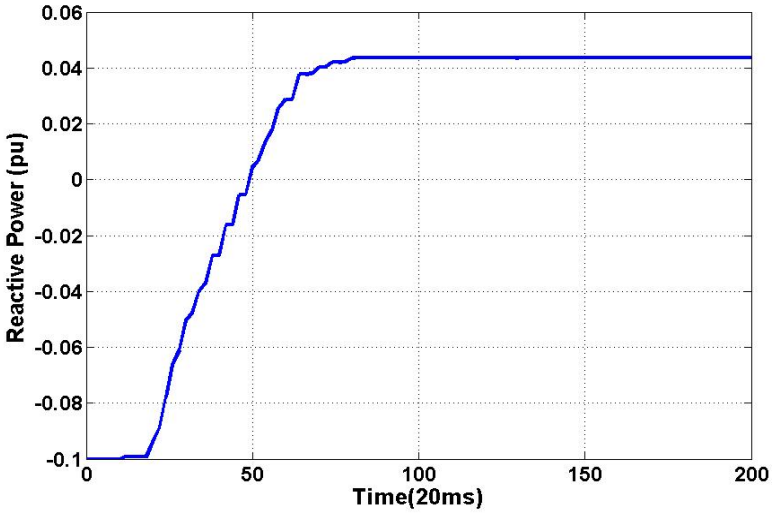

(b)

Figure 5.12 WRWSF Plant Response to a 5% Voltage Setpoint Change using the Virtual Impedance Method (a) POC Voltage, and (b) Individual Wind Turbine Reactive Power [28]

5.5.2.3 *Capacitor Switching Test*

In this test the comparison is performed to explore the difference between the new proposed method and conventional droop control. For this test, a 10 MVAr capacitor bank switched in, remained in for some time and then switched out. Figure 5.13 shows the performance of the system according to both the conventional and the new method.

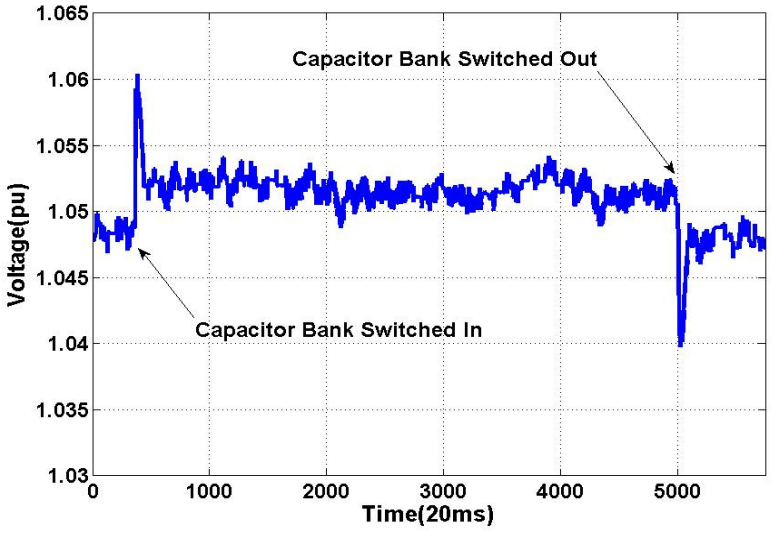

(a)

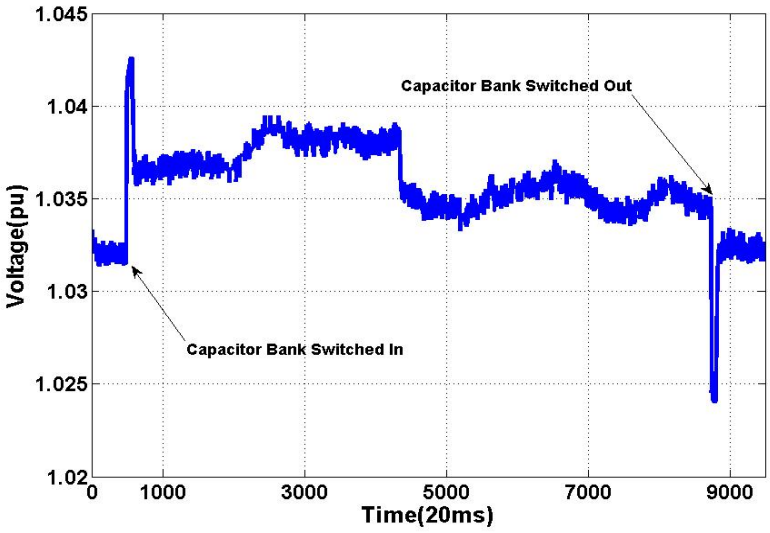

(b)

Figure 5.13 WRWSF Plant Response to Cap Switching in the Network Using (a) Droop Control, and (b) Virtual Impedance Control [28]

There is no significant difference between the transient response of the two control schemes; however, the steady-state in the voltage controlled by virtual impedance appears with less fluctuation. This is while the ripples and fluctuations in the voltage with the droop controller could have been caused by many other factors, as this was not significant under other conditions. Therefore, the ripples could have caused by grid elements at the time of the test. The location of capacitor bank used in this test was several kilometres away from the farm (refer to figure 5.2). Therefore, the actual reactive power step magnitude delivered to WRWSF was less than 10 MVar.

Figure 5.14 a) and b) show some of the equipment used in the Goldwind farm to implement the logic including the SCADA, VMP panel and IEDs [28].

(a)

(b)

Figure 5.14 WRWF Substation Equipment; (a) VMP and SCADA Systems, (b) Substation Automation and IEDs Proposed to be used in the Presented New Communication Platform.

5.6 Conclusion

This chapter has presented the implementation of the Adaptive Petri Net equipped with the fast communication protocol discussed in previous chapters. The fast communication platform assists the proposed adaptive Petri Net to achieve an enhancement of the voltage control of MGs in the remote area of the utility grid. This chapter has presented the results of the simulation and field implementation of the conventional and the new voltage control method for a 5% step response. The two control methods are also compared for a 10 MVAr capacitor switching that occurs in the grid.

The droop control method is well recognised and currently utilised in many grid-connected utility scale MGs and renewable plants such as wind farms and solar farms. The second method is proposed to be used with an adaptive Petri Net to control the voltage in certain remote parts of the grid. This method is particularly proposed for

microgrids that are significantly inductive. However, as no MG was available to see the impact of this method, a wind-solar farm was chosen as a substitute to implement this control scheme equipped with the new fast communication method.

The fast communication was only used between the measurement device and the main controller and because the inverter was not equipped with IEC 61850. The conventional Modbus TCP was used for the communication between the inverters and the VMP. The results show a significant improvement, and therefore the proposed data exchange is recommended for implementation on all inverters, so that a more significant improvement can be observed. Moreover, the proposed voltage control can only be practically guaranteed if all parts of the communication network become IEC 61850 bases and, in this case study, due to physical limitations on the operational system, the inverters could not change to support the proposed IEC 61850 protocol, although the simulation part of the study used and validated the functionality of the proposed IEC 61850 data type.

Nevertheless, the virtual impedance control method has been completely implemented and tested. The main outcomes from the Simulink and field studies are:

- The proposed virtual impedance strategy provides a fast response for reactive power and voltage compensations. The proposed voltage control scheme using fast communication and with access to the virtual impedance of the point of connection could also minimize overshoot. Less error in the steady state was observed as more of the farm's reactive power capability was used.
- The conventional fixed-ratio droop controller does not consider the variable reactive power consumption of the POC transformer. The proposed method equipped with fast communication resolves this issue by continuously and quickly updating the level of reactive power and the virtual impedance of the grid.
- The two methods indicated a satisfactory response for capacitor bank switching transients in the event of small voltage changes from the perspective of rise and settling times.
- The proposed control method showed a better response to larger disturbances, but this can be significantly improved if all parts of the communication network support the proposed IEC 61850 data model. This method can only be enhanced if the fast communication can be improved.

5.7 References

[1] M. Hedayati-Mehdiabadi, J. Zhang and K. W. Hedman, "Wind Power Dispatch Margin for Flexible Energy and Reserve Scheduling With Increased Wind Generation," in IEEE Transactions on Sustainable Energy, vol. 6, no. 4, pp. 1543-1552, Oct. 2015.

[2] J. Kiviluoma et al., "Short-Term Energy Balancing With Increasing Levels of Wind Energy," in IEEE Transactions on Sustainable Energy, vol. 3, no. 4, pp. 769-776, Oct. 2012.

[3] J. Liang, S. Grijalva and R. G. Harley, "Increased Wind Revenue and System Security by Trading Wind Power in Energy and Regulation Reserve Markets," in IEEE Transactions on Sustainable Energy, vol. 2, no. 3, pp. 340-347, July 2011.

[4] https://www.cleanenergycouncil.org.au/policy-advocacy/reports/clean-energy-australia-report.html

[5] C. Andalib-Bin-Karim, X. Liang, N. Khan and H. Zhang, "Determine Q–V Characteristics of Grid-Connected Wind Farms for Voltage Control Using a Data-Driven Analytics Approach," in IEEE Transactions on Industry Applications, vol. 53, no. 5, pp. 4162-4175, Sept.-Oct. 2017.

[6] C. T. Lee, C. C. Chu and P. T. Cheng, "A New Droop Control Method for the Autonomous Operation of Distributed Energy Resource Interface Converters," in IEEE Transactions on Power Electronics, vol. 28, no. 4, pp. 1980-1993, April 2013.

[7] H. Mahmood, D. Michaelson, and J. Jiang, “Accurate reactive power sharing in an islanded microgrid using adaptive virtual impedances,” IEEE Trans. Power Electron., vol. 30, no. 3, pp. 1605–1617, Oct. 2014.

A. Micallef, M. Apap, C. Spiteri-Staines, J. Guerrero, and J. Vasquez, “Reactive power sharing and voltage harmonic distortion compensation of droop controlled single phase islanded microgrids,” IEEE Trans. Smart Grid, vol. 5, no. 3, pp. 1149–1158, May 2014.

[8] Y. Zhang and H. Ma, “Theoretical and experimental investigation of networked control for parallel operation of inverters,” IEEE Trans. Ind. Electron., vol. 59, no. 4, pp. 1961–1970, Apr. 2012.

[9] Yu, A. M. Khambadkone, H. Wang, and S. T. S. Terence, “Control of parallel-connected power converters for low-voltage microgrid—Part I: A hybrid control architecture,” IEEE Trans. Power Electron., vol. 25, no. 12, pp. 2962–2970, Dec. 2010.

[10] M. Roslan, K. H. Ahmed, S. J. Finney, and B. W. Williams, “Improved instantaneous average current-sharing control scheme for parallel-connected inverter considering line impedance impact in microgrid networks,” IEEE Trans. Power Electron., vol. 26, no. 3, pp. 702–716, Mar. 2011.

[11] H. Mahmood, D. Michaelson, and J. Jiang, “Accurate reactive powersharing in an islanded microgrid using adaptive virtual impedances,” IEEE Trans. Power Electron., vol. 30, no. 3, pp. 1605–1617, Oct. 2014.

[12] J. He, Y. W. Li, J. M. Guerrero, J. C. Vasquez, and F. Blaabjerg, “An islanded microgrid reactive power sharing scheme enhanced by programmed virtual impedances,” in Proc. IEEE Int. Symp. Power Electron. Distrib. Gener. Syst., Aalborg, Denmark, 2012, pp. 229–235.

[13] J. He, Y. W. Li, J. M. Guerrero, F. Blaabjerg, and J. C. Vasquez, “An islanding microgrid power sharing approach using enhanced virtual impedance control scheme,” IEEE Trans. Power Electron., vol. 28, no. 11, pp. 5272–5282, Nov. 2013.

[14] J. He and Y. W. Li, “An enhanced microgrid load demand sharing strategy,” IEEE Trans. Power Electron., vol. 27, no. 9, pp. 3984–3995, Sep. 2012.

[15] Q. Shafiee, J. M. Guerrero, and J. C. Vasquez, “Distributed secondary control for islanded microgrids—A novel approach,” IEEE Trans. Power Electron., vol. 29, no. 2, pp. 1018–1031, Feb. 2014.

[16] White Rock Wind and Solar Farm Generator Performance Standard, 2018.

[17] Gullen Range Wind and Solar Farm Generator Performance Standard, 2017.

[18] Stockyard Hill Wind Farm Generator Performance Standard, 2018.

[19] C. J. Melhorn and M. F. McGranaghan, “Interpretation and analysis of power quality measurements,” IEEE Trans. Ind. Appl., vol. 31,

[20] K. Turitsyn, P. Sulc, S. Backhaus, and M. Chertkov, “Options for control of reactive power by distributed photovoltaic generators,” Proc. IEEE, vol. 99, no. 6, pp. 1063–1073, Jun. 2011.

[21] IEC 61850-7-1: 'IEC for basic communication structure for substation and feeder equipment Principles and models', 2003

[22] F, Milano., and M, Anghel.: 'Impact of time delays on power system stability', IEEE Trans Circuits and Systems I: Regular Papers, 2012, vol. 59, no. 4, pp. 889-900.

[23] H, Liang., B, J, Choi., W, Zhuang., et al.: 'Stability enhancement of decentralized inverter control through wireless communications in microgrids', IEEE Trans Smart Grid, 2013, vol. 4, no. 1.

[24] N. Aghanoori, M. A. S. Masoum, S. Islam and S. Nethery, "Investigation of microgrid instability caused by time delay," 2017 10th International Conference on Electrical and Electronics Engineering (ELECO), Bursa, 2017, pp. 105-110.

[25] J. Z. Zhou, A. Rajapakse and A. M. Gole, "Effects of control systems time delay on the performance of direct harmonics elimination [power network active filters]," Canadian Conference on Electrical and Computer Engineering 2004 (IEEE Cat. No.04CH37513), 2004, pp. 609-612 Vol.1.

[26] Y. Hu, J. Xiang, Y. Peng, P. Yang and W. Wei, "Decentralised control for reactive power sharing using adaptive virtual impedance," in IET Generation, Transmission & Distribution, vol. 12, no. 5, pp. 1198-1205, 3 13 2018.

[27] NER published by Australian Energy Market Operator.

[28] “Improving Voltage of Remote Connection Using Wind-Solar Farms Equipped with New Voltage Control Strategy Using Virtual Impedance Monitoring Enabled by IEC 61850 Communication” being published in IET special issue journal.

6 CHAPTER SIX: Thesis Summary, Conclusions and achievement

6.1 Thesis Proposal and Implementation Summary

This thesis introduces a comprehensive power management model which covers the following key aspects of controlling a utility size renewable microgrid.

1. High-level supervision and monitoring
2. Power Management
    a. Active Power Management
    b. Stability analysis and control
    c. Voltage control and reactive support
3. Communication architecture

The high-level supervision and monitoring layers of the platform are developed on an adaptive Petri Net, which runs to determine and indicate the status of the plant. The Petri Net has been selected due to its ability to adapt to any complex logic and the simplicity of its implementation on any SCADA platform. The Petri Net also provides a very simple brief of the system to all the plant users in a single view.

The power management and stability of the microgrid are considered in the proposed Petri Net via two streams. This main version of the Petri Net is equipped with CPSO optimisation so the Petri Net is not a conventional Petri Net and is referred to as a Petri PSO. This version of the control system is implemented and discussed in Chapter 4 of the thesis. This thesis for the first time develops a power management system that considers the cascaded impact of time delays on system stability and the impact of system stability on power management.

The Voltage-Reactive control of the microgrid at the POC, is the other stream of the Petri Net. This has been separated from the primary version because of its criticality in terms of reaction time. Normally, the power plant reacts to voltage changes at the POC within 1 second or 2, so there should be no optimisation onto this pathway. Basically, for this pathway of control the PSO is bypassed. The proposed voltage control and this main version is independently captured and explored in Chapter 5 of this thesis.

IEC 61850 communication architecture is also proposed here to equip the proposed management scheme with a fast communication platform. The proposed communication platform is comprehensively discussed in Chapter 3.

6.2 Conclusions and Achievements

6.2.1 Power System Related Conclusion

6.2.1.1 Investigation of the Impact of Time Delays on Power System Performance

In Chapter 3 it was indicated that improving the time delay could significantly improve the phase and gain margin in the microgrid control. For instance, the simulation results show that by improving the time delay from 5 ms to 1 ms without adjusting any other parameters of the system, the phase margin and gain margin improve by 12% and 18% respectively.

It was also discussed that in the real system there are solutions to reduce the impact of time delays caused by the communication system; however, communication is proposed to avoid any cost for the solution. For example, by making a system that responds faster to compensate for the time delay caused by the communication platform, engineers need to tune the controller parameters. Tuning the controller parameters to be more aggressive can cause instability or undesired behaviour such as overshoot or oscillation in the system.

The simulation in Chapter 3 also indicated that improving the time delay enhances the power quality by providing purer sinusoidal waves in voltage and current. Therefore, it is expected that total harmonic distortion is reduced by decreasing the time delay.

6.2.1.2 Petri PSO Power Demand management and Stability

In the case study discussed in Chapter 4, unlike other examples in the existing literature, the minimum communication delay was illustrated as was how the system can achieve such a minimum delay. This time delay was calculated using eigenvalue analysis by considering all the modes of the system. The simulation in this case study shows how increasing the time delay moves the eigenvalues of the system towards the right half plane which is the unstable zone.

This proposed scheme managed to maintain the stability of the microgrid by including an adaptive Petri PSO in the active power management while providing all the necessary microgrid demand from the load.

This study also showed a better response in the DC bus voltage in terms of fluctuation and power output.

6.2.1.3 Voltage and Reactive Power Management Control

The virtual impedance voltage control provided faster responses at the POC with less overshoot. This means that based on Australian NER rules, this method provides better rise time and settling time in a 50% step response, which is the AEMO's benchmark response to a voltage disturbance within the normal operation of a renewable plant connected to the Australian utility grid.

The proposed method equipped with communication platform also provided better steady-state response. This was observed in terms of a smaller steady-state error after the settling time of a 5% step response at the POC. This was achieved using more of the reactive power capacity of the turbine in the event of extreme voltage changes such as 5%.

This method added adaptivity in the amount of reactive power depending on the current reactive power consumption of the grid and POC's transfers. It was shown that conventional droop control does not adapt itself to different levels of active power production. For instance, droop control considers the same reactive power consumption at the POC transformer, while this varies from 50 MW active production to 150 MW active production. Basically, existing methods do not consider the variable component of the transformer's reactive power. This directly impacts the accuracy of voltage control at the POC, which using the proposed method, is significantly improved.

6.2.2 Communication Related Platform Conclusion

The proposed data class for the IEC 61850 standard could make the control system achieve less than 5 ms seconds of delay between any two control elements that supports this standard. For instance, any two inverters, PLCs or merging units can communicate within a few milliseconds, which in the current conventional platforms is only achievable on protection layouts. This fast communication is achievable based on the

proposed communication layout discussed in Chapter 3 by taking the packets from SCSM to the ethernet layer of OSI.

This will enable any inverter or electronic device to communicate with its peer with no need for a media converter, which bypasses all the time delays caused by mediating ware converting one protocol to the other. This can expand the stability margins such as phase margin and gain margin; therefore, the controllers do not need to be tuned aggressively, which in many cases can create undesired behaviour such as oscillatory behaviour, overshoots and others.

6.3 Future Works

This thesis delivery is limited to the materials discussed in chapters one to six; however, the proposed platform has more future research and development. This section briefly explores the future works that are relevant to this project in three main different categories including complete real-time implementation of the platform in a microgrid, studying the effectiveness of the proposed platform at the grid level in relation to enhancing the grid stability and establishing a network security platform for the proposed communication platform.

6.3.1 Implementation of the proposed platform

The field implementation of the proposed platform has been negotiated with one inverter manufacturer. This implementation requires to develop a prototype in a single manufacturing. Once the prototype is completely developed, tested and certified by IEC standard certifiers, the platform can be proposed to all the inverter and automation manufacturers.

The implementation of the proposed platform has the following main aspects:

- Populating the CPSO and generate a modular code. If the CPSO's objective function gets customised to a function that provides the optimal parameters of controllers, the platform can then optimise the response of the plant to the condition. This new condition can be a different SCR of the connection point that dynamically changes.
- Developing the source code into the format that can be integrated with different power system software platforms such as PSCAD which is widely

used in power system industry these days. This will be significantly helpful for the large scale microgrids as it simplifies the integration of the platform to other power system elements such as inverters and plant controllers.

- Populating the Petri Net components of the platform so that it can be simply added into power system software platforms and easily implementable in real-time controllers such as PLCs.
- Extending the data class model to new application. The current data class model has been developed to cover the microgrid applications. Should this platform be extended to wide area power system, the data class model may need to be extended to accommodate the new set logical nodes, logical devices and data attributes.
- Developing a modular communication firmware that can establish the communication between two peers of the proposed data class model of IEC 61850.

Developing these abovementioned codes requires some programming skills such as C code. Additionally, it requires knowledge of other third-party platforms such as PSCAD library for the purpose of integrating these components to the third-party software and hardware platforms.

All the above points are required before the proposed platform are used in industry as a standard tool otherwise the usage will be limited to MATLAB users.

6.3.2 Utilising the proposed platform to utility grid

Once this proposed platform is implemented as per section 6.3.1, a wider range of power system platform will be able to utilise this method. This makes it possible to assess the compatibility of the proposed platform to different generator's model provided by the vendors. This integration will cover two main features of this project. These features include the communication protocol and the Petri PSO.

It is worth noting that implementing these two features can be entirely independent of each other. Therefore, delay in implementing one will not cause any delay to the other component.

6.3.2.1 *Implementing CPSO for grid power system model*

Currently all the grid connected generators to Australia's electricity network have a constant set of control system parameters. These parameters are set to provide the best and the most optimal responses to the minimum fault level determined for the connection point; however, in some parts of the network, the fault level of the connection point can vary during the operation as a result of other changes within the network.

For instance, in some parts of Tasmanian grid, fault levels are significantly dependent on the import and the export power from and to Victoria's network. The generators in these conditions remain unchanged in terms of their controller's configurations. Therefore, the performance of these connection points will not be optimal to the new condition while they may remain compliant. This can be improved if the changes in SCR is dynamically monitored and considered by the proposed platform.

For example, as it was discussed in former chapter, some generators shall provide reactive power support to assist with the voltage disturbances. Some of the responses require to have 2 second-rise time and 5 second-settling time. On the other hand, the connected generators have the controllers with a constant set of gains to comply with agreed constant SCR with the voltage regulator. Under this condition, when the SCR of the connection point changes, the response of the plant to the voltage disturbance changes even with the same amount of reactive power support. Dynamically updating the SCR of connection point and adaptively regulating the controller gains are within the capability of the proposed Petri-PSO and will be considered in the future work of this proposed platform.

6.3.2.2 *Communication protocol within national electricity*

Currently all the control communication elements between the network operators, NSPs and grid generators are based on the conventional communication protocol such as ICCP, DNP3 or Modbus. Based on the discussions in chapter three of this thesis, replacing the old protocols with the proposed data class of IEC 61850 will significantly reduce the time delay.

It is proposed that a new scope of work is defined to develop a network layout for the whole grid that can connect the key elements of the network with such high-speed communication. While this is a large scope of work and requires cooperation from NSPs and network operators.

6.3.2.3 Improvement of the optimisation tool

As suggested in the above section, the proposed Petri PSO platform can be applied to whole grid application. Once this is practically considered, it is expected that the number of the optimisation constraints within CPSO will increase, and the data processing will be largely challenging. To overcome these challenges a new investigation needs to be carried out to ensure the selected optimisation method will satisfy the requirement of the application in terms of response time.

6.3.3 IEC 61850 network security

Once the proposed platform is implemented between different vendors and it becomes a part of a large network infrastructure, it is important to ensure the established communication system is secure. This network security of the proposed communication platform has been out of the scope of this thesis while within the interest of author due to the critical necessity of it.

Establishing proper security is expected to be critical as it shall be in such a way that does not slow an adverse impact on the communication delay.

The author intents that with a corporation from the expert in network security, this perspective of the proposed communication protocol will be further explored and added to the proposed power management platform.

APPENDIX A

List of the items on the proposed data class model for the inverter's IEC 61850 new data class model to Power Plant Controller

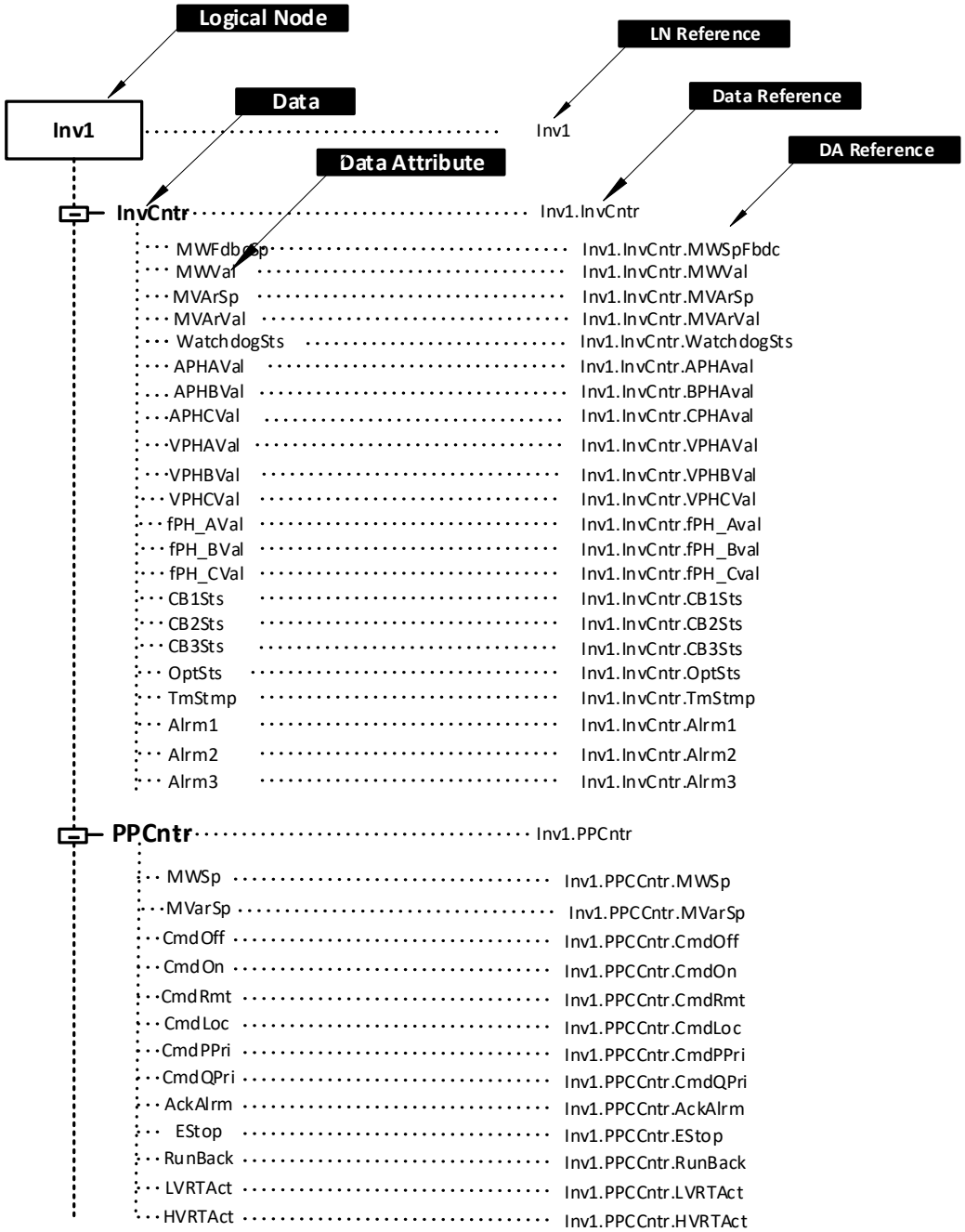

APPENDIX B

List of other supporting papers published or under review for conferences or journals:

1- "Improving Voltage of Remote Connection Using Wind-Solar Farms Equipped with New Voltage Control Strategy Using Virtual Impedance Monitoring Enabled by IEC 61850 Communication".

This paper is the outcome of the results of the case study discussed in chapter five of the thesis and has been published in IET Generation Transmission and Distribution.

2- "Investigation of microgrid instability caused by time delay".

This paper is the outcome of the results of study of time delay in the power systems which was discussed in chapter three. This paper was published in IEEE conference in 2017.

3- "Voltage sag compensation in renewable plant using hydro-pump storage".

This paper investigated the requirement of fast response for reactive power support from a hydro station in the event of grid fault for preventing a wind farm from tripping.

4- "Enhancement of Microgrid Operation by Cascaded Consideration of Communication Delay on System Stability and System Stability on Power Management"

This paper is the result of chapter four of the thesis and has been published in Elsevier-International Journal of Electrical Power and Energy System

APPENDIX C

Every reasonable effort has been made to acknowledge the owners of copyright material. I would be pleased to hear from any copyright owner who has been omitted or incorrectly acknowledged.

Authorship and declaration of the paper published or submitted:

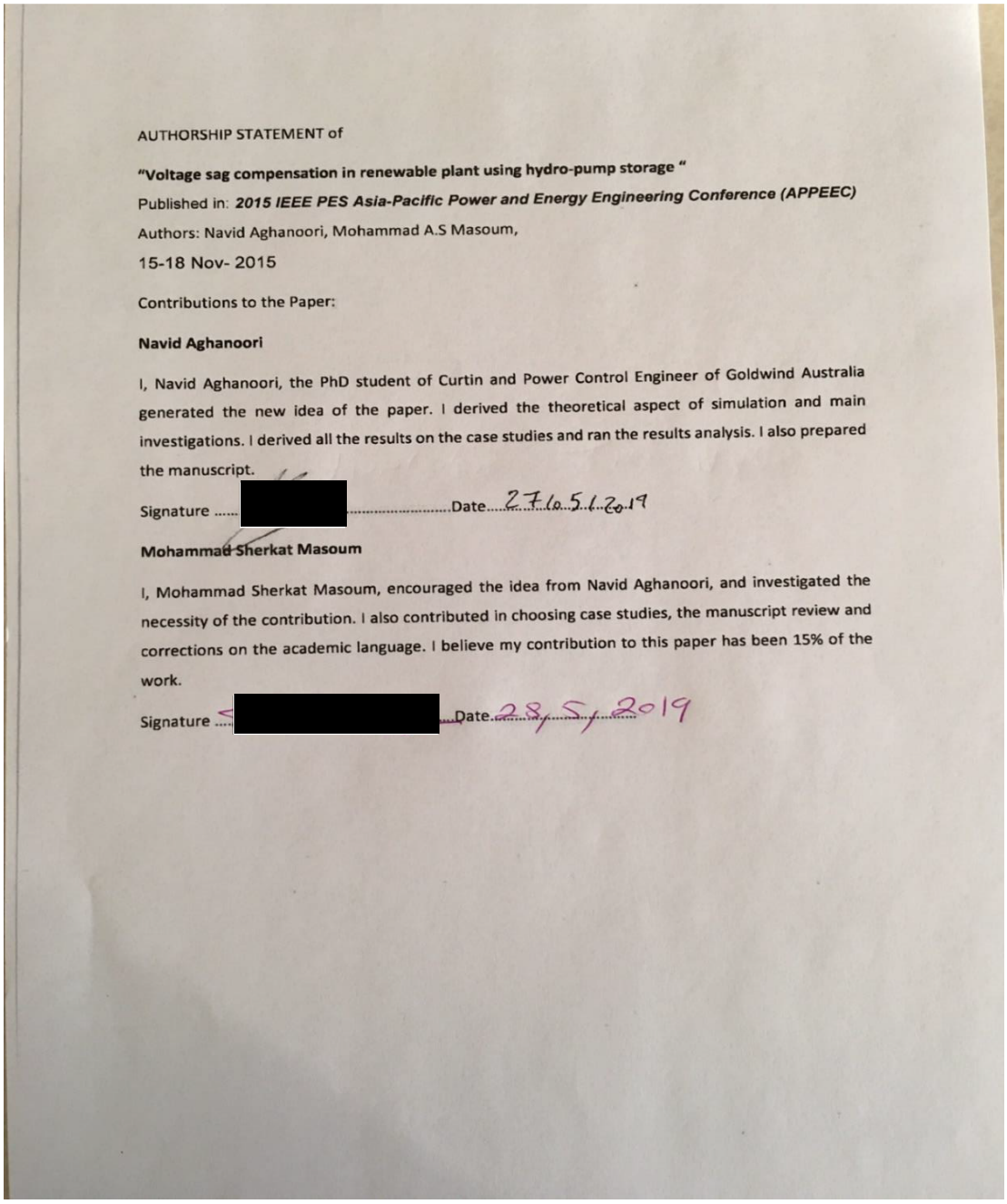

AUTHORSHIP STATEMENT of

"Voltage sag compensation in renewable plant using hydro-pump storage "

Published in: ***2015 IEEE PES Asia-Pacific Power and Energy Engineering Conference (APPEEC)***

Authors: Navid Aghanoori, Mohammad A.S Masoum,

15-18 Nov- 2015

Contributions to the Paper:

Navid Aghanoori

I, Navid Aghanoori, the PhD student of Curtin and Power Control Engineer of Goldwind Australia generated the new idea of the paper. I derived the theoretical aspect of simulation and main investigations. I derived all the results on the case studies and ran the results analysis. I also prepared the manuscript.

Signature [redacted] Date 27.05.2019

Mohammad Sherkat Masoum

I, Mohammad Sherkat Masoum, encouraged the idea from Navid Aghanoori, and investigated the necessity of the contribution. I also contributed in choosing case studies, the manuscript review and corrections on the academic language. I believe my contribution to this paper has been 15% of the work.

Signature [redacted] Date 28/5/2019

AUTHORSHIP STATEMENT of

"Investigation of microgrid instability caused by time delay "

Published at 2017 IEEE conference (ELECO)

Authors: Navid Aghanoori, Mohammad A.S Masoum, Syed Islam, Steven Nethery

2017 30 Nov- 2 Dec

Contributions to the Paper:

Navid Aghanoori

I, Navid Aghanoori, the PhD student of Curtin and Power Control Engineer of Goldwind Australia generated the new idea of the paper. I derived the theoretical aspect of simulation and main investigations. I derived all the results on the case studies and ran the results analysis. I also prepared the manuscript.

Signature [redacted] Date 27/05/2019

Mohammad Sherkat Masoum

I, Mohammad Sherkat Masoum, encouraged the idea from Navid Aghanoori, and investigated the necessity of the contribution. I also contributed in choosing case studies, the manuscript review and corrections on the academic language. I believe my contribution to this paper has been 10% of the work.

Signature [redacted] Date 28/5/2019

Syed Islam

I, Syed Islam, reviewed the results analysis and manuscript review and provided consultation about the control and stability margin improved on using the proposed method. I believe my contribution is 10% on this work

Signature [redacted] Date 23/8/18

Steven Nethery

I, Steven Nethery, contributed in supporting the idea based on practical experience gained in dealing with challenges on wind and solar plants. I provided consultations about the harmonic distortions. I reviewed the manuscript and provided some comments as well.

Signature [redacted] Date 7.6.19

AUTHORSHIP STATEMENT of

"Improving voltage of remote connection using wind-solar farms equipped with new voltage control strategy based on virtual impedance monitoring enabled by IEC 61850 communication "

Accepted by Special Issue: *IET Emerging Technologies for Virtual Power Plant and Microgrid*

Authors: Navid Aghanoori, Mohammad A.S Masoum, Syed Islam, Ahmed Abu-Siada Steven Nethery

12-05-2019

Contributions to the Paper:

Navid Aghanoori

I, Navid Aghanoori, the PhD student of Curtin and Grid Connection Manager of Goldwind Australia generated the new idea of the paper. I derived the theoretical aspect of simulation and field study on the wind-solar farm. I also did all the simulation and field tests. I developed all the results on the case studies and ran the results analysis. I also prepared the manuscript.

Signature [redacted] Date 27/05/2019

Mohammad Sherkat Masoum

I, Mohammad Sherkat Masoum, encouraged the idea from Navid Aghanoori, investigated the theory of IEC 61850 data type model and reviewed the results. I also contributed in the manuscript review and corrections on the academic language and formatting. I believe my contribution to this paper has been 10% of the work.

Signature [redacted] Date 28/5/2019

Syed Islam

I, Syed Islam, reviewed the results analysis and manuscript review and provided consultation about the power system featured improvement on using the proposed method. I believe my contribution is 10% on this work.

Signature [redacted] Date 27/5/2019

Ahmed Abu-Siada

I, Ahmed Abu Siada, reviewed the final version of the paper and results and provided consultation on the control aspect and quality of the material. I believe my contribution is 10% on this work.

Signature [redacted] Date 29/05/2019

Steven Nethery

I, Steven Nethery, contributed in growing and encouraging the idea of work specially the communication protocol development. I assisted Navid Aghanoori to be able to perform the test on the voltage management platform of wind-solar farm and at the end reviewed the results and the manuscript. I believe my contribution is 5% on this work.

Signature [redacted] Date 7-6-17

AUTHORSHIP STATEMENT of

"Enhancement of Microgrid Operation by Considering the Cascaded Impact of Communication Delay on System Stability and Power Management"

International Journal of Electrical Power and Energy Systems

Authors: Navid Aghanoori, Mohammad A.S Masoum, Ahmed Abu-Siada, Syed Islam

04-02-2020

Contributions to the Paper:

Navid Aghanoori

I, Navid Aghanoori, the PhD student of Curtin conceived and presented the idea of the paper. Navid Aghanoori developed the theory and computations, also derived all the simulations and lab tests. The results were generated by the work from my coding and programming. I analyzed the results, performed trouble shooting on the modelling and lab tests, and prepared the manuscript.

Signature .....[redacted].....Date 04/02/2020

Mohammad Sherkat Masoum

I, Mohammad Sherkat Masoum, encouraged and supported the idea from Navid Aghanoori, investigated the practicality of the idea and reviewed the results. I also contributed in the manuscript review and corrections on the academic language and formatting. I believe my contribution to this paper has been 10% of the work.

Signature [redacted] Date 4/02/2020

Ahmed Abu-Siada

I, Ahmed Abu-Siada, investigated the feedbacks received in the first and second review of the paper. I provided technical suggestions to the main author to respond to the comments. I also contributed in the manuscript review and corrections on the academic language and formatting. I believe my contribution to this paper has been 10% of the work.

Signature .....[redacted].....Date 05/02/2020

Syed Islam

I, Syed Islam, contributed in growing and encouraging the idea of work, results analysis and manuscript review. I believe my contribution is 10% on this work.

Signature ..... 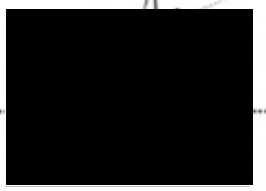 .....Date..... 4/2/2020

APPENDIX D

```
clc;
%clear;
close all;
%% Problem Definition
global NFE;
NFE=0;
model=CreateModel();
CostFunction=@(p) MyCost(p,model);        % Cost Function
nVar=model.N;       % Number of Decision Variables
VarSize=[1 nVar];   % Size of Decision Variables Matrix
VarMin=model.pmin;         % Lower Bound of Variables
VarMax=model.pmax;         % Upper Bound of Variables
PL=model.PL;
%% PSO Parameters
MaxIt=15;      % Maximum Number of Iterations
nPop=100;        % Population Size (Swarm Size)
w=1;             % Inertia Weight
wdamp=0.99;      % Inertia Weight Damping Ratio
c1=2;            % Personal Learning Coefficient
c2=2;            % Global Learning Coefficient
% % Constriction Coefficients
% phi1=2.05;
% phi2=2.05;
% phi=phi1+phi2;
% chi=2/(phi-2+sqrt(phi^2-4*phi));
% w=chi;          % Inertia Weight
% wdamp=1;        % Inertia Weight Damping Ratio
% c1=chi*phi1;    % Personal Learning Coefficient
% c2=chi*phi2;    % Global Learning Coefficient
% Velocity Limits
VelMax=0.1*(VarMax-VarMin);
VelMin=-VelMax;
%% Initialization
empty_particle.Position=[];
empty_particle.Cost=[];
empty_particle.Sol=[];
empty_particle.Velocity=[];
empty_particle.Best.Position=[];
empty_particle.Best.Cost=[];
empty_particle.Best.Sol=[];
%empty_particle.PL=[];
%empty_particle.Alpha=[];
particle=repmat(empty_particle,nPop,1);
GlobalBest.Cost=inf;
for i=1:nPop
    % Initialize Position
    particle(i).Position=CreateRandomSolution(model);
    % Initialize Velocity
    particle(i).Velocity=zeros(VarSize);
    % Evaluation
    [particle(i).Cost particle(i).Sol]=CostFunction(particle(i).Position);
    % Update Personal Best
    particle(i).Best.Position=particle(i).Position;
    particle(i).Best.Cost=particle(i).Cost;
    particle(i).Best.Sol=particle(i).Sol;
    % Update Global Best
    if particle(i).Best.Cost<GlobalBest.Cost
```

```
        GlobalBest=particle(i).Best;

    end

end
BestCost=zeros(MaxIt,1);
nfe=zeros(MaxIt,1);
%% PSO Main Loop
for it=1:MaxIt
    for i=1:nPop

     % Update Velocity
        particle(i).Velocity = w*particle(i).Velocity ...
            +c1*rand(VarSize).*(particle(i).Best.Position-particle(i).Position)
...
            +c2*rand(VarSize).*(GlobalBest.Position-particle(i).Position);

        % Apply Velocity Limits
        particle(i).Velocity = max(particle(i).Velocity,VelMin);
        particle(i).Velocity = min(particle(i).Velocity,VelMax);

        % Update Position
        particle(i).Position = particle(i).Position + particle(i).Velocity;

        % Velocity Mirror Effect
        IsOutside=(particle(i).Position<VarMin | particle(i).Position>VarMax);
        particle(i).Velocity(IsOutside)=-particle(i).Velocity(IsOutside);

        % Apply Position Limits
        particle(i).Position = max(particle(i).Position,VarMin);
        particle(i).Position = min(particle(i).Position,VarMax);

        % Evaluation
        [particle(i).Cost particle(i).Sol] = CostFunction(particle(i).Position);
        % Eigenvalue Evaluation
        NewAlpha=particle(i).Position./PL;
        %Parameter_edited;
        %Model_edited;
        %Eigenvalue_edited;
        Run main program;
                % Update Personal Best
        if particle(i).Cost<particle(i).Best.Cost %& Eig_Mode1_real(:,:)<0
            particle(i).Best.Position=particle(i).Position;
            particle(i).Best.Cost=particle(i).Cost;
            particle(i).Best.Sol=particle(i).Sol;
            % Update Global Best
            if particle(i).Best.Cost<GlobalBest.Cost
            GlobalBest=particle(i).Best;
            end
         end

    end

    BestCost(it)=GlobalBest.Cost;
    nfe(it)=NFE;
    disp(['Iteration ' num2str(it) ': Best Cost = ' num2str(BestCost(it))]);
```

```
    w=w*wdamp;
    end
 %% Results
LastAlpha=GlobalBest.Position./sum(GlobalBest.Position)
 figure;
plot(BestCost,'LineWidth',2);
%xlabel('NFE');
ylabel('Best Cost');
```